On the Morphology of Vesicles

Dissertation
zur Erlangung des akademischen Grades
Doctor rerum naturalium (Dr. rer. nat.)
in der Wissenschaftsdisziplin Theoretische Physik

eingereicht an der
Mathematisch–Naturwissenschaftlichen Fakultät der Universität Potsdam

angefertigt am


Max-Planck-Institut
für Kolloid- und Grenzflächenforschung

von

Dipl.-Ing. Erwin Johann Gutlederer
geboren in Amstetten (Österreich)

Potsdam, im März 2007

”Jenseits des Weihrauchs, dort wo es klar wird und heiter und durchsichtig, beginnen die Offenbarungen; dort gibt es keine Launen, Roderigo, wie in der menschlichen Liebe; was heute gilt, das gilt auch morgen, und wenn ich nicht mehr atme, es gilt ohne mich, ohne euch. Nur der Nüchterne ahnt das Heilige, alles andere ist Geflunker, glaub mir, nicht wert, daß wir uns aufhalten darin.” Don Juan.
Max Frisch: Don Juan oder die Liebe zur Geometrie

Abstract

This dissertation contains theoretical investigations on the morphology and statistical mechanics of vesicles. The shapes of homogeneous fluid vesicles and inhomogeneous vesicles with fluid and solid membrane domains are calculated. The influence of thermal fluctuations is investigated. The obtained results are valid on mesoscopic length scales and are based on a geometrical membrane model, where the vesicle membrane is described as either a static or a thermal fluctuating surface. The thesis consists of three parts.

In the first part, homogeneous vesicles are considered. The focus in this part is on the thermally induced morphological transition between vesicles with prolate and oblate shape. With the help of Monte Carlo simulations, the free energy profile of these vesicles is determined. It can be shown that the shape transformation between prolate and oblate vesicles proceeds continuously and is not hampered by a free energy barrier.

The second and third part deal with inhomogeneous vesicles which contain intramembrane domains. These investigations are motivated by experimental results on domain formation in single or multicomponent vesicles, where phase separation occurs and different membrane phases coexist. The resulting domains differ with regard to their membrane structure (solid, fluid). The membrane structure has a distinct effect on the form of the domain and the morphology of the vesicle. In the second part, vesicles with coexisting solid and fluid membrane domains are studied, while the third part addresses vesicles with coexisting fluid domains. The equilibrium morphology of vesicles with simple and complex domain forms, derived through minimisation of the membrane energy, is determined as a function of material parameters. The results are summarised in morphology diagrams. These diagrams show previously unknown morphological transitions between vesicles with different domain shapes. The impact of thermal fluctuations on the vesicle and the form of the domains is investigated by means of Monte Carlo simulations.

Zusammenfassung

Die vorliegende Arbeit enthält theoretische Untersuchungen zur Morphologie und statistischen Mechanik von Vesikeln. Es wird die Gestalt homogener fluider Vesikel und inhomogener Vesikel mit fluiden und festen Membrandomänen berechnet. Der Einfluss thermischer Fluktuationen wird untersucht. Die erzielten Ergebnisse beziehen sich auf mesoskopische Längenskalen und basieren auf einem geometrischen Membranmodell, in welchem die Vesikelmembran als statische, beziehungsweise thermisch fluktuierende Fläche beschrieben wird. Die Arbeit besteht aus drei Teilen.

Im ersten Teil werden homogene fluide Vesikel betrachtet. Das Interesse gilt dem thermisch induzierten Morphologieübergang zwischen prolaten und oblaten Vesikelformen. Mit Hilfe von Monte-Carlo-Simulationen wird ein freies Energieprofil für diese Vesikel ermittelt. Es kann gezeigt werden, dass die Formumwandlung zwischen prolaten und oblaten Formen kontinuierlich verläuft und mit keiner freien Energiebarriere verbunden ist.

Der zweite und dritte Teil beschäftigt sich mit inhomogenen Vesikeln, die intramembrane Domänen enthalten. Ausgangspunkt und Motivation der Berechnungen sind experimentelle Studien über Domänbildung in ein- oder mehrkomponentigen Vesikelmembranen, bei denen Phasentrennung stattfindet und unterschiedliche Membranphasen koexistieren. Die dabei auftretenden Domänen unterscheiden sich hinsichtlich ihrer Membranstruktur (fest, fluid). Diese beeinflusst die Form der Domäne und des gesamten Vesikels auf entscheidende Weise. Im zweiten Teil werden Vesikel untersucht, bei denen feste und fluide Membrandomänen koexistieren, Teil drei widmet sich Vesikeln mit zwei koexistierenden fluiden Membranphasen. In Abhängigkeit von Materialparametern werden durch Minimierung der Membranenergie die Grundzustandsformen von Vesikeln mit einfachen und komplexen Domänenformen bestimmt. Die Ergebnisse werden in Morphologiediagrammen zusammengefasst. Dabei werden bisher unbekannte Morphologieübergänge zwischen Vesikeln mit unterschiedlichen Domänformen beobachtet. Die Auswirkungen thermischer Fluktuationen auf die Vesikel und die Form ihrer Domänen werden mittels Monte-Carlo-Simulationen untersucht.

Contents

Chapter 1

Introduction

"When a man is born, he is weak and flexible; when he dies, he is sturdy and stiff. When a tree grows, it is soft and flexible, and when it is dry and stiff, it dies. Stiffness and strength are companions of death, flexibility and weakness express freshness of being. Thus, what has hardened will not win." Stalker. [1]

1.1 Soft matter(s)

Soft matter physics, a relatively new and rapidly developing branch in physics, is concerned with a vast variety of classical systems which exhibit types of order that lie in between simple disordered fluids and simple ordered crystals [1–5]. Soft condensed matter includes supramolecular assemblies or substances structured on nanoscopic to mesoscopic length scales, which – as the name indicates – are rather soft and flexible. These materials (sometimes also referred to as complex fluids) are ubiquitous in everyday life, and play an important role in various technological and biological applications. Ranging from milk to butter, from paints to lubricants, from beer foam to smoke, and from DNA to proteins, soft matter not only represents an integral part of everyday life, but actually forms the physical basis of life itself. Accordingly, especially in the last several years a major motivation for the study of such systems has come from the fields of biomaterials and biological matter [6, 7].

Vesicles and *membranes*, which are the focus of this thesis, are examples of biologically inspired soft matter. Vesicles are microscopically small, flexible bags composed of a molecular thin bilayer (membrane) of amphiphilic molecules [8–10]. These small bags are formed in a self-assembly process initiated when molecules with a dual hydrophilic-hydrophobic character are dissolved in water under appropriate conditions. Vesicles are interesting from a number of perspectives.

First, from a biological point of view, vesicles and membranes made of a bilayer of lipids are important because they serve as model systems for the far more complex biological membrane. Biological membranes are one of the fundamental structural components of all living cells. They consist of a core phospholipid bilayer, in which various other macromolecules are

[1] Когда человек родится, он слаб и гибок, когда умирает, он крепок и чёрств. Когда дерево растёт, оно нежно и гибко, а когда оно сухо и жёстко, оно умирает. Чёрствость и сила спутники смерти, гибкость и слабость выражают свежесть бытия. Поэтому что отвердело, то не победит. Arcady and Boris Strugatsky. Script for the film 'Stalker'. Director: Andrei Tarkovsky. (Thanks to Peter Saparin for providing me with the Russian original.)

embedded.

Then, from a technological point of view, research in this field has direct ramifications for potential applications. Vesicles are utilised as microcapsules in biochemistry and pharmacology [10]. From an experimental physicist's point of view, vesicles are convenient to study because they are easily visible and manipulated under an optical microscope.

Finally, vesicles and membranes have unique material and physical properties, whose theoretical description poses manifold scientific challenges. One intriguing property of vesicles is that they occur in a variety of different morphologies, including spherical forms, oblate and prolate shapes, and biconcave morphologies which resemble the shape of red blood cells. The shapes of vesicles are found to depend on a few material and control parameters and change, when these parameters are varied [11].

In this dissertation, we investigate selected aspects of the *morphology* and *morphological transitions* of vesicles. The thesis consists of three parts. In each part, transitions between vesicle shapes are caused by a different mechanism.

In the first part we study homogeneous fluid vesicles which are composed of a single component. Besides material parameters, the shape of vesicles is strongly influenced by thermal forces. Vesicles are not static objects, but, being embedded in an aqueous solution, they are subject to permanent thermal collisions with the water molecules. Vesicles are soft objects in the sense that the elastic deformation energies are in the order of the thermal energy. Therefore, thermal fluctuations are strong enough to cause membrane deformations and to affect the geometry of the vesicle. The first part of this dissertation centres on statistical properties of fluid vesicles in thermal equilibrium, focussing on vesicles with prolate and oblate shapes. We will investigate the transition between prolate and oblate shapes which is induced by thermal fluctuations.

The second and third part concern heterogeneous vesicles, made of a mixture of different lipid molecules. Understanding vesicles with a complex composition is important in view of biological membranes, which consist of a large number of different molecules. Heterogeneous vesicles made of a mixture of lipids are interesting because, under certain conditions, the lipids do not mix homogeneously but phase segregate. As a consequence, domains are formed in the vesicle membrane. These domains affect the shape of the vesicle in a distinct way. As a result, morphological transitions of the vesicle occur which are caused by the formation of membrane domains.

Beyond heterogeneities in their composition, membranes may also exhibit differences in their internal structure. Like ordinary matter, they can exist in different thermodynamic phases and show different degrees of internal or in-plane order. Biologically most relevant are fluid membranes, where the membrane molecules can diffuse freely in the lateral direction. Typically, biological membranes are fluid at physiological temperatures. At lower temperatures, the membrane molecules freeze and order on a crystal lattice. This in-plane order crucially influences the membrane behaviour.

In this dissertation, two different kinds of membrane domains are distinguished, based on the membrane structure: *solid* (gel) *domains* with longer-range positional order, and *fluid domains* which are in-plane disordered. In the second part, fluid vesicles with solid domains are studied, while in the third part, vesicles with coexisting fluid domains are investigated. We will address the question of how these different types of membrane domains affect the vesicle morphology.

The remainder of the introduction provides a brief introduction to the basic physical properties of vesicles and membranes, and gives an outline of the thesis.

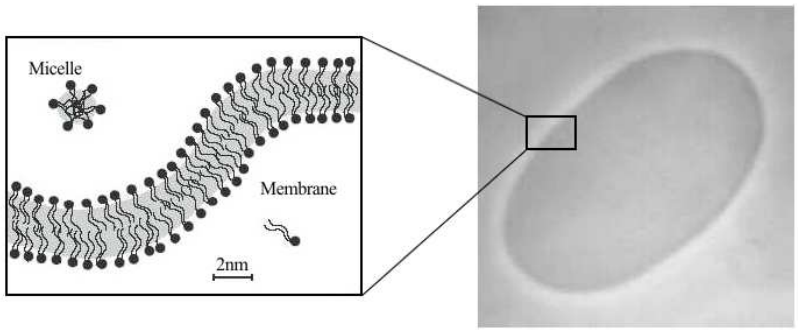

Figure 1.1: Sketch of a lipid bilayer membrane and image of a giant unilamellar vesicle obtained via phase contrast microscopy; adapted from [12].

1.2 Vesicles and membranes

Vesicles [2] are fluid, semipermeable soft shells which are composed of a thin bilayer membrane of amphiphilic molecules (see Fig. 1.1) [8, 9, 13–17]. Amphiphiles such as lipids consist of two parts covalently bound together, a hydrophilic (water 'liking') part which interacts attractively with water molecules and a hydrophobic (water 'fearing') part that shuns water and aggregates with other hydrophobic molecules. Exposed to an aqueous environment, these molecules assemble spontaneously into different structures above the so-called critical micelle concentration. This structure formation is due to the hydrophobic effect [18, 19]. Depending on the specific molecular properties of the amphiphile and on physical conditions such as their concentration or the temperature, one obtains spherical and cylindrical (worm-like) micelles, inverted micelles, hexagonal and lamellar structures.

A very prominent arrangement is the bilayer [20]. Bilayers are thin, sheet-like structures, composed of two adjacent mono-molecular layers, which are hold together by weak, non-covalent forces. The amphiphiles are arranged such that the hydrophobic parts are confined in the interior and face each other, while the hydrophilic parts are oriented towards the water surrounding. At physiological temperatures the bilayer membrane exhibits an in-plane fluid-like nature which means that the molecules can diffuse freely within their monolayers.

At the edge of the membrane, the hydrophobic parts are exposed to water. Therefore, in order to avoid energetic disadvantageous configurations at the edges, membranes often form closed shells called vesicles. By closure of the membrane an inner compartment is created, which separates the interior solvent from the exterior surrounding solvent. The size of vesicles created in the lab can reach dimensions in the order of tens of micrometers, even though the bilayer is only a few nanometers thick [10].

Vesicles are sometimes named according to their main constituents, for example, liposome (when made of lipids) or polymerosome (when the basic constituents are amphiphilic diblock-copolymers of modest molecular weight [21]), etc.

In the following, we concentrate on bilayer membranes and vesicles composed of lipids. Phospholipid molecules are amphiphilic, with a charged or polar hydrophilic head group, and typically one or two hydrophobic hydrocarbon tails. A schematic picture of a phospholipid molecule is illustrated in Fig. 1.2. The importance of lipid bilayers is related to their function in biological cells, lipid bilayers form the backbone of all biological membranes [22].

[2] from Latin vesicula small blister

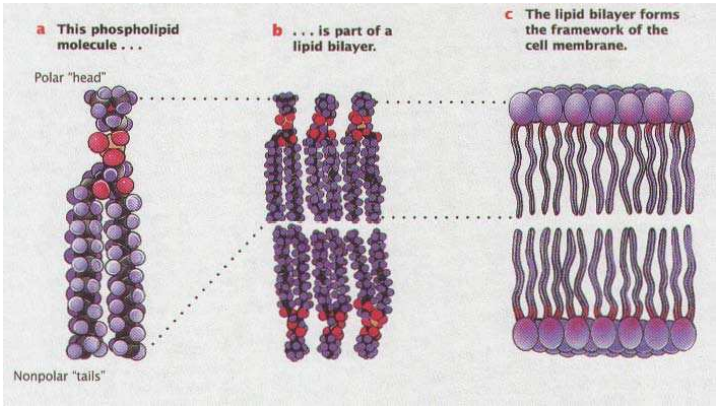

Figure 1.2: Schematic picture of a phospholipid forming a bilayer. Phospholipids, the major compound of biological membranes, consist of a hydrophilic phosphate-containing polar headgroup which is attached to two hydrophobic nonpolar hydrocarbon chains. These so-called amphiphilic molecules aggregate into bilayers in aqueous solution. The lipid bilayer forms the backbone of all cell membranes; from [23].

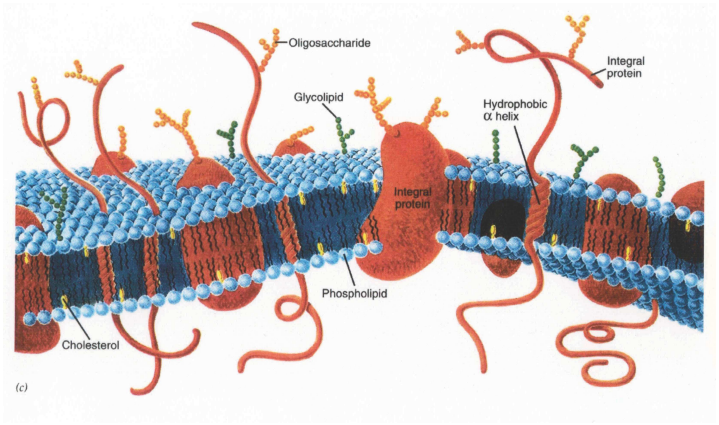

Figure 1.3: Schematic picture of a cell membrane. The lipid bilayer forms a fluid matrix where various macromolecules are embedded or associated; from [24].

1.2.1 Biological and biomimetic membranes

Biological membranes are essential structural as well as functional elements in biological cells [23]. The so-called plasma membrane envelopes the cell and controls the interface between the cell and its environment. Membranes also structure the interior of eukaryotic cells by forming different intracellular compartments. Their main purpose is to act as a selectively permeable barrier that enables enclosed spaces to maintain a biochemical environment that differs from the surrounding medium. Biomembranes actively participate in many cellular processes. They are involved in the communication between different compartments. Small vesicles bud from donor compartments and fuse with others.

Biological membranes are highly organised assemblies, consisting of a multi-component lipid bilayer core which acts as a fluid matrix for various macromolecules such as proteins or sugars (fluid mosaic model [25]), see Fig. 1.3. Biological membranes possess hundreds of

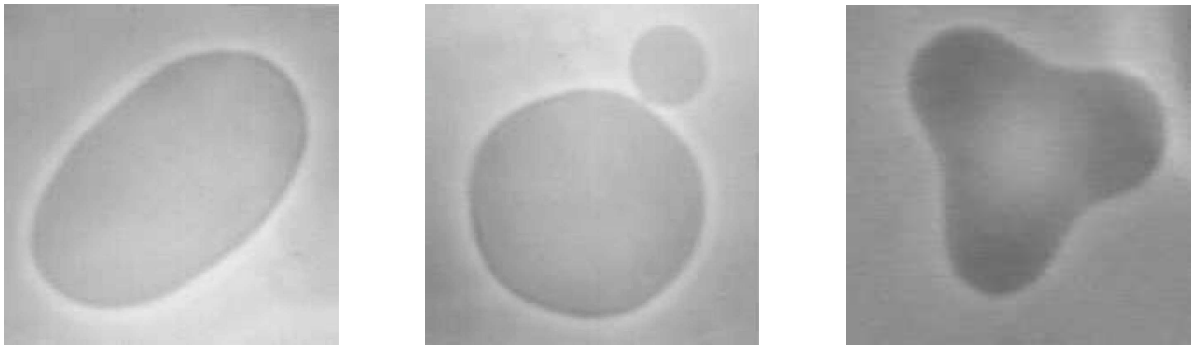

(a) (b) (c)

Figure 1.4: Morphologies of homogeneous fluid vesicles: (a) vesicle with prolate shape, (b) vesicle with a small bud, (c) star-shaped vesicle; (a)-(b) from [12], (c) by courtesy of Rumy Dimova.

different species of lipids, the most common lipid classes are phospholipids, sphingomyelin and sterols.

Due to their intrinsic complexity, a systematic study of biological membranes is very complicated. Therefore, one introduces model systems (biomimetic systems). These are strongly simplified systems which are supposed to capture main physical features of biomaterials and allow to focus more systematically on basic and generic aspects. Apart from their relevance to basic research, biomimetic membrane systems such as vesicles are promising research objects which lead to biotechnological applications. One example is the use of liposomes as biocompatible microcapsules in targeted drug delivery and gene therapy [26], another example are vesicles which are applied as microreactors for biochemical reactions [27, 28].

Biomimetic lipid vesicles have proven to be very convenient model systems for studying various aspects of biomembrane behaviour. During the past years different issues have been investigated: equilibrium phenomena of homogeneous single-component vesicles [29–31], polymer-decorated membranes and vesicles [32–35], inclusions in membranes [36, 37], adhesion of membranes and vesicles [38–40], fission and fusion of vesicles [41], vesicles in external fields [42, 43]; out-of-equilibrium aspects like vesicles in shear fields [44, 45] and 'active membranes' (i.e. membranes with local dissipative elements which reflect the activity of membrane proteins) [46–48].

In this thesis, a main focus is on vesicles which are made of a mixture of different lipids. These vesicles have interesting properties because the different lipids do not always mix homogeneously, but under appropriate condition phase segregate and form domains within the vesicle membrane. Before we turn to such vesicles composed of different lipids, we briefly describe main properties of homogeneous, single-component vesicles.

1.2.2 Morphology of vesicles

An intriguing aspect of phospholipid vesicles is the multiplicity of geometrical shapes they can attain [29–31]. Apart from spherical forms the conformations include oblate and prolate ellipsoids, biconcave discocytes, which resemble the shape of a red blood cell under normal physiological conditions [49], cup shaped stomatocytes, pears, dumb-bells, budded shapes, where a smaller vesicle is expelled from a larger one and remains connected via a small neck,

and various non-axisymmetric shapes like boomerangs or starfish [50]. Some of the observed morphologies are illustrated in Fig. 1.4. By changing temperature or osmotic conditions, transitions between these morphologies can be induced. Furthermore, vesicles with a more complex topology, for example, toroidal vesicles, have been observed [3].

At first glance, the richness of vesicle shapes, including non-convexity, is rather astonishing. One may just recall the shape of other soft surfaces like soap bubbles. Closed liquid films such as soap bubbles are always found to be spherical. The reason for this is that soap bubbles are governed by surface tension and try to minimise their surface area. As a consequence, they acquire a surface of constant mean curvature. Since the only closed embedded surface of constant mean curvature is a sphere (shown in [53]), the shape of a closed, isotropic liquid film is unique and has to be spherical [4].

Fluid membranes, on the contrary, do not behave as a thin liquid film. Their properties resemble more closely those of a smectic liquid crystal film. This fact has been recognised in the early seventies of the last century [55–57]. Fluid membranes are primarily governed by bending elasticity, hence they acquire shapes with minimal bending energy or, in its mathematical formulation, minimal curvature.

1.2.3 Basic physical properties of membranes and vesicles – Surface model

Fluid membranes are remarkable materials with interesting physical properties. Like almost all soft matter, vesicles feature a hierarchy of spatial and temporal scales. In particular, there is a huge discrepancy in the involved length scales. While the vesicle membrane is very thin with a thickness of a few nanometers, the lateral size of a vesicle can extend up to tens of micrometers. We briefly describe their main material properties.

An important characteristic of fluid membranes is their resistance to bending deformations. Although membranes are quite flexible, they tend to avoid curved configurations. This is quite intuitive from a molecular point of view since one leaflet of the bilayer is squeezed when the membrane is bent. For fluid membranes, bending modes are rather soft. The elastic modulus for bending deformations is in the order of the thermal energy at room temperature.

Membranes can be bent much more easily than they can be stretched (extended) or compressed. This follows from similar considerations regarding thin plates [5]. In contrast to liquid interfaces, for membranes, surface tension is less relevant. The elastic modulus for changing the area per molecule is exceedingly high compared to the thermal energy. The area of the membrane is essentially determined by the number of lipid molecules in the membrane. This number is constant on experimentally relevant time scales because the interchange of lipids between the membrane and the solution is negligible. Thus, the membrane area remains approximately constant.

Fluid membranes are further characterised by a zero shear-modulus. The membrane molecules can diffuse freely in the membrane plane. Thus, any shear deformation relaxes

[3] For vesicle shapes with topological genus 2 (or higher), the energetic ground state is degenerated. This fact leads to the first theoretically predicted [51], then experimentally confirmed effect called conformal diffusion [52].

[4] This holds under the assumption that the liquid film does not self-intersect. For immersions i.e. hypersurfaces with self-intersection, closed surfaces of constant mean curvature are not necessarily spherical. There exist other surfaces with constant mean curvature which have a more complex topology [54].

[5] For a solid plate, the ratio between stretching energy and bending energy diverges as the thickness vanishes [58].

by flow within the membrane. This happens on time scales fast compared to the time scale of shape deformations.

In this dissertation, we are interested in the morphology of vesicles with a size in the micrometer range. On this length scale, most details of the membrane molecules become irrelevant, and the relevant properties can be described by a few material parameters. In the early 1970s, Canham [55] and Helfrich [56] introduced a coarse-grained continuum model which lays the foundation for the understanding of vesicle shapes. In the Canham-Helfrich model, the vesicle membrane is described as a flexible two-dimensional surface which resists bending. The (free) energy of the membrane consists of bending energy and depends on the curvature of the membrane surface

$$\mathcal{H}_{CH} = \frac{1}{2}\kappa \int dA\,(2H - C_0)^2 + \kappa_G \int dAK\,. \tag{1.1}$$

The integral extends over the membrane area. In Eq. (1.1), the mean curvature H and the Gaussian curvature K are geometric quantities and describe the curvature of the membrane (mathematical details are recalled in appendix A.1). The bending rigidity κ, the Gaussian bending rigidity κ_G and the spontaneous curvature C_0 are material parameters. Eq. (1.1) describes the bending energy of the membrane from its preferred curvature C_0. The bending rigidity κ quantifies the energetic costs associated with bending of the membrane. For phospholipid bilayers, a typical value for κ is around $10^{-19}J$ [20], which is in the order of $10-20\ T_0$ where T_0 is the thermal energy at room temperature including the Boltzmann constant k_B [6]. The Gaussian elastic modulus κ_G is associated with the energetic costs of deformations which change the topology of the vesicle. It is difficult to determine experimentally, recent measurements yield a value $\kappa_G \sim -0.8\kappa$ (for a phospholipid monolayer) [59]. A nonvanishing spontaneous curvature C_0 takes a possible asymmetry of the membrane into account.

In equilibrium, the vesicle adapts a morphology which minimises the bending energy under given constraints on the vesicle area and, depending on the osmotic conditions, on the enclosed volume of the vesicle.

1.2.4 Thermal fluctuations

Membranes and vesicles are not static structures. Analogously to colloid particles which (if sufficiently small) undergo Brownian motion, they are subject to thermal forces. Fluid membranes are soft, deformable objects with bending rigidities in the order of the thermal energy at room temperature. Therefore, thermal fluctuations not only affect the centre of mass and the overall orientation of the vesicle, but also excite soft internal deformation modes and thus influence its morphology. Vesicles exhibit pronounced shape fluctuations whose long wavelength modes are visible in the optical light microscope [60].

Typically, the shape fluctuations occur around a mean shape which corresponds to the shape of minimum bending energy. Yet, thermal fluctuations may cause morphological transitions of the whole vesicle. Such thermally induced shape transformations are frequently observed in experiments between vesicles with prolate and oblate shape [61]. These vesicles with prolate and oblate shape are the subject of the first part of this dissertation where a detailed study of this shape transition is provided.

[6] Throughout the thesis, the Boltzmann constant is set to one, $k_\mathrm{B} = 1$.

1.3 Multi-component membranes

While homogeneous fluid membranes already give rise to a rich physical behaviour, interesting new effects occur for membranes with additional (internal) degrees of freedom. In this dissertation, we concentrate on vesicle membranes composed of a mixture of different lipid molecules. These multi-component membranes mimic real biological membranes more closely than single-component membranes. The interesting aspect of such vesicles is that the different lipids do not always mix uniformly to form homogeneous membranes. Instead, at appropriate conditions they segregate into different phases and form intramembrane domains [62].

The study of domain formation in vesicles is inspired by recent findings of biologists about the lateral distribution of lipids in biomembranes [63]. The bilayer core of the cell membrane is made out of a mixture of hundreds of different lipid species. In the conventional view of Singer and Nicolson [25], these lipids were believed to be distributed laterally rather homogeneously within the cell membrane. This picture of the cell membrane, however, has been challenged in the recent years by the hypothesis that the lipids do not mix randomly but instead certain saturated lipids, like sphingomyelin and cholesterol, aggregate and cluster. These lipids are conjectured to form lateral assemblies, small microdomains called lipid 'rafts', which float in the sea of other (unsaturated) lipids [64, 65]. This spatial organisation of the membrane is believed to be of vital importance in biological systems. Lipid rafts may play an important role in the control of the activity of membrane proteins. Certain membrane proteins are found to partition preferentially into one or the other lipid assembly.

Rafts are difficult to detect experimentally *in vivo*. Up to now, the evidence for their existence in biomembranes is still rather indirect and controversial. Especially their size is a matter of current debate, estimates range from 20 to 700 nm [66]. One has to bear in mind that in vivo the formation of domains may not only be due to the interaction between different lipids. When discussing biomembranes, the issue is complicated by the presence of many components, other than lipids, and manifold active and passive processes. Therefore, domain formation might be influenced by the interaction with other membrane molecules.

In contrast, phase separation and domain formation has been demonstrated clearly for *in vitro* systems [67]. An experimentally well explored model system are vesicles composed of a ternary mixture of cholesterol, a high-melting point lipid (such as sphingomyelin) and a lipid whose melting point is lower. Fig. 1.5 shows the phase diagram for such a system. Depending on the membrane composition and temperature, the membrane exists in different phases with different type of internal order. There are fairly large regions in the phase diagram where different phases coexist. When the vesicle is prepared at conditions providing phase coexistence, one obtains vesicles with membrane domains. The vesicle morphology and the shape of the domains depends decisively on the particular phase the membrane is in [62].

Before we have a closer look at the observed vesicle shapes and different domain morphologies, we discuss different lipid bilayer phases, starting first with the phases that already occur for a single-component membrane.

1.3.1 Phases of lipids in bilayer arrangement

Similar to ordinary matter lipid bilayers can exist in different thermodynamic states and exhibit varying degrees of internal order [69]. The generic phase at higher temperatures is the fluid phase, also called L_α-phase (or smectic A), the state of the membrane already encountered before. Physiologically, the L_α phase is the most important phase. Therefore, it has attracted

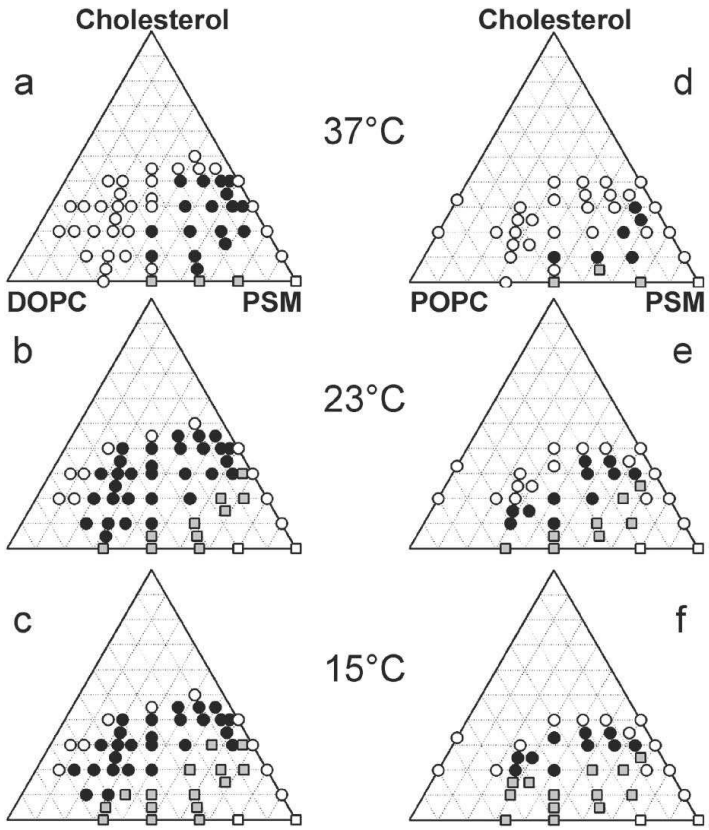

Figure 1.5: Partial phase diagrams for vesicles composed of a ternary mixture of lipids at different temperatures. Figures (a)-(c) correspond to a mixture of DOPC/PSM/cholesterol (DOPC (dioleoyl-phosphatidylcholine) is a phospholipid and PSM (palmitoyl sphingomyelin) a sphingolipid); figures (d)-(f) correspond to a mixture of POPC/PSM/cholesterol (POPC (palmitoyl-oleoyl-phosphatidylcholine) is a different phospholipid). White symbols denote that the membranes are in one uniform phase, either liquid (circles) or solid (squares). Black circles denote coexisting liquid phases, and gray squares denote coexisting solid and liquid phases; from [68].

the most interest and research activities of all the different lipid bilayer phases. As noted before, the lipid molecules are liquid-like disordered in plane and free to diffuse in the lateral direction. The hydrocarbon chains of the lipids are in a conformationally disordered state and undulate due to thermal fluctuations (see Fig. 1.6a).

If the temperature is reduced below the so-called main transition temperature, the hydrocarbon chains freeze and positional ordering of the molecules on a lattice sets in. In the crystalline or solid phase, diffusion of the molecules is slowed down substantially. Owing to a usually rich defect structure, which is caused by the different packing constraints of the hydrocarbon chains and the lipid headgroups, solid phases are commonly also referred to as gel-phases. Most probably, crystalline phases do not have any biological implications. Nevertheless, from a physical perspective, as two-dimensional crystals with unique properties, they certainly deserve attention. Most lipids have more than one crystalline phase. Typical phases

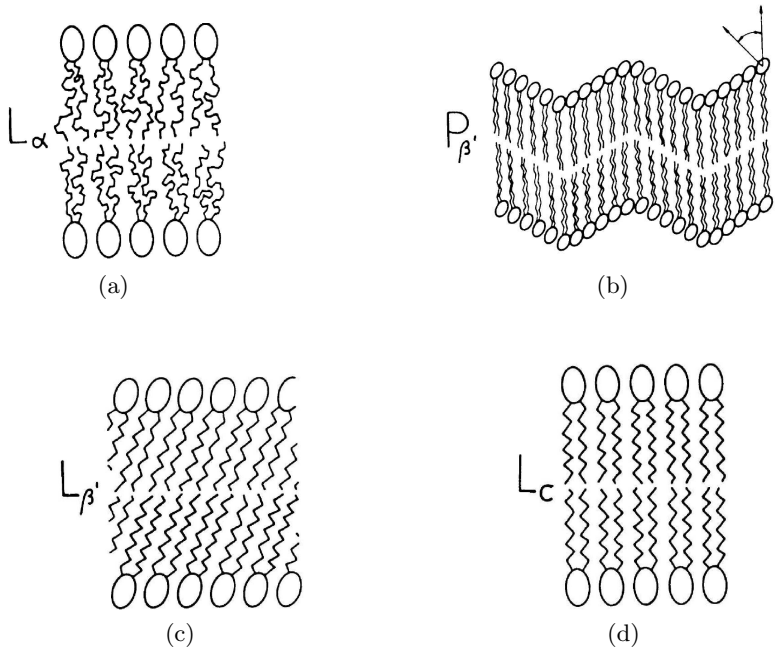

Figure 1.6: Schematics of the bilayer structure of different lipid phases: the fluid phase L_α (a), and the gel phases $P_{\beta'}$ (b), $L_{\beta'}$ (c) and L_c (d); from [14].

are the gel phases $P_{\beta'}$, L_β, and $L_{\beta'}$ [7] as well as the sub-gel phase L_c (see Fig. 1.6b-Fig. 1.6d). In the $P_{\beta'}$ phase, or 'ripple' phase, the bilayer exhibits a corrugated surface profile (asymmetric sawtooth), and the molecules are arranged on a hexagonal lattice. In the lamellar phases L_β and $L_{\beta'}$ the bilayer is flat with orthorhombic molecular packing. For most common lipids, the low-temperature phase is the subgel L_c ('c' denoting crystalline). It exhibits a greater order in the conformation of the hydrocarbon chains as well as in the lattice arrangement. In general, the transition to an equilibrium L_c phase is a slow process and may be accompanied by long-lived metastable intermediates.

A more complex scenario exists for membranes made of a mixture of different lipids. The addition of cholesterol has the most striking implications. The major effect of cholesterol is that it disturbs (respectively stimulates) the conformational order of the hydrocarbon tails in the L_α (respectively L_β) state. At sufficiently high amounts of cholesterol chain ordering and positional ordering decouple so that a new phase appears between the solid and fluid phases – without cholesterol both ordering transitions occur together at the main transition [70]. This new phase is termed 'liquid-ordered', L_o. It is fluid, characterised by lateral fluid disorder such as in the L_α phase, but exhibits larger conformational order of the lipid hydrocarbon tails. In this context, the L_α state is also termed 'liquid-disordered' phase L_d. According to current knowledge, lipid rafts are associated with liquid-ordered domains.

[7] In general, 'β' represents the fact, that the bilayer is in a gel phase, and the prime denotes a tilting of the hydrocarbon chains with respect to the bilayer normal.

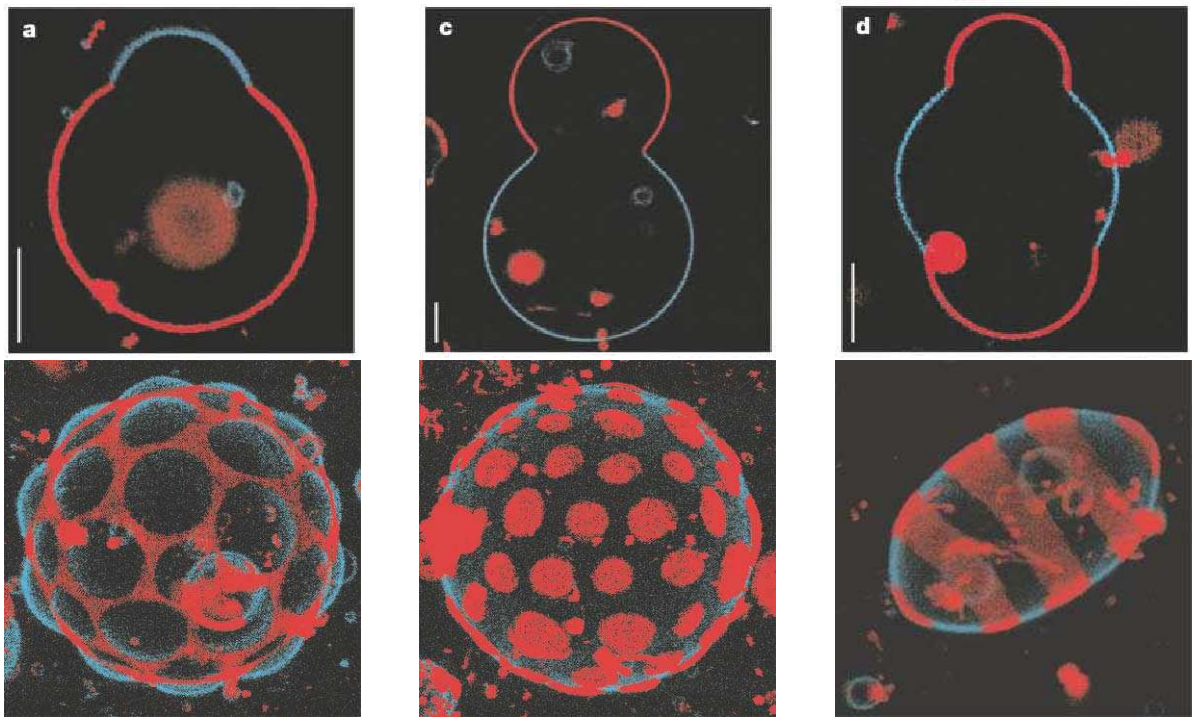

Figure 1.7: Coexisting fluid domains in a vesicle formed by a mixture of DOPC (dioleoyl-phosphatidylcholine)/sphingomyelin/cholesterol obtained by optical microscopy. Liquid-ordered domains (L_o) are labelled blue, liquid-disordered domains (L_d) domains red; in the top row images of equatorial sections of the vesicles are shown, the vesicles have rotation symmetry with respect to an axis in the vertical direction within the image plane; scale bars $5\mu m$; from [67].

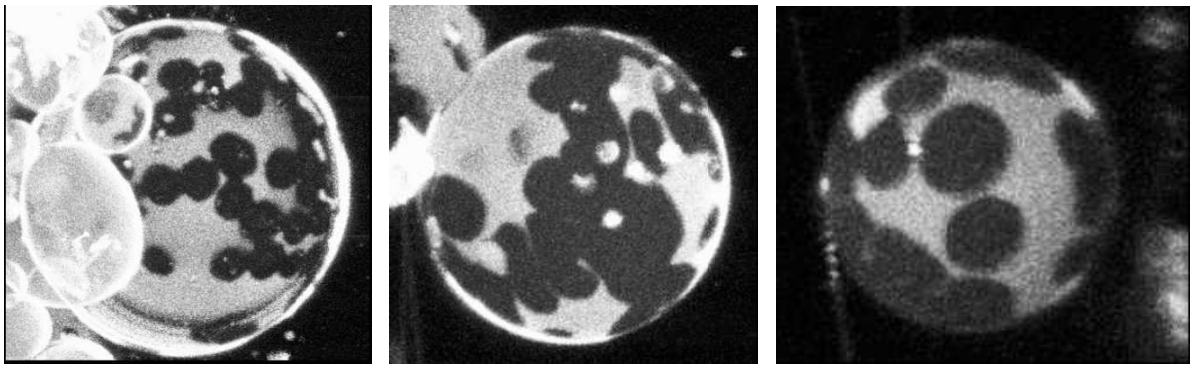

Figure 1.8: Vesicles composed of a mixture of DPPC (dipalmitoyl-phosphatidylcholine)/DPPE (dipalmitoyl-phosphoethanolamine) lipids grow domains in the L_β phase: the gel domains are predominantly round. The gel phase can be observed as dark areas on the vesicle membrane; from [71].

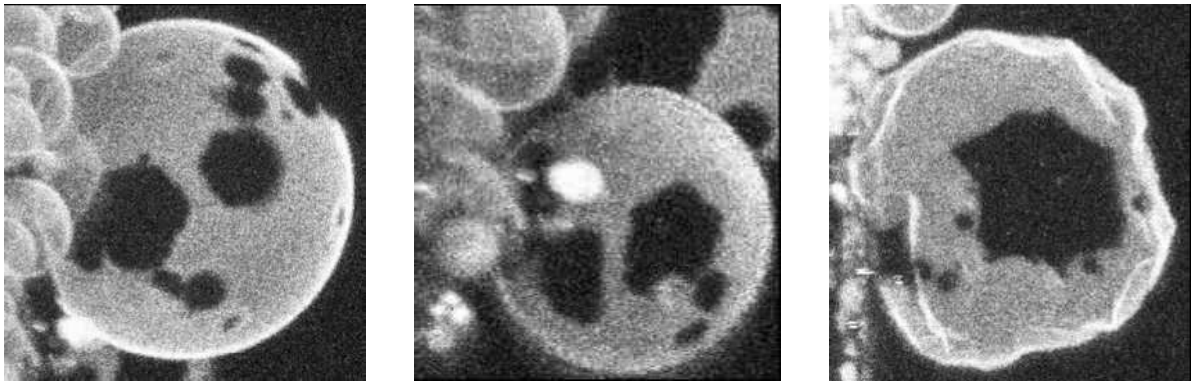

Figure 1.9: Vesicles made of a mixture of DPPC (dipalmitoyl-phosphatidylcholine)/DPPS (dipalmitoyl-phosphatidylserine) lipids with domains in the $L_{\beta'}$ phase: the gel domains have polygonal and hexagonal shape; from [71].

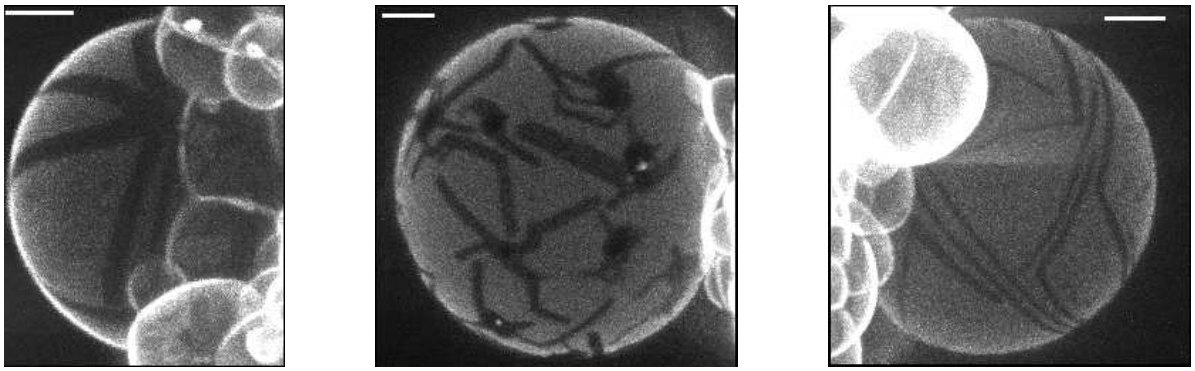

Figure 1.10: Vesicles with domains in the $P_{\beta'}$ (ripple) phase: the gel domains have stripe shape; from [72].

1.4 Fluid and solid membrane domains

When a vesicle is prepared at appropriate conditions so that different phases coexist, its membrane components segregate and form domains. Fig. 1.7 - Fig. 1.10 display examples of the resulting vesicle shapes which have been obtained by optical microscopy. Vesicles are shown with coexisting fluid-fluid membrane domains (Fig. 1.7) as well as with coexisting solid-fluid domains (Fig. 1.8 - Fig. 1.10). The morphologies of the vesicle and the fluid and solid domains differ considerably and depend on the structure of the membrane phases. We summarise the main experimental observations:

Fluid domains are predominantly circular (see Fig. 1.7). They tend, quite generally, to bulge and form buds. Besides vesicles with two coexisting domains, one in each phase, vesicles with several cap domains are observed. At temperatures closer to the mixing/demixing temperature, there are also vesicle-spanning ring domains. The domains are not static but diffuse around. When two smaller fluid domains collide, they coalesce and continuously merge into a larger circular domain. In vesicles with budding domains the fusion step sometimes seems to be impeded. Budding domains tend to repel each other upon approach, avoiding high curvature build-up of the membrane between [67, 73].

The shapes of solid domains are different to the shape of fluid domains and more intricate, see Fig. 1.8 - Fig. 1.10 [71, 72, 74–78]. The observed domain morphologies seem to be correlated with the structure or lipid packing of the gel phase [71, 78].

In the lipid composition of Fig. 1.8, which is believed to exhibit L_β-L_α coexistence, small, round conformations of gel-domains are observed which float in the fluid vesicle membrane [71]. Contrary to fluid domains, these gel domains do not deform or rearrange upon contact, which is due to the slow diffusion constant of the molecules in the gel phase. Sometimes, they are found to adhere to one another and form morphologies which resemble two-dimensional dumbbells, or more complicated shapes if more than two domains cluster. Since many shapes show round morphologies, the underlying phase is expected to be isotropic on the length scale of micrometers.

Solid domains in the $L_{\beta'}$ phase are polygonal in shape [71]. At optical resolution, they show straight edges and sharp corners (see Fig. 1.9). Many of the domains are hexagonal. The angles of the polygons appear to be quantised close to $2\pi/3$ respectively $2\pi/6$, reflecting the angles of the underlying orthorhombic (nearly hexagonal) lattice. It is assumed that in the $L_{\beta'}$ phase the tilting of the molecules promotes a longer ranged positional order compared to the previous L_β phase.

In the $P_{\beta'}$ gel phase, preferentially domains with stripe morphology are observed (see Fig. 1.10) [72]. During growth, the stripes grow longitudinally, increasing in length while their width remains constant. Within each vesicle, the stripes are found to be quite monodisperse in width. It is conjectured that the strong anisotropy is due to the directional anisotropy of the ripple phase [72].

It should be mentioned that for all the different gel-domain morphologies the domain shapes are to a certain extent history-dependent and seem to be influenced by nucleation and growth processes. As a consequence, the observed morphologies may be non-equilibrium in nature.

The objective of the second and third part of this dissertation is to provide a theoretical analysis of the morphology of vesicles with coexisting solid-fluid and fluid-fluid membrane domains, respectively.

1.5 Outline of the thesis

The present thesis is organised as follows. It consists of three parts. The first part, including chapter 3, is concerned with homogeneous vesicles. The second and third part, including chapter 4 and 5, investigates properties of inhomogeneous vesicles with solid and fluid membrane domains.

The thesis starts with a short presentation on foundations. In chapter 2 we introduce models for a mesoscopic description of fluid and crystalline membranes which are applied for the vesicle membrane later on.

Chapter 3 is concerned with statistical properties of fluid vesicles with geometries close to a sphere. The focus is on the transition between vesicles with prolate and oblate shape which is induced by thermal fluctuations. We determine the free energy landscape of unconstrained vesicles and of vesicles whose volume is fixed.

In chapter 4 we study the morphology of fluid vesicles with solid membrane domains. We consider the limit where the solid membrane cannot undergo stretching deformations. The equilibrium shapes of minimum energy are determined for a fluid vesicle with one or several solid domains for various material parameters. Vesicles which can change their volume and

vesicles with fixed volume, in particular vesicles with almost spherical geometry, are discussed. We observe morphological transitions between vesicles with different domain shapes as the material parameters change. The impact of thermal fluctuations on the domain shapes is analysed.

Chapter 5 is dedicated to vesicles with coexisting fluid membrane domains. Analogous to solid domains we calculate the equilibrium shapes of vesicles with simple and complex domain topology. The emphasis is on vesicles with a comparably small line tension at the domain boundary. As material parameters are varied, morphological transition between vesicles with different domain shapes are observed.

The thesis closes with general conclusions. A short outlook is given.

Throughout the thesis, the vesicle membrane is modelled on a mesoscopic level as a static or fluctuating geometric surface.

Chapter 2

Membranes - models and methods

In this chapter, continuum and discrete models for membranes with different types of internal order are presented. These models are applied later on in the thesis to describe fluid and crystalline phases of lipid bilayers. We give a brief account of known results of their statistical mechanics.

2.1 Introduction

In this chapter we introduce models for isotropic elastic membranes which are used in this thesis to describe the different phases of the vesicle membrane. Membranes such as lipid bilayers can be modelled on a mesoscopic level as self-avoiding geometric surfaces [8, 79, 80]. At zero temperature, these surfaces acquire a state of minimum energy and can be regarded as static, whereas at finite temperatures they are subject to thermal fluctuations and undulate. The statistical mechanics of membranes is rather complex because membranes can undergo phase transitions and exist in different states with different types of internal order. Although thermal fluctuations act to destroy any conventional true long-range order in a two-dimensional system with a continuous symmetry [81], membranes may exhibit longer-ranged order where the correlations in the order parameter decay slowly in an algebraic manner. Such longer-ranged order is commonly termed quasi-long-range (QLR) order. The shape and the fluctuation spectra of membranes crucially depend on their internal structure.

Which types of order generically exist for a homogeneous, isotropic membrane? For a thin planar layer of an isotropic material, which effectively constitutes a quasi two-dimensional system, the generic phases are a crystalline or solid phase with QLR positional order at low temperatures and a disordered fluid phase at higher temperatures. In a two-dimensional system the transition between the solid and liquid state does not necessarily have to be of first order, but it may also occur via two distinct continuous transitions [82]. This gives rise to an intermediate phase, the hexatic phase. The hexatic phase is characterised by the translational disorder of a fluid but – and this is reminiscent of the crystalline phase – exhibits QLR correlations in the orientation of bonds connecting neighbouring particles (bond orientational order). It is a unique two-dimensional feature and results from the interplay of thermal fluctuations and defects in the melting process of a two-dimensional system.

Membranes are more complex than flat layers. They are not confined to two dimensions, but undulate and can bend or buckle into the transversal third direction. This out-of-plane buckling significantly lowers the energies of the conventional in-plane topological defects, which therefore

can be initiated more easily by thermal fluctuations. Thermal fluctuations in combination with membrane undulations may cause disruptions of the internal membrane structure. As a matter of fact, certain defects (dislocations) will be present even at low temperatures in a very large membrane, which can fluctuate freely and which is not stabilised by covalent bonds. Viewed on a sufficiently large length scale, the generic low temperature phase of a fluctuating membrane is therefore not crystalline, but hexatic.

In the present chapter, we concentrate on two different classes of membranes which will be relevant in this thesis. First, we consider a model for fluid membranes, which are characterised by short-range translational and orientational order. This membrane model is used to describe the fluid phases of lipid bilayers, the L_α phase in homogeneous lipid bilayers and the liquid ordered L_o and liquid disordered L_d phase in bilayers with lipid-cholesterol mixtures. The second membrane model considered are crystalline membranes with QLR translational and long-range orientational order whose internal order is not affected by thermal fluctuations. Due to their fixed internal connectivity, they are also called tethered or polymerised membranes. This model has been originally devised to describe membranes where the internal structure is guaranteed by strong (covalent) bonds between the membrane molecules. However, if thermally induced rearrangements of the internal structure can be neglected, it can also be applied to membranes which are held together by weaker (van der Waals) forces as in the case of gel and solid phases of lipid bilayers. This should be valid on length scales below a translational correlation length ξ_T which corresponds to the typical separation distance between free dislocations in the membrane. Using this membrane model is justified as in our studies we do not consider defects.

Due to fluctuations the crystalline order is destroyed on large length scales, which results in a membrane with hexatic order. The hexatic membrane exhibits short-range translational order but QLR orientational order. For sake of completeness, we briefly touch hexatic membranes at the end of this chapter, a short discussion of their properties is given in the appendix C.1.

The membranes are modelled on a mesoscopic level as static or fluctuating geometric surfaces with appropriate elastic energies for their conformation, in accordance with their internal structure [1]. The membranes investigated are not subject to any external forces or constraints, but undulate freely. We consider thermal equilibrium throughout. Aspects of the presented material can be found in a number of reviews [79, 80, 83, 86–93].

2.2 Fluid membranes

Fluid membranes are soft sheets that behave as quasi two-dimensional fluids which resist bending. A canonical example is given by the lipid bilayer in the fluid phase. The word 'fluid' emphasises that the individual membrane molecules are free to move laterally within the plane of the membrane. It is this fluidity which allows the membrane to adapt itself to any particular

[1] Field theories of fluctuating geometric objects such as the surface models for bilayer membranes are a common and widespread theme in theoretical physics, with applications in many different areas of physics [83]. In the realm of soft condensed matter, one considers thermally undulating, low-dimensional manifolds: fluctuating lines describe the conformational properties of linear polymers, flexible surfaces are used to describe interfaces and membranes on mesoscopic length scales [84]. The currently most promising attempts for a unified theory of all known fundamental forces or interactions (gravity, electroweak and strong interaction) are based on (quantum mechanically) fluctuating geometric objects, one-dimensional manifolds (strings) and corresponding higher dimensional objects (branes) [83, 85].

shape and to undergo remarkable morphological changes. In a fluid membrane, there is no low-frequency response to shear stress. However, a fluid membrane behaves differently to a fluid film because it involves energy to deform or bend it from its preferred curvature state. This is because bending of the membrane causes splay of the molecules. The bending modes are soft, involving energies in the order of the thermal energy. A fluid membrane is characterised by a rather high compressibility modulus. Therefore, it can be considered to some extent as incompressible. This implies that the membrane area is essentially determined by the number of constituent molecules.

Given these main physical properties, fluid membranes can be modelled on a mesoscopic length scale as flexible surfaces with a fixed area whose shape and fluctuations are controlled primarily by bending (or curvature) elasticity.

2.2.1 Continuum model

The membrane is considered as a two-dimensional surface embedded in three-dimensional Euclidean space $\mathbb{R}^3$. The membrane surface is parametrised by a suitable set of the coordinates $\xi = (\xi^1, \xi^2) \in \mathbb{R}^2$, its position is given by the vector function $\mathbf{X}(\xi^1, \xi^2) \in \mathbb{R}^3$.

The free energy or Hamiltonian of a specific membrane configuration depends on geometric quantities of its embedding. Due to the membrane's fluidity the free energy has to be invariant under a reparametrisation of the surface, i.e. under a change of the coordinate system $\xi^a \to \xi'^a(\xi^1, \xi^2)$. Since the energy has to be invariant under translations and rotations of the whole membrane, only scalars containing derivatives of the position vector $\mathbf{X}$ should contribute to the membrane energy.

The most general free energy up to quadratic order in the curvature which respects these symmetries reads

$$\mathcal{H}_{\text{fluid}}(\mathbf{X}(\xi)) = \int d^2\xi \sqrt{g} \left(\sigma + \frac{\kappa}{2} (2H - C_0)^2 + \kappa_G K \right) . \tag{2.1}$$

The integral extends over the membrane area, $dA = d^2\xi\sqrt{g}$, where g is the determinant of the induced metric $g_{\mu\nu} = \partial_\mu \mathbf{X} \cdot \partial_\nu \mathbf{X}$ (see appendix A.1). The functional, Eq. (2.1), equals the Canham-Helfrich Hamiltonian which has been encountered in Eq. (1.1), extended with a term proportional to the surface area. The expressions in this energy are geometric quantities, the mean curvature H and the Gaussian curvature K (see appendix A.1 for a definition), and material parameters, the bending rigidity κ, the Gaussian bending rigidity (or saddle splay modulus) κ_G and the spontaneous curvature C_0. The bending rigidity κ quantifies the energetic costs of bending deformations. For a phospholipid bilayer, its value is typically in the order of 10-20 T_0 [20]. The Gaussian bending rigidity κ_G is associated with the energetic costs related to deformations which change the topology of the membrane. Recent measurements give an estimate of $\kappa_G \sim -0.8\kappa$ [59]. For homogeneous membranes the integral over the Gaussian curvature is a topological invariant (Gauss-Bonnet theorem). Therefore, contributions from the Gaussian curvature can be neglected when membrane deformations which alter the topology are not possible. The spontaneous curvature C_0 describes a possible preferred curvature of the membrane.

The interpretation of the parameter σ, which is conjugate to the (microscopic) membrane area, gives rise to conceptual problems [94]. In the context of interfaces, it is commonly referred to as a surface tension. In the context of fluctuating membranes, it is more appropriate to regard σ not as a surface tension, but rather as a chemical potential for the addition of

new surfactant molecules to the membrane. The term surface tension – as will become clearer further below – should be attributed to the parameter conjugated to the coarse-grained, projected area [94, 95].

In the following we are interested in the statistics of the membrane in thermal equilibrium at temperature T. An important quantity is given by the canonical partition function $\mathcal{Z}(T)$. It is defined as the phase-space integral over all microstates that are accessible to the system, weighted with the Boltzmann factor $e^{-\mathcal{H}/T}$ ($\mathcal{H}$ stands for the energy of the microstate) [2]. The canonical partition function $\mathcal{Z}(T)$ is related to the free energy $F(T)$ via

$$F(T) = -T \ln \mathcal{Z}(T) \,. \tag{2.2}$$

For fluid membranes the partition function can be written as a functional integral and reads

$$\mathcal{Z}(T) = \int \mathcal{D}\{\mathbf{X}(\xi)\}\, e^{-\mathcal{H}_{\text{fluid}}(\mathbf{X}(\xi))/T} \,, \tag{2.3}$$

where the integral covers all different shapes of the membrane. With Eq. (2.3) a few comments have to be made:

First, since any continuum theory starts to loose its validity at some short-distance scale, the functional integral has to be supplemented with some short distance cut-off for the undulation modes. This length scale represents the minimal wave length possible for any shape deformations and is in the order or slightly above the thickness of the membrane.

Second, the measure $\mathcal{D}\{\mathbf{X}(\xi)\}$ deserves some care because of the reparametrisation symmetry of the integrand [96]. Apparently, the result of Eq. (2.3) should not depend on the chosen parametrisation of the integrated membrane surfaces. One has to be careful when evaluating the functional integral, Eq. (2.3), because the integral should not extend over all different embedding functions $\mathbf{X}(\xi)$, but only over embedding functions which describe physically different membrane configurations. Different embedding functions which are related via a reparametrisation transformation must be counted only once. How this can be accomplished at least formally is briefly sketched in appendix B.1.

Scale dependence of elastic parameters

A popular strategy in statistical mechanics to learn about a system which cannot be solved analytically is provided by the renormalisation procedure: by iteratively thinning out degrees of freedom in the partition function on smaller length scales one arrives at effective interactions on larger length scales. As a result of this coarse-graining the coupling parameters have to be adapted and depend on the length scale of interest.

In membranes thermal fluctuations become evident through the scale dependence of elastic coefficients. The effects of fluctuations on shorter length scales can be expressed in renormalised elastic parameters on larger length scales. If one traces in Eq. (2.3) over the short-distance modes with wavenumber q in a shell $2\pi/q_0 < 2\pi/q < 2\pi/q_l$ above the wavelength $\Lambda_0 = 2\pi/q_0$ (this can be done in a perturbative expansion), one finds for the renormalised bending stiffness $\kappa(q_l)$ a scale-dependence of the form [97, 98]

$$\kappa(q_l) = \kappa(q_0) + \frac{3}{4\pi} T \ln(q_l/q_0) + \dots \,. \tag{2.4}$$

[2] Throughout the thesis, the temperature T is expressed in energy units so that the Boltzmann constant k_B is contained in T.

The bending stiffness decreases when viewed on larger length scales and becomes ineffective beyond a 'persistence length'

$$\xi_p \simeq e^{4\pi\,\kappa/(3T)}\,. \tag{2.5}$$

The persistence length ξ_p is a correlation length associated with the order in the local normals $\mathbf{n}$ to the surface. It defines the length scale beyond which the orientations of the membrane between two positions $\mathbf{r}_1$ and $\mathbf{r}_2$ become decorrelated

$$\langle \mathbf{n}(\mathbf{r}_1)\cdot\mathbf{n}(\mathbf{r}_2)\rangle \simeq e^{-|\mathbf{r}_1-\mathbf{r}_2|/\xi_p}\,. \tag{2.6}$$

The persistence length separates two different regimes of the membrane: For a membrane patch much smaller than the persistence length, the fluctuations of the normal vector around the average orientation are small. The membrane exhibits pronounced undulations on this scale, but globally it looks almost planar. This regime applies to membrane parts of a vesicle. At room temperature, the persistence length of phospholipid bilayers is usually orders of magnitude larger than the size of the vesicle. Membrane undulations relevant on the length scales of vesicles are investigated in more detail in the next subsection.

Membrane patches, on the contrary, which are much larger than the persistence length have a wildly fluctuating normal vector and appear crumpled. For fluid membranes, the persistence length is finite, albeit large, at nonzero temperature. Thus, on large enough scales they are expected to be crumpled. Since for phospholipid bilayers at ambient temperature the persistence length by far exceeds the size of the vesicle, we do not consider fluctuations on this length scale any further.

In the considerations so far it has been neglected that real membranes cannot self-intersect. Self-avoidance plays a role when parts of the membrane come close to each other. This typically occurs on length scales beyond the persistence length where the membrane is crumpled and folds back. In fact, self-avoidance may prevent crumpling and act to stabilise the membrane. Self-avoidance is difficult to treat theoretically, because interactions, although local in the embedding physical space, are highly nonlocal in the coordinates that parametrise the membrane. Apart from simulation studies, no real satisfactory theoretical treatment for interacting self-avoiding fluid membranes exists.

Thermal fluctuations do not only renormalise the bending rigidity, but also amount in entropic corrections to the surface tension and the Gaussian bending rigidity, respectively [94]. Fluctuations tend to decrease the effective (or projected) area of the membrane. As a consequence, the effective surface tension, in terms of this projected area, gets positive contributions. The membrane develops a stretching elasticity which is entropic in nature. This stretching elasticity arises from the suppression of fluctuations as the membrane is stretched out.

Fluctuations around a flat state

Fluctuating membranes with finite bending stiffness exhibit undulations on a broad range of length scales. They are locally smooth, rough on intermediate scales and crumpled on large length scales. In the following we consider membrane undulations relevant on length scales of the size of the vesicle in more detail. In this regime fluctuations do not deviate too strongly from a planar reference plane and we can use the Monge gauge to describe the membrane surface. As long as there are no overhangs, the membrane configuration can be described by

its deviation from a flat plane

$$\mathbf{X}(x) = \mathbf{X}(x_1, x_2) = \begin{pmatrix} x_1 \\ x_2 \\ h(x_1, x_2) \end{pmatrix} . \tag{2.7}$$

The coordinates $x = (x_1, x_2)$ are Cartesian coordinates on a flat reference plane, and $h(x) = h(x_1, x_2)$ is a single valued function which measures the distance from this reference plane in the orthogonal direction.

We start with the assumption that the membrane deviations are small so that an expansion in powers of $|\nabla h(x)|$ can be justified. In this case the Canham-Helfrich-Hamiltonian simplifies considerably. Omitting contributions from the spontaneous and Gaussian curvature and neglecting the surface tension one gets

$$\mathcal{H}_{\text{fluid}}(h(x)) \simeq \frac{1}{2}\kappa \int dx \left(\nabla^2 h(x)\right)^2 . \tag{2.8}$$

With this, one can calculate the fluctuation spectrum of the undulation modes and the correlation of lateral height fluctuations [80]. For a tensionless fluid membrane, one obtains for the correlation between position $\mathbf{r}_1$ and $\mathbf{r}_2$ [84]

$$\langle |h(\mathbf{r}_1) - h(\mathbf{r}_2)|^2 \rangle \sim |\mathbf{r}_1 - \mathbf{r}_2|^{2\zeta} , \qquad \text{with} \qquad \zeta = 1 . \tag{2.9}$$

The character of the shape undulations is quantified by the roughness exponent ζ which is $\zeta = 1$ for a fluid membrane. Its power-law form implies that the membrane undulations are scale-invariant. This scaling relation of the correlation function holds on intermediate length scales, $a \ll L_{\|} \ll \xi_p$ (where a is a typical molecular dimension).

2.2.2 Discrete model

In order to perform numerical calculations or simulations one needs a discrete membrane model. Various computational approaches and techniques have been devised, which consider different levels of microscopic details. The approaches include full atomistic simulations, which describe the individual membrane molecules with chemical accuracy [99], coarse-grained techniques, where some of the molecular degrees of freedom are integrated out and effective membrane particles with effective interactions are considered [92, 93], and mesoscopic approaches, which start from a continuum membrane model and discretise the membrane surface [79]. Microscopical detailed models are limited to small length and time scales and do not allow to address membrane properties on the size of a micron-sized vesicle. For the numerical work in this thesis we therefore apply a triangulated membrane surface. At zero temperature, the triangulated surface is static and acquires a conformation with minimum energy. If thermal fluctuations are included and the surface is fluctuating, this leads to the so-called tether and bead model [79].

Tether and bead model

A simple and well established method, appropriate for mesoscopic length scales, is provided by triangulated surface models [79]. They have originally been developed in a different context for discrete models in quantum gravity [100–102]. The smooth membrane surface

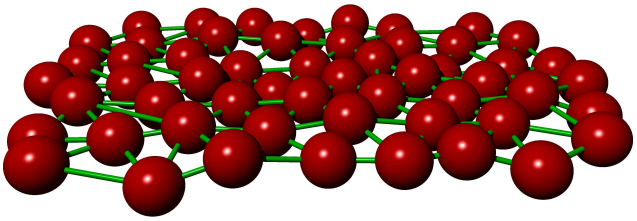

Figure 2.1: Tether and bead model: The continuous membrane surface is triangulated and replaced by a mesh of hard spheres. To assure the stability of the membrane the beads are connected by tethers. Dynamic triangulation of the tether network guarantees fluidity of the membrane.

is triangulated and approximated by an inscribed mesh of N_v interconnected vertices, see Fig. 2.1. The configuration of the membrane is specified by the triangulation $\mathcal{T}_{N_v} = (\{\mathbf{X}_i\}, S)$ $(i = 1, \ldots, N_v)$. The vector $\mathbf{X}_i$ denotes the position vector of the i^{th} vertex, and S is the adjacency matrix which contains nearest-neighbour vertex pairs, $S_{ij} = 1$ or 0 according to whether $\mathbf{X}_i$ and $\mathbf{X}_j$ are connected by a 'tether' ('bond') or not. The stability of the membrane is accomplished by a tethering potential $V_{ij}(r)$, which acts between tethered nearest neighbour vertices i and j, and which in the simplest case is given by

$$V_{ij}(r) = \begin{cases} 0 & \text{if} \quad r < l_0 \\ \infty & \text{otherwise} \end{cases} , \tag{2.10}$$

with $r = |\mathbf{X}_i - \mathbf{X}_j|$. The potential $V_{ij}(r)$ ensures that the distance between nearest neighbours is less than l_0. In order to guarantee self-avoidance of the membrane, one usually places at each vertex a hard sphere. A discretised membrane surface with hard spheres at the vertices is illustrated in Fig. 2.1. The diameter σ_0 of the hard spheres is chosen such that they cannot pass through the network mesh. The potential $V_{ij}(r)$ is augmented by

$$V_{\text{HS}}(r) = \begin{cases} \infty & \text{if} \quad r < \sigma_0 \\ 0 & \text{otherwise} \end{cases} , \tag{2.11}$$

which acts between all beads. Self-avoidance requires that $l_0 < \sqrt{3}\sigma_0$.

Once the membrane surface is suitably triangulated, appropriate terms for the involved energies have to be found. A general introduction to methods for discretising differential operators on triangulated random surfaces is given in [103]. As an apparent need one requires that in the limit of an infinitesimal triangulation the values of the continuum limit are reproducible. It turns out that the discretisation of the bending energy is quite subtle and not straightforward [104]. Some aspects of the occurring difficulties are recollected in the appendix A.2. In this thesis we apply a discretisation of the bending energy which is based on the square of the local average of the discretised mean curvature around a vertex as it is proposed in [105]. For a membrane patch with vertices v_i, the bending energy in Eq. (2.1) is approximated by a sum over the vertices v_i (see appendix A.2)

$$\mathcal{H}_{\text{fluid, bend}} = \sum_{v_i} \left(\frac{\kappa}{2} \frac{\left(\sum_{e_j} \frac{1}{2} l_j \phi_j - C_0 \bar{A}_i \right)^2}{\bar{A}_i} + \kappa_G \frac{2\pi - \sum_{f_j} \alpha_j}{\frac{3}{2}\bar{A}_i - \frac{1}{8}\sum_{f_j} \operatorname{cotg}(\alpha_j) \bar{l}_j^2} \right)_i . \tag{2.12}$$

Figure 2.2: Dynamic triangulation: In a bond flip the common edge between two neighbouring triangles is cut and re-attached in such a way that the formerly unconnected vertices are connected.

The first term in Eq. (2.12) describes the elastic bending energy. The inner sum extends over all edges e_j which are connected to the vertex v_i. The length of the edge e_j is denoted with l_j, ϕ_j is the tilting angle between the neighbouring triangles that share the edge e_j. The area $\bar{A}_i$ is the area associated to the vertex v_i. It is given by one third of the sum of the areas A_j of the adjacent triangles f_j, $\bar{A}_i = \sum_{f_j} \frac{1}{3} A_j$ where A_j is the area of the triangle f_j. The second term is the discretisation of the Gaussian bending energy. The Gaussian curvature at vertex v_i is proportional to the deficit angle of the vertex v_i to 2π, i.e. $(2\pi - \sum_{f_j} \alpha_j)_i$, where the sum goes over all triangles f_j adjacent to v_i and α_j is the angle of f_j which is incident to the vertex v_i. $\bar{l}_j$ is the length of edge opposed to the angle α_j in triangle f_j [106].

In the continuum model the fluidity of the membrane is reflected by the reparametrisation invariance of the free energy functional. Apparently, one also has to account for the fluidity of the membrane in the discrete model. In order to allow for the lateral diffusion of the membrane molecules, in the simulations with a triangulated surface the triangulation is therefore not kept fixed, but varies dynamically. The partition function, Eq. (2.3), is realised by an integration over different embeddings $\mathbf{X}_i$ and a sum over different triangulations S [100]

$$\mathcal{Z}_{\mathcal{T}_{N_v}}(T) = \int \Pi_{i=1}^{N_v} d\mathbf{X}_i \sum_S e^{-\mathcal{H}(\mathcal{T}_{N_v})/T} \,. \tag{2.13}$$

Monte Carlo simulations

In this dissertation, thermal averages of membrane observables are evaluated with the help of Monte Carlo simulations. Monte Carlo simulations are stochastic techniques which generate an appropriate random set of microstates of the phase space (i.e. different membrane configurations) according to a desired probability distribution. In the canonical ensemble this is the Boltzmann distribution. Thermal averages of the physical properties of interest are then estimated as averages over a representative sequence of microstates (see appendix D.1).

Most frequently, trajectories through phase space are obtained via a Markov process which has the desired probability density as its limiting equilibrium distribution. A Markov process is a 'memoryless' stochastic process, where only the knowledge of the current state, but not of previous states is relevant for determining the subsequent state. The evolution of states is specified by the probability $\rho(x, x')$ which is the conditional probability that the system goes from the microstate x to the state x'. Provided that the Markov process is ergodic (i.e. every microstate can be reached from every other microstate in a finite number of transition steps), a sufficient condition that the sequence of microstates asymptotically converges towards the desired equilibrium distribution is given by the detailed balance or microscopic reversibility condition

$$\rho(x, x')p(x) = \rho(x', x)p(x') \,. \tag{2.14}$$

Here, $p(x)$ is the probability density that the system is in the state x. Usually, the transition probability $\rho(x, x')$ is factorised into two parts,

$$\rho(x, x') \equiv g(x, x')\, p_{\mathrm{acc}}(x, x')\,. \tag{2.15}$$

It consists of the selection function $g(x, x')$, which is the conditional probability that a new 'trial' state x' is proposed given that the current state is x, and the acceptance probability $p_{\mathrm{acc}}(x, x')$, which gives the conditional probability that the proposed move is accepted. In our simulations we employ the Metropolis algorithm (see appendix D.1) and use a symmetric selection function, i.e. $g(x, x') = g(x', x)$. In this case, the acceptance probability is given by

$$p_{\mathrm{acc}}(x, x') = \min[1, e^{-(E(x')-E(x))/T}]\,, \tag{2.16}$$

where $E(x)$ and $E(x')$ are the energy of state x and x', respectively. In practice, an important step in the implementation of a Monte Carlo algorithm is the choice of the selection function, or proposed Monte Carlo 'moves'.

In the simulations of fluid membranes, the attempted Monte Carlo moves consist of two different classes:

First, there are vertex moves, the positions of the vertices $\mathbf{X}_i$ are randomly displaced within a cube of size $[-\Delta x, \Delta x]^3$ centred at their former position. This corresponds to performing the integral over $\mathbf{X}_i$ in Eq. (2.13). By varying Δx the acceptance rate can be adjusted.

Second, there are bond moves where the connectivity matrix S is changed by a local bond flip (dynamic triangulation). The bond or edge flip proceeds as follows (cf. Fig. 2.2): Two neighbouring triangles, which are defined by four vertices, share a common edge. In an edge flip this common edge is cut and re-attached in such a way that it connects the formerly unconnected vertices. It can be shown that the bond flip moves are ergodic, i.e. every triangulation can be transformed by a finite sequence of local-bond flips into any other with the same number of vertices [107] [3]. By this dynamic triangulation, the sum over all possible triangulations S in Eq. (2.13) is realised.

2.3 Crystalline membranes

Crystalline membranes, sometimes also termed tethered or polymerised membranes, are membranes with a fixed internal connectivity between neighbouring membrane molecules. They exhibit in-plane QLR positional and true long-range orientational order. Tethered membranes occur naturally in a biological context, examples are the triangulated protein network given by the spectrin skeleton in red blood cell membranes. They can also be made artificially, such as polymerised amphiphilic bilayers or thin inorganic sheets of graphite oxide in aqueous suspension.

In principle, crystalline membranes with a fixed internal structure have to be distinguished from crystalline membranes like the solid or gel phases of lipid bilayers. There, the bilayers are held together by weaker, van der Waals forces. Major distortions or even disruptions of the crystalline order may occur in principle. Thermally induced rearrangements of the in-plane structure are not possible in a polymerised membrane due to strong covalent forces between the membrane molecules. However, in cases where severe rearrangements of the internal membrane

[3] The proof in [107] considers an arbitrary triangulation and neglects implications of the tether and bead model, the finite size of the hard spheres at the vertices and a finite tether length.

structure can be neglected, the elastic energies derived for crystalline-tethered membranes apply equally well to the crystalline phase of lipid bilayers. This is the case on length scales below a translational correlation length ξ_T. This length scale is set by the typical distance of thermally induced defects. Since for the gel phases of lipid bilayers we neglect defects as a first approximation, we employ this model.

Crystalline membranes have, in contrast to fluid membranes, a preferred in-plane ground-state which is associated with the unperturbed crystalline lattice. Deviations from this ground state are suppressed by in-plane elastic energies. The properties of crystalline membranes are governed by the coupling of in-plane elastic deformations (stretching and shearing) and of out-of-plane deformations (bending).

2.3.1 Continuum model

In a continuum description the positions of the individual membrane molecules $\mathbf{X}_i$ of the crystalline lattice are replaced by a coarse-grained coordinate vector $\mathbf{X}(\xi)$, which is a function of the continuous internal coordinate $\xi = (\xi^1, \xi^2)$. Deformations from the reference frame associated with the unperturbed lattice are described by the displacement vector field $\mathbf{u}(\xi)$. This vector field maps the coordinates of the undeformed state $\mathbf{X}(\xi)$ to the positions of the deformed media $\mathbf{X}(\xi) + \mathbf{u}(\xi)$.

If the membrane is stretched or sheared, the distance between two neighbouring points changes. The change is expressed by the strain tensor $u_{\mu\nu}(\xi)$, which is defined as the difference of the metric tensor $g_{\mu\nu}(\xi)$ of the deformed state from the metric tensor $g^0_{\mu\nu}(\xi)$ of the undeformed state

$$u_{\mu\nu}(\xi) = \frac{1}{2}\left(g_{\mu\nu}(\xi) - g^0_{\mu\nu}(\xi)\right) . \tag{2.17}$$

The mixed strain tensor $u^\nu_\mu(\xi)$ is obtained by raising one of the indices according to [4]

$$u^\nu_\mu(\xi) = u_{\mu\lambda}(\xi)\, g^{\lambda\nu}(\xi) , \tag{2.18}$$

where $g^{\lambda\nu}(\xi)$ is the dual metric tensor, see appendix A.1. With this, we are prepared to write down the deformation energy of an isotropic, two-dimensional material, following the elasticity theory of thin elastic sheets [58]

$$\begin{aligned}\mathcal{H}_{\text{cryst}}(\mathbf{X}(\xi)) = &\int d^2\xi \sqrt{g^0}\left(\frac{\kappa}{2}\left(2H - C_0\right)^2 + \kappa_G K\right) \\ &+ \int d^2\xi \sqrt{g^0}\left(\frac{1}{2} k_a u^\nu_\mu(\xi) u^\mu_\nu(\xi) + k_b\, \left(u^\mu_\mu(\xi)\right)^2\right) .\end{aligned} \tag{2.19}$$

This free energy or Hamiltonian includes a Helfrich-type bending energy, expressed by the first term, which penalises out-of-plane deformations, as well as an in-plane elastic energy, expressed by the second term, which penalises stretching and shearing deformations. Eq. (2.19) is invariant under translations and rotations of the membrane in the embedding space $\mathbb{R}^3$. The stretching energy is quadratic in the strain, it contains the trace of the square of the strain tensor $u^\nu_\mu(\xi) u^\mu_\nu(\xi)$ and the square of the trace of the strain tensor $(u^\mu_\mu(\xi))^2$. The stretching energy is a function of the metric tensor and thus depends on the intrinsic geometry of the membrane. This form of the stretching energy is assumed to be valid for small deformations. k_a and k_b are elastic moduli called Lamè coefficients, k_a is also referred to as the shear modulus.

[4] Here and below, Einstein's summation convention over repeated indices is implied.

Given the statistical weight for a specific membrane conformation, one can write down the partition function as the integral over all different embedding functions $\mathbf{X}(\xi)$ [5]

$$\mathcal{Z}(T) = \int \mathcal{D}\{\mathbf{X}(\xi)\}\, e^{-\mathcal{H}_{\rm cryst}(\mathbf{X}(\xi))/T}\,. \tag{2.20}$$

Geometrically speaking, one has a fluctuating surface with a distinguished (reference) metric. In contrast to fluid membrane surfaces, the metric of the crystalline membrane surface fluctuates only slightly and locally because larger deviations from the preferred metric are punished by in-plane elastic energies.

Next, we explore the effects of thermal fluctuations. Since we are interested in membranes of the size of a mesoscopic vesicle, we consider an expansion around the flat state. Contrary to fluid membranes, such an expansion would be justified even for larger length scales because tethered membranes – when including self-avoidance – are expected to be not only flat at small or intermediate length scales, but remain flat, though rough, on all length scales.

Fluctuations around a flat state

We assume that the membrane at rest is flat and the reference metric $g^0_{\mu\nu}$ is proportional to the unit matrix $\delta_{\mu\nu}$. In order to describe fluctuations of the membrane with inner coordinates $x = (x_1, x_2)$ around a flat configuration, it is advantageous to use the representation

$$\mathbf{X}(x_1, x_2) = \begin{pmatrix} x_1 + u_1(x_1, x_2) \\ x_2 + u_2(x_1, x_2) \\ h(x_1, x_2) \end{pmatrix}\,. \tag{2.21}$$

In Eq. (2.21), $u_a(x_1, x_2)$ $(a = 1, 2)$ describe in-plane phonon displacements while $h(x_1, x_2)$ denotes out-of-plane distortions. Using this ansatz, the strain tensor $u_{\mu\nu}(x)$ reads

$$u_{\mu\nu}(x) = \frac{1}{2}\left(\partial_\mu u_\nu(x) + \partial_\nu u_\mu(x)\right) + \frac{1}{2}\left(\partial_\mu h(x)\right)\left(\partial_\nu h(x)\right) + \frac{1}{2}\left(\partial_\mu u_\lambda(x)\right)\left(\partial_\nu u_\lambda(x)\right)\,. \tag{2.22}$$

We assume zero spontaneous curvature and disregard effects from the Gaussian bending rigidity. Then, one obtains for the elastic energy in Eq. (2.19) (expanding to lowest order in $h(x)$ and its derivatives)

$$\mathcal{H}_{\rm cryst}(h(x), u_a(x)) = \frac{1}{2}\kappa \int d^2x \left(\nabla^2 h(x)\right)^2 + \frac{1}{2}\int d^2x \left(2k_a\, u^2_{\mu\nu}(x) + k_b\, u^2_{\lambda\lambda}(x)\right)\,. \tag{2.23}$$

To proceed, it is useful to reformulate Eq. (2.23) only in terms of out-of-plane undulations $h(x)$. To this end, one has to eliminate the in-plane displacement vectors $u_a(x)$ (or phonon modes) and calculate an effective free energy for the out-of-plane undulations

$$\mathcal{H}_{\rm cryst,eff}(h(x)) = -T \ln\left(\int \mathcal{D}\{u_a(x)\}\, e^{-\mathcal{H}_{\rm cryst}(h(x), u_a(x))/T}\right)\,. \tag{2.24}$$

[5] Since Eq. (2.19) lacks the reparametrisation symmetry of fluid membranes, one does not encounter the difficulties with proper counting embedding functions. Strictly speaking, the integral in Eq. (2.20) should not extend over all different embedding functions, but cover all embedding functions modulo potential symmetries (isometries) of the reference metric $g^0_{\mu\nu}(\xi)$.

Evaluating this integral, one obtains for the effective elastic energy [108]

$$\mathcal{H}_{\text{cryst,eff}}(h(x)) = \frac{1}{2}\kappa \int d^2x (\nabla^2 h(x))^2 + \frac{1}{2} k_{\text{Y}} \int d^2x \int d^2x' \, K(x) \overline{\Gamma}(x,x') K(x') \,. \tag{2.25}$$

The elastic coupling k_{Y} is the Young's modulus

$$k_{\text{Y}} = \frac{4k_a(k_a+k_b)}{2k_a+k_b} \,. \tag{2.26}$$

In Eq. (2.25), $K(x) = \det(\partial_\mu \partial_\nu h)$ denotes the Gaussian curvature, and $\overline{\Gamma}(x,x')$ is given by $\overline{\Gamma}(x,x') = 1/\Delta^2 \sim (x-x')^2 \ln(|x-x'|/a)$, where Δ is the scalar Laplacian and a is a microscopic cut-off. The elastic energy, Eq. (2.25), is a reformulation and approximation to the general elastic energy, Eq. (2.19), which is valid for a membrane that has a flat ground state and undergoes only small deformations. It consists of the bending energy in the first term and an in-plane stretching energy in the second term. Both energies are expressed only in terms of the out-of-plane deformation $h(x)$. The advantage of this formulation of the in-plane elastic energy is that it directly gives the in-plane stretching energy which is caused by the out-of-plane deformation $h(x)$. For the initially flat membrane, which is characterised by zero Gaussian curvature, the in-plane elastic energy has the form of an effective, long-ranged interaction between local Gaussian curvatures. This means that all membrane distortions which alter the local Gaussian curvature (i.e. lead to a nonzero Gaussian curvature) cause high elastic strain and are suppressed by the Young's modulus k_{Y}. This coupling is absent for membranes with a vanishing shear modulus such as fluid membranes.

For an elastic membrane with an arbitrary reference metric, one can conclude that out-of-plane deformations which change the internal metric (and thus cause in-plane distortions) are suppressed by the elastic coupling k_{Y} [6]. Only isometric membrane deformations are possible without extra energy cost.

Scale dependence of elastic parameters

The resistance to in-plane stretching deformations crucially influences the character of the membrane undulations and the renormalisation behaviour of the elastic parameters. Thermal fluctuations lead to a stiffening of a self-avoiding tethered membrane on larger length scales. This stiffening dominates the logarithmic softening of the bending rigidity which is seen in fluid membranes. Simulations and a self-consistent perturbative expansion in k_{Y} propose a scale-dependence of the bending rigidity in the long wavelength limit of the form [80]

$$\kappa(q) \sim q^{-\eta_h} \,. \tag{2.27}$$

with $0 < \eta_h \leq 1$. At long wavelengths (q approaches zero) the effective bending rigidity $\kappa(q)$ is expected to diverge via a power law.

It is believed that self-avoiding tethered membranes exhibit an overall flat phase at all finite temperatures. This flat phase is characterised by an infinite persistence length and is not found with fluid membranes.

The fluctuation spectrum of a crystalline-tethered membrane is markedly different from a fluid membrane. This is reflected by the correlations of out-of-plane fluctuations and the

[6] Note that the Gaussian curvature is a measure for the intrinsic curvature of a surface and depends only on the metric.

corresponding roughness exponent ζ. One obtains as an estimate for the average amplitude of the membrane undulations between position $\mathbf{r}_1$ and $\mathbf{r}_2$ [80]

$$\langle |h(\mathbf{r}_1) - h(\mathbf{r}_2)|^2 \rangle \sim |\mathbf{r}_1 - \mathbf{r}_2|^{2\zeta} , \qquad \text{with} \qquad \zeta = \frac{1}{2}(2 - \eta_h) . \tag{2.28}$$

The currently most accurate estimates for η_h are around $\eta_h \simeq 0.72$, which gives $\zeta \simeq 0.64$ [80].

2.3.2 Discrete model

On a discrete level, a crystalline-tethered membrane is most naturally modelled as a triangulated surface with a fixed triangulation. The membrane surface is represented by a network of hard spheres which are connected by tethers (tether and bead model presented in subsection 2.2.2 before). Unlike fluid membranes, the connectivity of the network is kept fixed. Thus, when one samples thermal equilibrium configurations, bond flips are not performed. As Monte Carlo moves only vertex moves are attempted where single vertices are displaced randomly.

2.4 Hexatic membranes

In the preceding section we have been concerned with crystalline membranes that exhibit longer-ranged in-plane positional order. The obtained results hold when integrity of the internal membrane structure is given. For fluctuating membranes whose in-plane order is caused by weak, van der Waals forces this is not guaranteed from the beginning. It turns out that in these systems topological defects play an important role and rearrangements of the crystalline order do occur on sufficiently large length scales in the presence of thermal fluctuations. This can be seen from the following argument. The relevant defects are dislocations [7], which destroy translational order, and disclinations [8], which disrupt bond orientational order. In two-dimensional systems these defects are point-like, and, compared to three-dimensional systems, the energy associated with the creation of defects is comparably small. For a planar membrane confined to two dimensions, the crystalline phase is stable because both the energy and entropy of dislocations increase logarithmically with the system size. The situation changes, however, if the membrane is allowed to fluctuate and buckle out of the plane. The energy of dislocations is significantly reduced by buckling. It turns out that it grows sub-logarithmically with the system size. In this case, the entropy gain of the dislocations compensates the increase of energy associated with the formation of dislocations. As a consequence, fluctuating membranes of sufficiently large size are expected to show free dislocations at any finite temperature. On sufficiently large length scales, the resulting low-temperature phase is a hexatic [79]. Beyond a certain translational correlation length ξ_T the crystalline order is disrupted and only the bond orientational order of the original crystalline lattice preserves. This translational correlation

[7] Mathematically, a dislocation represents the breaking of the translational holonomy [109]. A path that would naturally close in a perfect lattice fails to close around a dislocation by a vector $\mathbf{b}$, the Burgers vector. The vector $\mathbf{b}$ (its magnitude is denoted $b = \mathbf{b}$) can be considered as a (vector-like) topological charge of the dislocation.

[8] A disclination is associated with the breaking of the rotational holonomy. The bond angle around the point defect is a multiple of the natural bond angle in the ground state ($2\pi/6$ in a triangular lattice). The charge s of the disclination is given by the defect angle, its sign is chosen according to the character of the defects (positive or negative). For a positive (five-fold) coordinated disclination we have $s = +2\pi/6$, while for a negative (sevenfold), $s = -2\pi/6$. A dislocation can be regarded as a tightly bound pair (or dipole) of opposite disclinations.

length ξ_T depends on the Young's modulus k_Y, the temperature and the elastic energy to create a defect.

The name hexatic accounts for the six-fold symmetry of the orientational order parameter. This symmetry of the orientational order is reminiscent from the symmetry of the underlying triangular crystal lattice. There is experimental evidence for a hexatic phase in various systems, including free standing liquid crystal films [110]. Although bond orientational order with six-fold symmetry is the most important one, phases with a different symmetry of the orientational order parameter do exist. Very recently, a liquid film with an orthorhombic orientational order has been demonstrated experimentally [111].

Undulating membranes with orientational order are comparably complex. They are governed by a coupling of in-plane elastic energies and out-of-plane bending energies. Orientational order in a hexatic membrane leads to an in-plane elastic energy, which is different and smaller than the in-plane elastic energy in membranes with crystalline order. It is introduced in the appendix C.1. A theoretical description of hexatic membranes is challenging as one has to account for a proper treatment of thermally created defects in a fluctuating surface.

Here, we do not consider hexatic membranes any further. In our investigations on solid membrane domains thermally induced defects will be omitted. The correlation length of in-plane translational order ξ_T is assumed to be larger than the membrane size of interest. This is justified when crystalline membranes at suitable low temperature are considered. For the solid membrane domains in vesicles, it is a reasonable approximation at room temperature. In a vesicle, the out-of-plane fluctuations are restricted by the confined geometry. Therefore, defects cannot be formed so easily by thermal fluctuations and out-of-plane bending.

Chapter 3

Homogeneous fluid vesicles

In this chapter we discuss statistical properties of homogeneous fluid vesicles in thermal equilibrium. In particular, we study the morphological transition between vesicles with prolate and oblate shape which is caused by thermal fluctuations. With the help of Monte Carlo simulations, we determine the free energy profile of these vesicles as a function of suitable order parameters. The shape transition between prolate and oblate vesicles is shown to be continuous and not hampered by a free energy barrier.

3.1 Introduction

The present chapter is concerned with physical properties of homogeneous fluid vesicles. Fluid vesicles constitute a paradigmatic soft matter system which has received intense research interest over the last three decades [8, 9]. As soft surfaces they occur in a large variety of different geometric shapes, undergo morphological transitions between those shapes and, due to thermal fluctuations, exhibit pronounced undulations. The theoretical description is based on the theory of fluid membranes, chapter 2, which requires some modification, since the vesicle membrane is closed. In general, the Canham-Helfrich free energy works well. Yet, for a more quantitative analysis especially near vesicle shape transitions it turns out that the bilayer aspect of the membranes should be paid more attention. For this reason several refined (free) energy models have been proposed [9]. Furthermore, the closing of the membrane to vesicles implies that the membrane does not undulate freely but is subject to geometric constraints. The area of the vesicle depends on the number of constituent molecules in the membrane and is basically fixed. The volume enclosed by the vesicle is controlled by the osmotic conditions of the solvent. Lipid membranes are semipermeable bilayers, they are permeable by water and small uncharged molecules such as CO_2 or N_2, but in experimental time-scales they are essentially impermeable to ions and larger uncharged molecules such as glucose and macromolecules. Concentration differences of molecules that cannot permeate the membrane give rise to an osmotic pressure between the interior and exterior. Two experimental situations have to be distinguished: if osmotically active solutes are absent, the vesicle volume can change. Otherwise the system tries to equilibrate the osmotic pressure difference by the inflow or outflow of water molecules. Since the energy associated with osmotic pressures is in general quite large compared to the other relevant energies of the vesicle, the volume is essentially fixed at the osmotically optimal value.

Based on these considerations, a firm understanding of the diversity of vesicle morphologies

has been established over the past 30 years [8, 9]. Important insights have been gained by determining the shapes of minimum bending energy, taking into account the constraints on area and, if required, volume [8, 9]. Furthermore, thermal fluctuations of the vesicle membrane have been included either by perturbative calculations around the shape of minimum energy, which are possible for simple vesicle geometries [112, 113], or by computer simulations in the general case [114, 115].

In the following we attempt to complete this picture by computing the free energy profile of fluid vesicles. For vesicles, calculations of the free energy profile have become possible only very recently due to increased computational power [116]. The free energy profile provides information about the equilibrium shape of minimum energy, metastable states and on free energy barriers in between. Knowledge of the free energy profile is therefore particularly valuable when the vesicle undergoes a morphological transition. In this chapter the emphasis is on the transition between vesicles with prolate and oblate shape. This shape transition is caused by thermal fluctuations and is frequently observed in experiments [61]. The goal of this chapter is to characterise details and the order of this transition.

The present chapter is organised as follows: We start with a brief introduction of the three standard models for the analysis of vesicle shapes: the Canham-Helfrich or spontaneous curvature model (SC) [55, 56], the bilayer-couple model (BC) [117, 118] and the area-difference elasticity model (ADE) [119]. A short discussion on shapes of minimum energy follows. Then, we turn to thermal equilibrium properties, concentrating on the transition between vesicles with prolate and oblate shapes. We reexamine suitable asphericity parameters which enable us to characterise prolate and oblate vesicle morphologies. Results of Monte Carlo simulations are presented which give insight into the free energy profile between prolate and oblate vesicles.

3.1.1 Curvature models

The Canham-Helfrich or spontaneous curvature model (SC), already encountered in the introduction, chapter 1, describes the membrane as a structure-less two-dimensional surface which resists bending deformations. Any possible physical or chemical bilayer asymmetry is taken into account via a nonzero spontaneous curvature. To characterise the vesicle, it is useful to introduce two dimensionless parameters, the reduced volume v and the reduced spontaneous curvature c_0. The constraint on the total area A allows to define a length scale R_0 which is defined as the radius of a sphere with the same surface area, $R_0 = (A/(4\pi))^{1/2}$. The reduced volume v is defined by

$$v \equiv \frac{V}{4\pi/3R_0^3} \tag{3.1}$$

and the reduced spontaneous curvature is given by

$$c_0 \equiv R_0 C_0 \,. \tag{3.2}$$

In the SC model the vesicle shapes are characterised by v and c_o.

The SC model neglects one aspect of the bilayer architecture. The exchange of lipid molecules between the two monolayers ('flip-flop') is suppressed for most phospholipids and slow compared to the experimental time-scale of the experiments. Therefore, besides the total number of molecules in the bilayer also the individual number of molecules in each monolayer is approximately conserved. The number difference $N^{\rm out} - N^{\rm in}$ of molecules in the inner and outer leaflet of the bilayer gives a preferred area difference between the two monolayers,

$\Delta A_0 \equiv (N^{\text{out}} - N^{\text{in}})a_0$, where a_0 is the equilibrium area per lipid molecule. In a vesicle, the actual area difference ΔA is related to the integrated mean curvature $\Delta A \simeq 2d \int dA H$, where d is the distance between the neutral surfaces of the two monolayers, i.e. roughly half the bilayer thickness. In the bilayer couple model (BC) it is assumed that the area of each molecule is strictly conserved and thus ΔA is conserved, too. This implies a constraint on the total mean curvature $M = \int dA\, H$. In the BC model, if a spontaneous curvature is not considered, there are two parameters to describe the vesicle, the reduced volume v and the reduced total mean curvature $m = M/R_0$.

The SC and the BC model can be seen as two limiting cases of a generalised curvature model which is known in the literature as the area-difference-elasticity model (ADE)

$$\mathcal{H}_{\text{ADE}} = \frac{\kappa}{2} \int dA\, (2H)^2 \, + \, \frac{\alpha_\kappa \kappa}{2} (m - m_0)^2 \,. \tag{3.3}$$

In the ADE model the hard constraint on the area difference between the two monolayers ΔA of the BC model is released. Instead, a softer harmonic potential is introduced which penalises deviations from the preferred integrated mean curvature m_0. The preferred integrated mean curvature m_0 is related to the optimal area difference A_0 by $m_0 = \Delta A_0/(2dR_0)$, which is essentially given by the number difference of lipid molecules in the two monolayers. A spontaneous curvature is not introduced explicitly because it is not an independent parameter. It corresponds merely to a shift in the optimal integrated mean curvature $m_0 \to m_0 + 2C_0R_0/\alpha_\kappa$. The dimensionless parameter α_κ is in the order of one and interpolates the ADE model between the SC and the BC model. In the limit of large α_κ, the ADE model becomes the BC model, while in the limit of vanishing α_κ, it reduces to the SC model without spontaneous curvature. The ADE model has two independent parameters, v and m_0, and one additional material parameter α_κ.

All experiments on vesicle shapes and shape transitions that have been performed so far are in quantitative agreement with the ADE model. For our investigations it is sufficient to use the simpler Canham-Helfrich free energy.

3.2 Equilibrium configurations

The vesicle performs small fluctuations around an average shape which corresponds to the conformation of minimum bending energy. In order to determine the equilibrium morphology of the vesicle one has to minimise the free energy functional of the vesicle for a given fixed area and (in the presence of osmotically active particles) fixed volume. This can be done by functional variation of the vesicle's free energy. The constraints on area and volume are thereby incorporated via Lagrange parameters. The parameter σ is introduced as the Lagrange parameter for the area conservation, the parameter p is introduced as the Lagrange parameter for a fixed volume (p is related to the pressure difference between the outside and inside of the vesicle). Extremising the Canham-Helfrich free energy with respect to a deformation directed along the surface normal yields the Euler-Lagrange equation, or shape equation, first derived in [120]

$$p - 2\sigma H + \kappa(2H + c_0)(2H^2 - c_0 H - 2K) + \kappa\Delta(2H) = 0\,, \tag{3.4}$$

where Δ is the scalar Laplace operator, see appendix A.1. Eq. (3.4) is equivalent to the equation which one gets when one balances the forces (stresses and bending moments) on an infinitesimal membrane segment [121]. Thus, this equation also expresses the state of

mechanical equilibrium of the membrane [1]. In the limit of vanishing κ it reduces to the familiar Laplace equation which describes an interface under a surface tension σ. The shape equation, Eq. (3.4), provides a necessary condition for the vesicle shape of being a local minimum. To investigate the stability of a vesicle shape, one has to analyse the second or higher variation of the energy functional.

It is noteworthy that in the shape equation, Eq. (3.4), the Gaussian bending modulus drops out. This is because we have considered a closed surface with a constant Gaussian bending modulus, where by virtue of the Gauss-Bonnet theorem the Gaussian energy term yields only a constant contribution. In the general case of arbitrary boundary conditions the contribution from the Gaussian energy may not be neglected. The general influence of a varying Gaussian bending rigidity is seen in the generalised shape equation where the analysis is extended from constant bending moduli κ and κ_G to varying bending moduli, see [124].

Furthermore, we note that for vesicles the pressure inside is not necessarily larger than outside. An inner excess pressure is required for systems governed by interfacial tension like liquid droplets. In contrast to such systems, a homogeneous vesicle with a reduced volume smaller than one typically exhibits an outer excess pressure at mechanical equilibrium.

For practical calculations, Eq. (3.4) has to be written in terms of a coordinate function $\mathbf{X}$ that describes the membrane surface. This leads to a highly nonlinear partial differential equation of fourth order in $\mathbf{X}$, which can be solved analytically only in a few exceptional cases. In the past years efforts have been concentrated on finding solutions to this equation in the axisymmetrical case (which is then a second order ordinary differential equation) or alternatively on the direct numerical minimisation of the vesicle free energy. The resulting minimum energy shapes are arranged in morphology diagrams (bifurcation diagrams) which give the equilibrium shape of the vesicle as a function of the parameters of the particular vesicle model [9, 125]. As an example, which will be referred to later on, we give the results for the simple case of the SC model with $c_0 = 0$. For $0.65 < v < 1$, the equilibrium shape is a prolate. For $0.58 < v < 0.65$, the ground state is a biconcave discocyte, and for $v < 0.58$ a stomatocyte has lowest energy. Examples of the different vesicle morphologies are displayed in Fig. 3.1.

In summary, equilibrium morphologies of vesicles are well understood, for a detailed discussion see [9, 31].

[1] Recently, Eq. (3.4) has been reinterpreted as one element of the conservation law which follows from the Euclidean symmetry of the Helfrich Hamiltonian. Generally, a continuous symmetry implies the conservation of a corresponding Noether charge. From the translational symmetry of the functional it follows that the stress tensor is conserved. Three equations describe the conservation of the stress tensor: The normal projection is identified as the shape equation describing equilibrium configurations, while the tangential projections are consistency equations on the stresses which are related to the fluid character of the membrane [122, 123].

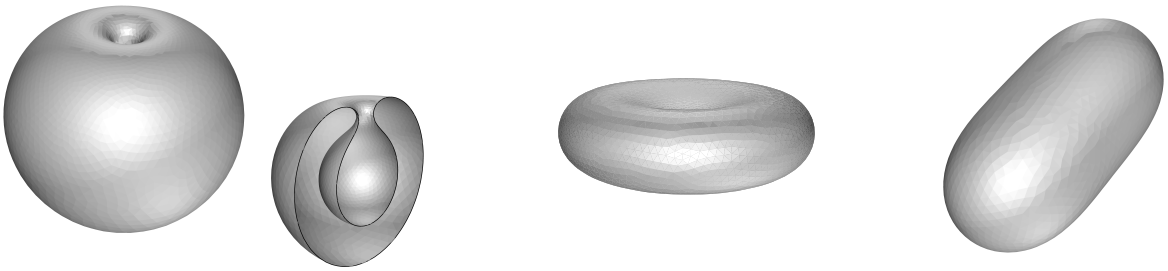

(a) (b) (c)

Figure 3.1: Equilibrium conformations of vesicles with different reduced volume v (spontaneous curvature $c_0 = 0$): (a) stomatocyte ($v = 0.57$), (b) discocyte ($v = 0.6$), and (c) prolate ($v = 0.9$).

3.3 Thermal fluctuations

Vesicle membranes are not static objects. Being embedded in an aqueous solution, they are subject to permanent thermal collisions with water molecules and thus in continuous exchange of energy with the environment. Thermal forces lead to fluctuations of the membrane shape. The membrane fluctuations extend over a broad range of length scales. On length scales comparable to or smaller than the membrane thickness, thermal fluctuations give rise to protrusion modes. These are relative displacements of the lipid molecules which change the surface area of the lipid-water interface and which, consequently, are governed by an effective interface tension. The roughness arising from these fluctuations occurs on the length scale of a few angstroms. On intermediate and larger length scales the occurring fluctuations are out-of-plane bending modes which are governed by the bending rigidity. The focus in this dissertation is on bending modes with a longer wavelength, which are visible in the optical microscope.

Thermal fluctuations have several effects on the vesicle. In the experiments, the analysis of the shape fluctuations is based on the optically resolvable membrane contour. The measured shape is an average image of the true, microscopic vesicle geometry. While the microscopic membrane area can be assumed to be approximately constant, the optically resolvable membrane area fluctuates. This leads to an entropic stretching elasticity of the vesicle membrane [95, 126]. As explained in detail in chapter 2, the bending rigidity κ gets entropic contributions. Due to the interaction of fluctuation modes on smaller length scales the bending modulus becomes scale dependent. Therefore, instead of the bare microscopic (mechanic) bending rigidity κ one has to use the renormalised value for the bending rigidity adequate for the length scale of interest.

An intriguing effect of thermal fluctuations is that they can induce changes in the morphology of the vesicle. As noted above, for $v > 0.65$ the energetic favoured vesicle morphology is prolate, oblate shapes always have higher bending energies. Nevertheless, in this regime transitions between prolate and oblate shapes are frequently observed in the light microscope. The transition is caused by thermal fluctuations [61]. The aim of this section is to provide details and the order of this transformation between vesicle with prolate and oblate shape.

How can thermally excited shape fluctuations be included in the theoretical description? If

the equilibrium shape has a simple geometry, the fluctuations can be calculated in a (perturbative) expansion around the equilibrium conformation [113]. For axisymmetric vesicles, the spherical harmonics are a convenient basis. For a quasi-spherical vesicle in the limit of large bending rigidities, $\kappa/T \gg 1$, the thermal spectrum of undulation modes can be calculated analytically. The vesicle shape is expressed in polar coordinates $\Omega = (\Theta, \Phi)$ with a normalised radial height field $h(\Omega)$ over the sphere of radius R_0

$$\mathbf{X}(\Omega) = R_0(1 + h(\Omega))\mathbf{e}_r \,, \tag{3.5}$$

where $\mathbf{e}_r$ is the radial unit vector. Expanded in spherical harmonics, $h(\Omega)$ reads

$$h(\Omega) = \sum_{l=1}^{l_M} \sum_{m=-l}^{l} a_{lm} Y_l^m(\Omega) \,. \tag{3.6}$$

In Eq. (3.6), modes up to the wavenumber cutoff l_M are considered. The fluctuation amplitudes are found to be [112]

$$\langle a_{lm}^2 \rangle \simeq \frac{T}{\kappa} \frac{1}{l(l+1)(l-1)(l+2)} \,. \tag{3.7}$$

Analytic or perturbative calculations are practicable only for special cases. For the general case of not so simple vesicle geometries, this is not possible and one has to resort to computer simulations. For mesoscopic length scales there is a well established Monte Carlo method in which the shape of the fluid vesicle membrane is simulated with a dynamic network of triangles (tether and bead model) [114, 115]. This method, presented in chapter 2, has been applied very successfully in interpreting and fitting experimental data, for example in the analysis of the vesicle fluctuation spectrum obtained by optical spectroscopy [127].

In the following we are interested in the free energy profile of vesicles. The free energy profile gives information about the local minima of the free energy and free energy barriers in between. Knowledge of the free energy profile is therefore particularly valuable when the vesicle undergoes a morphological transition. In the article [116], the free energy profile of a vesicle with a reduced volume v considerably smaller than one has been determined. There, prolate-discocyte and discocyte-stomatocyte shape transformations occur. The emphasis in this section is on the free energy profile of vesicles with a reduced volume close to one where transitions between prolate and oblate configurations occur.

To study the free energy profile between prolate and oblate shapes, an appropriate measure to distinguish between prolate and oblate shapes is needed. Unfortunately, the asphericity parameter from [128] used in [116] does not permit to discriminate between prolate and oblate conformations and cannot be applied. In the article [129] an alternative order parameter is proposed which is capable to distinguish between prolate and oblate morphologies. However, the order parameter in [129] has some disadvantages which make it less suited to explore the free energy landscape of prolate and oblate shapes and to study (possible) free energy barriers between them. The order parameter jumps discontinuously from positive to negative values as the vesicle is deformed continuously from a prolate to an oblate shape without crossing an exact spherical shape. Furthermore, it does not allow to distinguish intermediate vesicle shapes which are neither exact spherical nor pronounced oblate nor pronounced prolate (intermediate biaxial shapes) [2]. These intermediate shapes, however, are important because they dominate

[2] The order parameter in [129] classifies these intermediate biaxial shapes (the eigenvalues of the shape tensor $\mathbf{Q}$ fulfil $\lambda_3 - \lambda_2 \simeq \lambda_2 - \lambda_1$) as pronounced prolate respectively oblate shapes or even as spheres (for $\lambda_3 - \lambda_2 = \lambda_2 - \lambda_1$). For a definition of the shape tensor $\mathbf{Q}$ see the following subsection 3.3.1.

the probability density of configurations for an unconstrained vesicle.

Next, we reexamine suitable asphericity parameters for vesicles with a reduced volume close to one.

3.3.1 Asphericity parameters

We consider a triangulated vesicle described by N_v vertices with the coordinate vectors $\mathbf{X}_k$ $(k = 1, \ldots, N_v)$ embedded in $\mathbb{R}^d$. To characterise the shape of the triangulated vesicle, it is useful to introduce a symmetric second rank tensor (shape tensor) $\mathbf{Q}$ with the components [130]

$$Q_{ij} = \frac{1}{N_v} \sum_{k=1}^{N_v} \left(X_{k,\,i} - \bar{X}_i\right) \left(X_{k,\,j} - \bar{X}_j\right) . \tag{3.8}$$

Here, $X_{k,\,i}$ denotes the i-th coordinate of the position $\mathbf{X}_k$ of the k-th vertex and $\bar{\mathbf{X}}$ with the coordinates $\bar{X}_i$ is the centre of mass

$$\bar{\mathbf{X}} = \frac{1}{N_v} \sum_{k=1}^{N_v} \mathbf{X}_k \,. \tag{3.9}$$

The shape tensor $\mathbf{Q}$ has also been used to quantify the conformation of random walks and polymers [128, 131, 132]. The trace of this tensor, $\mathrm{tr}\,\mathbf{Q}$, equals the square radius of gyration. It is related to the vesicle's moment of inertia tensor $\mathbf{I}$, evaluated about its centre of mass $\bar{\mathbf{X}}$, via

$$\mathbf{I} = (\mathrm{tr}\mathbf{Q})\,\mathbf{1} - \mathbf{Q} \,. \tag{3.10}$$

Information on the anisotropy of the shape is provided by the spread in the eigenvalues of $\mathbf{Q}$, $\lambda_1 \leq \cdots \leq \lambda_d$. If all the λ_i are equal, the shape is spherically symmetric.

To proceed, it is practical to define $\hat{\mathbf{Q}}$, the traceless version of $\mathbf{Q}$, by

$$\hat{\mathbf{Q}} = \mathbf{Q} - \bar{\lambda}\mathbf{1} \,, \tag{3.11}$$

where $\bar{\lambda}$ denotes the average eigenvalue of $\mathbf{Q}$

$$\bar{\lambda} = \frac{1}{d} \sum_i \lambda_i = \frac{1}{d}\,\mathrm{Tr}\mathbf{Q} \,. \tag{3.12}$$

For a spherical shape, $\hat{\mathbf{Q}}$ is $\mathbf{0}$.

A measure for the deviation from spherical symmetry is given by the relative variance of the eigenvalues λ_i of $\mathbf{Q}$. By definition one has

$$\sum_i \left(\frac{\lambda_i - \bar{\lambda}}{\bar{\lambda}}\right)^2 = d^2 \frac{\mathrm{Tr}(\hat{\mathbf{Q}}^2)}{(\mathrm{Tr}\mathbf{Q})^2} \,. \tag{3.13}$$

As a measure for the asphericity we define the asphericity parameter α_d as a normalised version thereof [131]

$$\alpha_d \equiv \frac{d}{d-1} \frac{\mathrm{Tr}(\hat{\mathbf{Q}}^2)}{(\mathrm{Tr}\mathbf{Q})^2} \,. \tag{3.14}$$

Upon averaging over a thermal ensemble, the following inequality holds

$$0 \leq \frac{d}{d-1}\frac{\langle \mathrm{Tr}(\hat{\mathbf{Q}}^2)\rangle}{\langle (\mathrm{Tr}\mathbf{Q})^2\rangle} \leq 1\,. \tag{3.15}$$

For $d = 3$, the asphericity parameter reads

$$\alpha \equiv \alpha_3 = \frac{3}{2}\frac{\mathrm{Tr}(\hat{\mathbf{Q}}^2)}{(\mathrm{Tr}\mathbf{Q})^2} = \frac{1}{6}\sum_i \left(\frac{\lambda_i - \bar{\lambda}}{\bar{\lambda}}\right)^2\,, \tag{3.16}$$

which is the order parameter used by in the article [116]. One has $\alpha_3 = 0$ for spheres, $\alpha_3 = 1$ for thin rods and $\alpha_3 = 0.25$ for thin disks.

The character of the anisotropy, whether it is prolate or oblate, is reflected by the third order measure $\mathrm{Tr}(\hat{\mathbf{Q}}^3)$. For $d = 3$,

$$\mathrm{Tr}(\hat{\mathbf{Q}}^3) = 3\det\hat{\mathbf{Q}} = 3(\lambda_1 - \bar{\lambda})(\lambda_2 - \bar{\lambda})(\lambda_3 - \bar{\lambda})\,. \tag{3.17}$$

The sign of $\det\hat{\mathbf{Q}}$ reflects the relative number of large and small eigenvalues in $\mathbf{Q}$. For a prolate shape ($\lambda_3 \gg \lambda_1 \simeq \lambda_2$) one has $\lambda_3 - \bar{\lambda} > 0$, while $\lambda_1 - \bar{\lambda} < 0$ and $\lambda_2 - \bar{\lambda} < 0$, so that $\det\hat{\mathbf{Q}}$ is positive. In contrast, an oblate conformation ($\lambda_3 \simeq \lambda_2 \gg \lambda_1$) has a negative value for $\det\hat{\mathbf{Q}}$. Thus, the sign of $\det\hat{\mathbf{Q}}$ determines whether a shape is prolate or oblate. Its magnitude probes how oblate or prolate a shape is. As a normalised measure of the character of the shape anisotropy we use in the following [3] [132]

$$\delta_d \equiv \frac{d^2}{(d-1)(d-2)}\frac{\mathrm{Tr}(\hat{\mathbf{Q}}^3)}{(\mathrm{Tr}\mathbf{Q})^3}\,, \tag{3.18}$$

which fulfils

$$-\frac{1}{(d-1)^3} \leq \frac{d^2}{(d-1)(d-2)}\frac{\langle \mathrm{Tr}(\hat{\mathbf{Q}}^3)\rangle}{\langle (\mathrm{Tr}\mathbf{Q})^3\rangle} \leq 1\,. \tag{3.19}$$

For $d = 3$,

$$\delta \equiv \delta_3 = \frac{9}{2}\frac{\mathrm{Tr}(\hat{\mathbf{Q}}^3)}{(\mathrm{Tr}\mathbf{Q})^3} = \frac{1}{2}\frac{(\lambda_1 - \bar{\lambda})(\lambda_2 - \bar{\lambda})(\lambda_3 - \bar{\lambda})}{\bar{\lambda}^3}\,, \tag{3.20}$$

and

$$-\frac{1}{8} \leq \frac{9}{2}\frac{\langle \mathrm{Tr}(\hat{\mathbf{Q}}^3)\rangle}{\langle (\mathrm{Tr}\mathbf{Q})^3\rangle} \leq 1\,. \tag{3.21}$$

3.3.2 Free energy profile

At this point, a few general remarks regarding free energy profiles are in order. To characterise the free energy of a system, the phase space of the system needs to be partitioned via an appropriate order parameter, which we denote by a. The probability density $p_a(T)$ for the system to acquire microstates assigned to the order parameter a at temperature T can be written as

$$p_a(T) = \frac{\mathcal{Z}_a(T)}{\mathcal{Z}(T)}\,. \tag{3.22}$$

[3] This definition of δ_d differs from that in [131] by a factor of two.

In Eq. (3.22), $\mathcal{Z}(T)$ denotes the (canonical) partition function of the system and $\mathcal{Z}_a(T)$ the restricted partition function, defined as

$$\mathcal{Z}_a(T) = \int d\Gamma e^{-\mathcal{H}(\Gamma)/T} \delta(a(\Gamma) - a)\,, \tag{3.23}$$

where the integral extends over all microstates in the phase space. With this, we can define the constrained free energy

$$F_a(T) = -T \ln \mathcal{Z}_a(T)\,. \tag{3.24}$$

A free energy profile refers to the free energy $F_a(T)$ as a function of a. The free energy difference $\Delta F_{a,a'}(T) = F_a(T) - F_{a'}(T)$ is related to the probability densities $p_a(T)$ and $p_{a'}(T)$ via

$$\Delta F_{a,a'}(T) = T \ln \frac{\mathcal{Z}_{a'}(T)}{\mathcal{Z}_a(T)} = T \ln \frac{p_{a'}(T)}{p_a(T)}\,, \tag{3.25}$$

which is in principle accessible by Monte Carlo simulations.

3.3.3 Simulation results

We perform Monte Carlo simulations with the Metropolis algorithm to obtain thermal equilibrium properties of vesicles. The focus is on the free energy profile of vesicles with reduced volumes close to one, where typically prolate and oblate morphologies occur. To characterise the vesicle shape two different order parameters are employed, the asphericity $\alpha = \alpha_3$ and the shape anisotropy $\delta = \delta_3$. The asphericity α allows to quantify the deviation from being a sphere, while the shape anisotropy δ distinguishes between prolate and oblate morphologies. The shape anisotropy δ is positive for prolates, and negative for oblates. Its magnitude quantifies how oblate or prolate the shape is.

Simulation details and units

In the simulations, the vesicle is represented by a triangulated surface with $N_v = 864$ vertices and edge lengths according to the tether-bead model, see section 2.2.2. Fig. 3.2 shows snapshots for a prolate (Fig. 3.2a) and an oblate morphology (Fig. 3.2b) taken during the simulation. The vesicle area is essentially fixed, up to small fluctuations in a harmonic potential around a given optimal area. We apply two types of Monte Carlo moves in a random order: vertex moves where the position of single vertices is displaced and bond-flips in which an edge between two triangles is relocated to connect the formerly unconnected vertices of the two triangles. We perform about $2 \cdot 10^7$ MC moves to obtain sufficient statistics. The system is equilibrated in an initial run. Thereby, a maximum step size Δx for the vertex translation is determined such that about 50% of the proposed translation moves are accepted.

In the following, all energies, including T, are given in units of κ.

We monitor in the simulations the probability densities $p_\alpha(T)$, $p_\delta(T)$ and $p_{\alpha,\delta}(T)$. The probability density $p_\alpha(T)$ gives the probability that at temperature T the vesicle acquires a conformation with asphericity α, it is related to the constrained free energy $F_\alpha(T)$ by $F_\alpha(T) = -T \ln p_\alpha(T)$ (up to a constant). The probability density $p_\delta(T)$ denotes the probability that the vesicle has the shape anisotropy δ, with the corresponding constrained free energy $F_\delta(T)$. The probability density $p_{\alpha,\delta}(T)$ gives the probability density that the vesicle has asphericity α and shape anisotropy δ, with the corresponding constrained free energy $F_{\alpha,\delta}(T)$.

(a) (b)

Figure 3.2: Snapshots of (a) a prolate ellipsoid (asphericity $\alpha = 0.060$, anisotropy $\delta = 0.014$) and (b) an oblate ellipsoid ($\alpha = 0.009$, $\delta = -0.0004$).

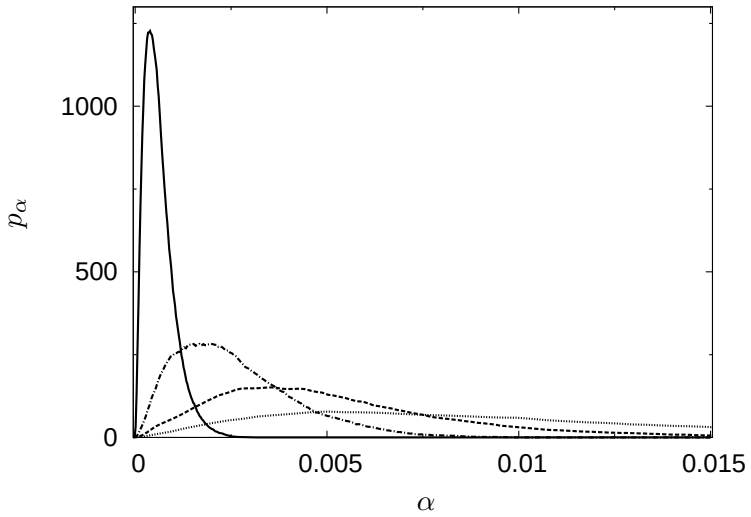

Figure 3.3: Probability density $p_\alpha(T)$ as a function of the asphericity α for vesicles without volume constraints at different temperatures T (in units of the bending rigidity κ) $T = 0.01\,\kappa$ (solid line), $T = 0.05\,\kappa$ (alternating dots and dashes), $T = 0.1\,\kappa$ (dashed line), and $T = 0.2\,\kappa$ (dotted line).

In the following we investigate vesicles which can change their volume and vesicles with a fixed reduced volume.

Vesicles without volume constraints

Vesicles embedded in a solvent without osmotically active particles can change their volume. For these vesicles, when $c_0 = 0$, the energetic ground state is a sphere ($v = 1$, $\alpha = 0$ and $\delta = 0$). If one includes thermal undulations of the membrane, the vesicle shape starts to deviate from an exact spherical geometry. This can be seen in Fig. 3.3, where the probability density $p_\alpha(T)$ of

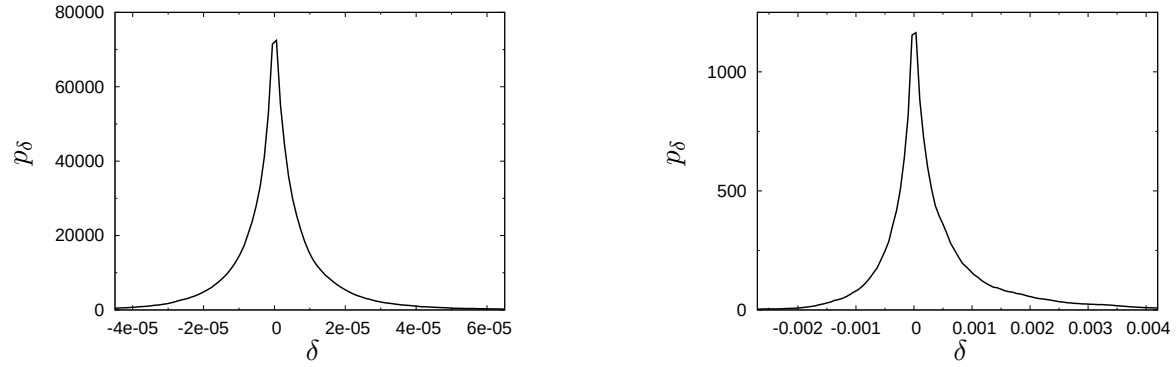

(a) (b)

Figure 3.4: Probability density $p_\delta(T)$ as a function of the shape anisotropy δ for vesicles without volume constraints at temperatures T (in units of the bending rigidity κ) (a) $T = 0.01\,\kappa$, and (b) $T = 0.2\,\kappa$. The shape anisotropy δ is positive for prolate shapes, negative for oblate and vanishes for intermediate shapes or spheres, its magnitude quantifies the anisotropy of the shape.

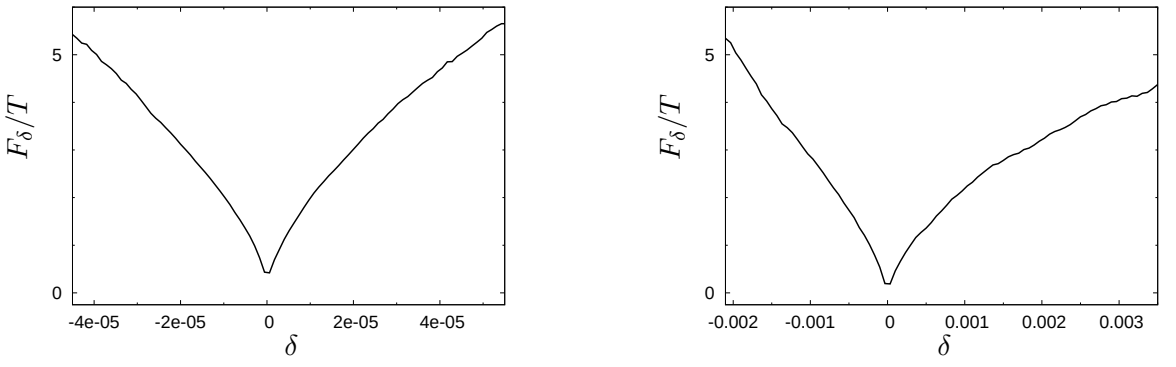

(a) (b)

Figure 3.5: Free energy profile $F_\delta(T)$ for vesicles without volume constraints as a function of the shape anisotropy δ at temperatures (a) $T = 0.01\,\kappa$, and (b) $T = 0.2\,\kappa$. The shape anisotropy δ is positive for prolates, negative for oblate and vanishes for intermediate biaxial shapes or spheres; its magnitude quantifies the anisotropy of the shape.

a vesicle with $c_0 = 0$ is plotted for different temperatures T varied between $0.01\,\kappa \leq T \leq 0.2\,\kappa$, corresponding to bending rigidities from $\kappa = 100\,T$ down to $\kappa = 5\,T$.

The data shows that at low temperatures or equivalently large bending rigidity, the maximum of $p_\alpha(T)$ is close to zero. The vesicle conformations are almost spherical. As the temperature increases, the maximum of $p_\alpha(T)$ shifts to larger values of α. The deviation from the spherical shape becomes larger. The asphericity is caused by thermal fluctuations and has an entropic origin.

To characterise the anisotropy of these conformations, we determine the probability density $p_\delta(T)$ for the same parameters. Fig. 3.4 displays some of this data. We assume in the following

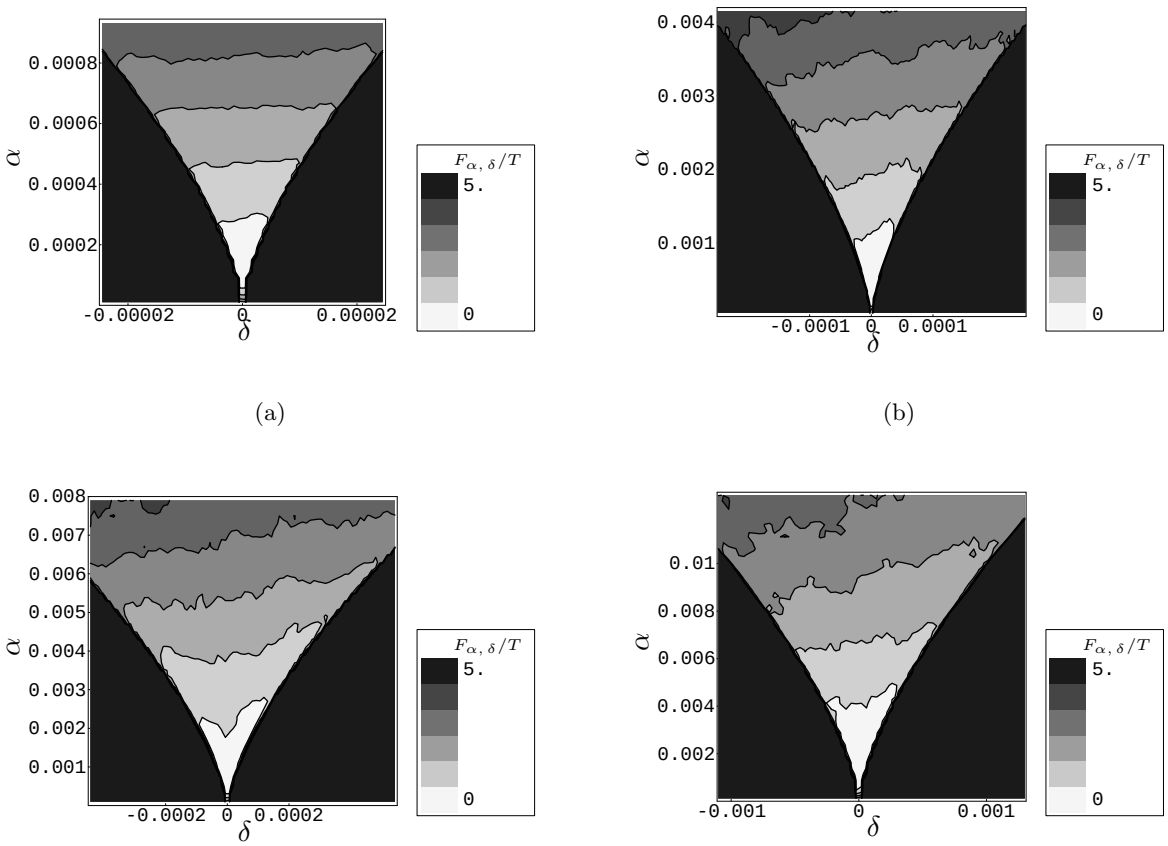

Figure 3.6: Contour plots of the free energy $F_{\alpha,\delta}(T)$ (asphericity α on the vertical axis versus anisotropy δ on the horizontal axis) for vesicles without volume constraints at different temperatures T (in units of the bending rigidity κ), from top left (a) $T = 0.01\,\kappa$, (b) $T = 0.05\,\kappa$, (c) $T = 0.1\,\kappa$, and (d) $T = 0.2\,\kappa$.

$\lambda_1 \leq \lambda_2 \leq \lambda_3$. As a first result we find that the conformations with maximum probability density are shapes with $\delta = 0$. These are intermediate shapes which are neither distinctly prolate ($\lambda_3 \gg \lambda_1 \simeq \lambda_2$) nor oblate ($\lambda_3 \simeq \lambda_1 \gg \lambda_2$), but slightly biaxial morphologies where the eigenvalues of the shape tensor are approximately equidistant, i.e. $\lambda_3 - \lambda_2 \simeq \lambda_2 - \lambda_1$. This result holds for all investigated temperatures. Furthermore, the distribution $p_\delta(T)$ is found to be asymmetric with respect to the sign of δ, i.e. between prolate and oblate shapes. It has a larger tail for prolate shapes, implying that the probability of prolate morphologies is slightly larger than that of oblate shapes. While the form of $p_\delta(T)$ is quite insensitive to the temperature – with increasing temperature the probability for prolate shapes increases slightly –, the absolute value of the distribution width changes considerably with varying temperature. As the temperature increases from $T = 0.01\,\kappa$ to $T = 0.2\,\kappa$, it increases by almost two orders of magnitude. This result is understood by recalling that the absolute magnitude of δ quantifies the anisotropy of the shape and reflects how prolate or oblate a shape is. Thus, for higher temperatures the eccentricity (elongations) of the vesicle shape is

T/κ	$\langle \sum_i \left(\frac{\lambda_i - \bar{\lambda}}{\bar{\lambda}}\right)^2 \rangle$	p_{prolate}	$\langle v \rangle$
0.01	0.0037	0.514	0.993
0.05	0.0154	0.573	0.981
0.1	0.0309	0.590	0.966
0.2	0.0651	0.600	0.935

Table 3.1: Thermal equilibrium properties of vesicles without volume constraints at different temperatures T (in units of the bending rigidity κ). The relative spread of the eigenvalues of the shape tensor $\sum_i \left(\frac{\lambda_i - \bar{\lambda}}{\bar{\lambda}}\right)^2 = 6\alpha$ measures the asphericity of the vesicle, p_{prolate} gives the probability of conformations with prolate shape, and v is the reduced volume. (The brackets $\langle\rangle$ denote thermal average.)

much more pronounced. This is of course the behaviour one would naturally expect.

To obtain the total probability for prolate conformations $p_{\text{prolate}}(T)$ one has to integrate the probability density $p_\delta(T)$ in the interval $0 < \delta < \infty$. Likewise, the total probability for oblate conformations $p_{\text{oblate}}(T)$ is given by the integration of $p_\delta(T)$ in $-\infty < \delta < 0$. The probability of prolate morphologies $p_{\text{prolate}}(T)$ is found to be slightly larger than $p_{\text{oblate}}(T)$. This is a result which has also been made in [129]. For $T = 0.01\,\kappa$, we find $p_{\text{prolate}}(0.01\,\kappa) = 0.514$. With increasing temperature $p_{\text{prolate}}(T)$ increases slightly. For $T = 0.2\,\kappa$ $p_{\text{prolate}}(0.2\,\kappa)$ is about $p_{\text{prolate}} = 0.6$. The findings are summarised in detail in Tab. 3.1. How can the preference of prolate shapes be explained? This fact is due to energetic reasons. For vesicles with v close to one, the prolate ground state energy is slightly smaller than that of the corresponding oblate at the same v [125].

Fig. 3.5 shows the profile of the constrained free energy $F_\delta(T)$ for $T = 0.01\,\kappa$ (Fig. 3.5a) and for $T = 0.2\,\kappa$ (Fig. 3.5b), which are derived from $p_\delta(T)$ and correspond to Fig. 3.4a and Fig. 3.4b, respectively. The single minimum in $F_\delta(T)$ at $\delta = 0$ shows that the transition between prolate and oblate morphologies is continuous and not hampered by a free energy barrier. This is an important issue and could not be clarified in [129].

To corroborate our findings we monitor $p_{\alpha,\delta}(T)$ and determine $F_{\alpha,\delta}(T)$. The free energy landscape as a function of α and δ provides more detailed information about the transition between prolate and oblate shapes. It is shown in contour plots in Fig. 3.6 for $T = 0.01\,\kappa$ (Fig. 3.6a) and $T = 0.2\,\kappa$ (Fig. 3.6d). The data shows clearly that in the free energy landscape there are no barriers. The transition between prolate and oblate vesicles proceeds in a continuous manner.

Vesicles with fixed reduced volume

For typical osmotic conditions in experiments, the osmotic energy exceeds the energy of curvature elasticity. To a good approximation, the volume is then fixed to a value for which the osmotic pressure is minimal. We analyse the statistics of a vesicle with vanishing spontaneous curvature $c_0 = 0$ at temperature $T = 0.1\,\kappa$ for different fixed volumes v, starting from $v = 0.75$ up to $v = 0.95$. For these values of v, the minimum energy configuration is a prolate shape. The results of our simulations are collected in Fig. 3.7, which shows histograms of $p_\alpha(T)$, Fig. 3.8, which shows histograms of $p_\delta(T)$ and Fig. 3.9, which shows contour plots of the constrained free energy $F_{\alpha,\delta}(T)$.

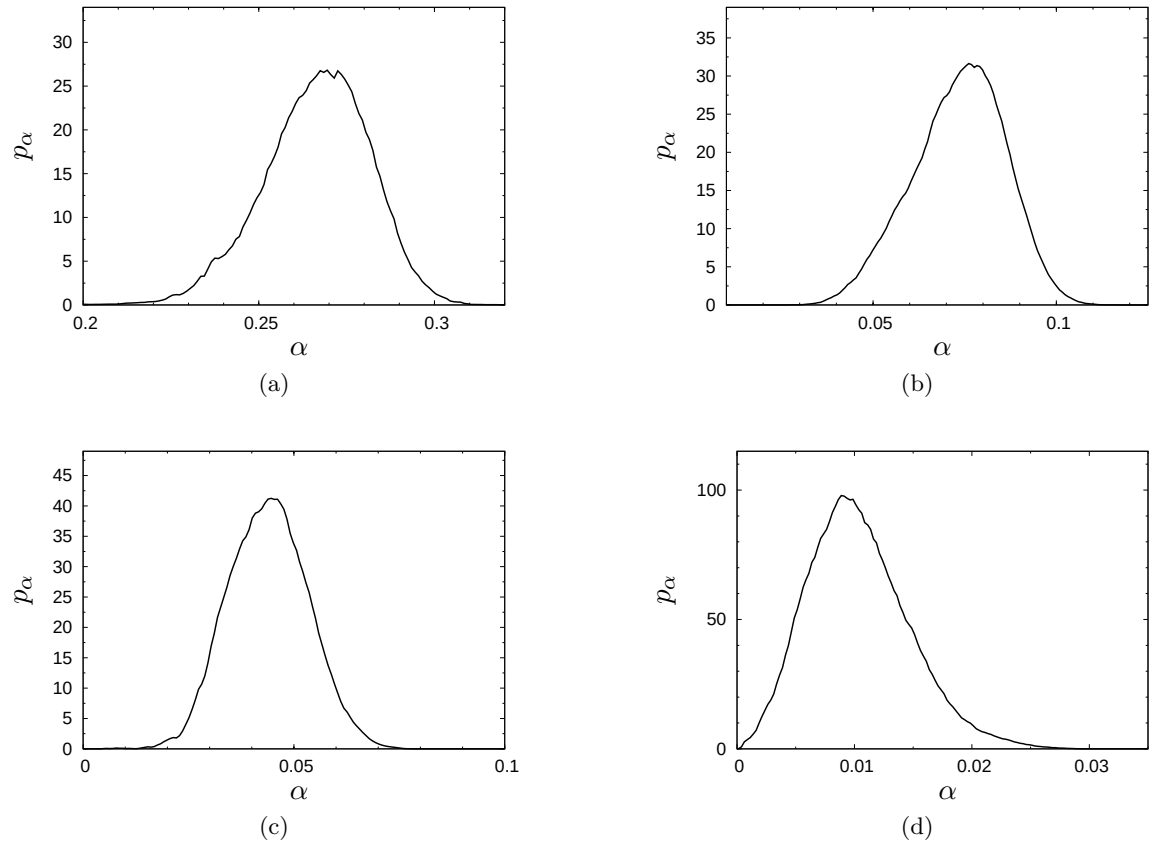

Figure 3.7: Histograms of the probability density $p_\alpha(T)$ as a function of the asphericity α for vesicles with bending rigidity κ and vanishing spontaneous curvature $c_0 = 0$ at temperature $T = 0.1\,\kappa$ for different reduced volumes v, from top left (a) $v = 0.8$, (b) $v = 0.9$, (c) $v = 0.92$, (d) $v = 0.95$.

v	p_{oblate}
0.9	0.054
0.92	0.104
0.95	0.38

Table 3.2: Thermal equilibrium properties of vesicles with bending rigidity κ at different reduced volumes v for temperature $T = 0.1\,\kappa$ and vanishing spontaneous curvature $c_0 = 0$. The probability p_{oblate} gives the probability that the vesicle has a prolate shape.

Our data shows that for comparably small values of v ($0.75 \leq v \lesssim 0.9$) only prolate configurations occur in thermal equilibrium (Fig. 3.8a). This is expected from energetic reasons because in this range of reduced volumes the difference in the ground state energy of oblate and prolate shapes is considerably larger than the thermal energy [125]. For vesicles with reduced volume close to one, this energy difference is small and thermal fluctuations also excite oblate configurations. For our parameter values chosen, this happens at about $v \gtrsim 0.9$, above which the statistical weight of oblate morphologies $p_{\text{oblate}}(T)$ is significantly larger than zero. The

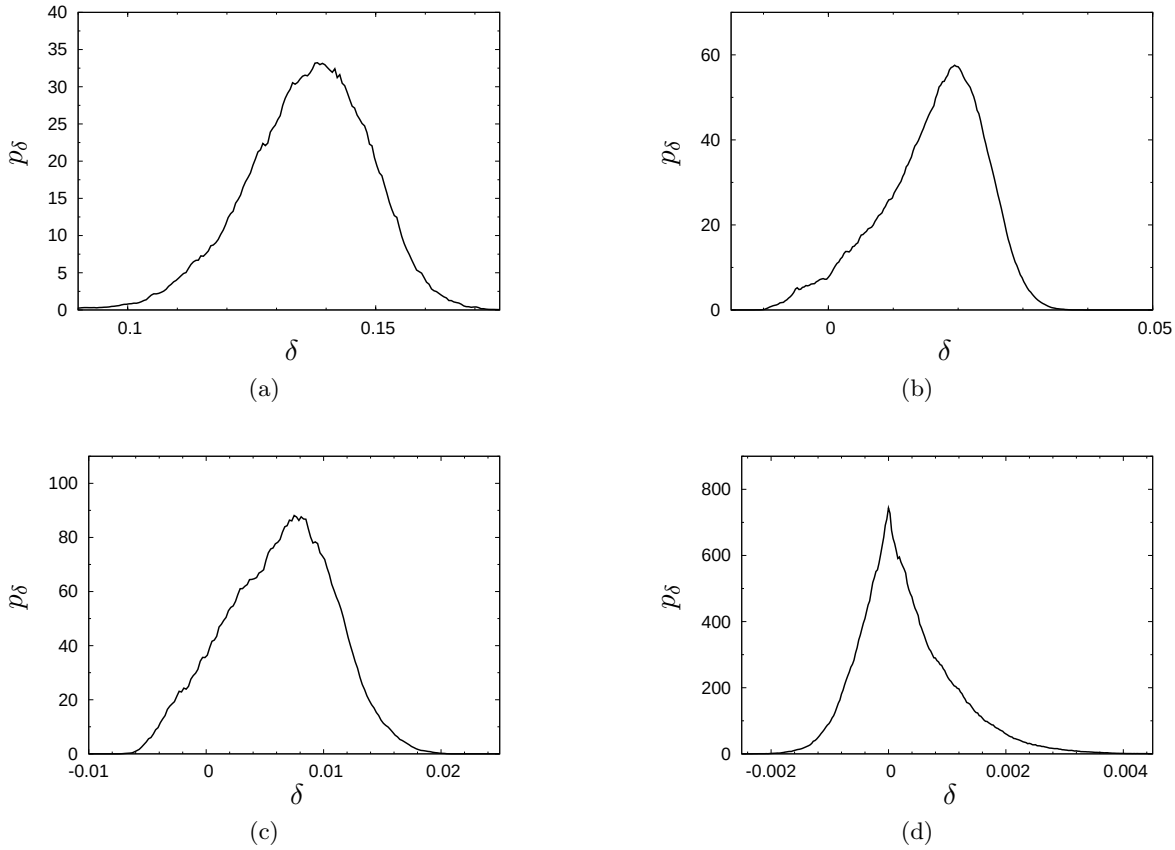

Figure 3.8: Histograms of the probability density $p_\delta(T)$ as a function of the shape anisotropy δ for vesicles with bending rigidity κ and vanishing spontaneous curvature $c_0 = 0$ at temperature $T = 0.1\,\kappa$ for different reduced volumes v, from top left (a) $v = 0.8$, (b) $v = 0.9$, (c) $v = 0.92$, and (d) $v = 0.95$.

probability $p_{\text{oblate}}(T)$ increases with increasing v. We find that for $T = 0.1\,\kappa$, $p_{\text{oblate}}(T) = 0.054$ for $v = 0.9$, $p_{\text{oblate}}(T) = 0.104$ for $v = 0.92$ and $p_{\text{oblate}}(T) = 0.38$ for $v = 0.95$, see Tab. 3.2.

A look at the distributions in Fig. 3.8 and the free energy profiles in Fig. 3.9 reveals that for vesicles with volume constraints the transition between prolate and oblate shapes is continuous. Again, no free energy barrier is involved. This result is similar to the observation made for vesicles without volume constraints.

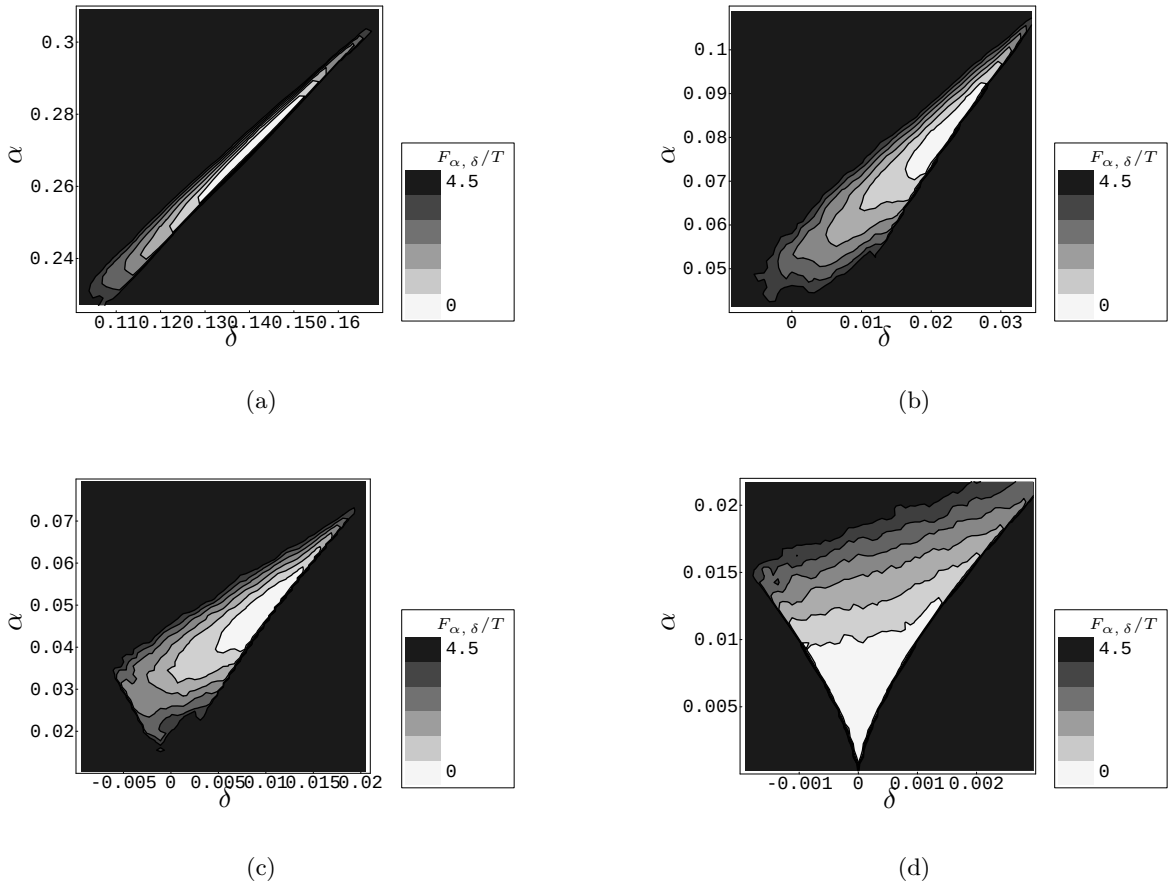

Figure 3.9: Contour plots of the free energy $F_{\alpha,\delta}(T)$ (asphericity α on the vertical axis versus anisotropy δ on the horizontal axis) for vesicles with bending rigidity κ and vanishing spontaneous curvature $c_0 = 0$ at temperature $T = 0.1\,\kappa$ for different reduced volumes v, from top left (a) $v = 0.8$, (b) $v = 0.9$, (c) $v = 0.92$, (d) $v = 0.95$.

3.4 Discussion and conclusion

In this chapter the conformation of fluid three-dimensional vesicles has been studied. Using Monte Carlo simulations, we have determined the free energy profile of vesicles with a reduced volume close to one. Both, unconstrained vesicles as well as vesicles with volume constraints have been analysed.

For unconstrained vesicles whose energetic ground state is an exact sphere, we find that in thermal equilibrium the most probable conformations deviate from an exact sphere. The deviation becomes larger when temperature increases and it is due to thermal fluctuations. A similar observation has also been made in the related work of [129]. We find that the shapes with the highest probability density are neither prolate (positive anisotropy) nor oblate (negative anisotropy), but intermediate biaxial shapes with vanishing anisotropy (i.e. the eigenvalues of the shape tensor $\mathbf{Q}$ fulfil $\lambda_3 - \lambda_2 \simeq \lambda_2 - \lambda_1$). We give estimates for the probabilities for the occurrence of prolate and oblate morphologies and show that vesicles with prolate shape are more likely than vesicle with oblate shapes. Furthermore, as an important result, we find that the transition between prolate and oblate shapes is smooth, i.e. it is not hampered by a free energy barrier.

For vesicles with fixed volume whose energetic ground state is a prolate we show that for sufficiently large v thermal fluctuations lead to shape transitions from prolate to oblate morphologies. Our simulations for fixed reduced volumes indicate that the transition between prolate and oblate shapes proceeds continuously without a free energy barrier. Again, we give estimates for the probabilities for the occurrence of prolate (oblate) morphologies.

Our findings provide a natural explanation for the experimentally observed transition from oblate to prolate morphologies [61]. It should be pointed out, however, that a direct comparison with the experiments may be difficult. While in the simulations the full three-dimensional information of the vesicle shape is given, in the experiments only a two-dimensional cross section of the vesicle shape is available. Given this limited information, it may be sometimes difficult to judge whether a vesicle is indeed prolate or oblate.

Chapter 4

Vesicles with solid and fluid membrane domains

This chapter surveys the morphology of fluid vesicles with solid membrane domains. The solid membrane is considered in the limit where it cannot undergo in-plane stretching deformations. We determine the *equilibrium* shape of fluid vesicles with one or several solid domains for various material parameters. As the material parameters change, morphological transitions are observed between vesicles with different domain shapes. Our results are corroborated by Monte Carlo simulations, which take into account effects of thermal fluctuations.

4.1 Introduction

In this chapter we investigate morphologies of fluid vesicles where some parts of the vesicle membrane exhibit in-plane order. Certain aspects of in-plane order in membranes have been encountered in chapter 2 for unconstrained membranes which undulate freely. Compared to free membranes, order phenomena in a closed surface such as a vesicle are more complex for topological reasons. For vesicle shells whose total membrane area is in an ordered state (for example the vesicle membrane is frozen in the solid (gel) phase), new vesicle morphologies appear. In contrast to fluid vesicles, the equilibrium shape for large, in-plane ordered vesicles is found to be non-spherical also in cases where the vesicle volume is unconstrained. This is because even in the energy ground state defects have to be present. These topological defects interact with each other, usually they repel and tend to be separated as far as possible, causing membrane deformations.

The focus in this chapter is not on homogeneously ordered vesicles, but on inhomogeneous vesicles where only a fraction of the vesicle area is in an ordered state, while the rest of the vesicle membrane is disordered and fluid [62]. Such a scenario arises when the membrane is prepared in a region of the phase diagram where a solid (or gel) phase coexists with a fluid phase. Phase separation then leads to the formation of intramembrane domains [62]. In the past, researchers did not show too much interest in solid membranes and the formation of solid domains because, in contrast to fluid domains, solid domains are not believed to be of immediate biological relevance. Nevertheless, from a physical point of view they certainly do deserve special attention. As two-dimensional crystals they have unique physical properties which are markedly different from their three-dimensional counterparts [133].

Very recently, confocal fluorescence microscopy studies allowed to investigate in detail the

formation of solid domains on giant unilamellar vesicles made of lipid mixtures [71, 72, 74–78]. These experiments reveal micron-sized domains with different morphologies, including stripes of different widths and orientations, polygonal domains as well as round shapes (see Fig. 1.8-Fig. 1.10). There is experimental indication that the shapes of the domains observed in solid-fluid coexistence are correlated with the structure of the gel phase [71]. It is also observed that, surprisingly, the domains do not grow beyond a limit but their size seems to be limited. This phenomenon has remained unexplained.

In the following we study the morphology of fluid vesicles with solid domains from a theoretical perspective. We consider phase separation in the so-called strong-segregation limit [134, 135]. This implies that the phases are homogeneous inside the domains and that a sharp interface separates the domains. The physics of the domain boundaries can therefore be described by a line tension. Basing on this assumption, the formation of solid domains in fluid vesicles has been the subject of recent work [136, 137]. In these studies the authors focused on the limit of exact spherical vesicles, where the solid domains are stretched onto the spherical geometry. In this case the shape of the domain is determined by an interplay between line tension and elastic stretching energy. In this chapter we address the opposite situation where the solid domains are considered to be essentially unstretchable and undergo only isometric bending deformations. This regime is supposed to be more relevant for lipid bilayer membranes. We consider non-spherical vesicle morphologies where domain shapes are governed by a competition between bending energy and line tension contributions.

The chapter is organised as follows. We start with a summary of in-plane order in a homogeneous vesicle membrane. Next, we turn to inhomogeneously ordered vesicles, and determine the equilibrium energy of vesicles with different solid domain morphologies. The shapes with minimum energy are arranged in morphology diagrams. Monte Carlo techniques are employed to include effects of thermal fluctuations.

4.2 Order on homogeneous vesicles

Even though the main topic of this chapter is the formation of solid membrane domains, it is instructive to have a brief look on vesicles whose whole membrane is in an ordered state. Internal or in-plane order is coupled to the local geometry of the membrane. If a surface has intrinsic curvature, in-plane order becomes frustrated. This affects translational order in a crystal [138] as well as order which is described by a vector or tensor field order parameter such as hexatic bond-orientational order or tilt (smectic C) order with two-fold rotation symmetry [139]. For example, a two-dimensional, initially flat crystal necessarily stretches if it is forced to lie on a surface which is curved in two directions, i.e. which has non-vanishing Gaussian curvature, cf. section 2.3.

In-plane order is not only connected with local properties of the membrane but in addition constrained by its topological properties. For a closed surface, new phenomena arise which are not present in a planar membrane. A closed surface is classified according to its genus g (number of handles) or equivalently its Euler-Poincaré characteristic $\chi_{\text{Euler}} = 2(1-g)$ which is a topological invariant. For these surfaces, the Poincarè theorem relates the sum of the charges of topological defects to the Euler-Poincaré characteristic χ_{Euler} [140]. For a triangulated surface, the elementary topological defects are given by disclinations. We associate the topological charge $s = +2\pi/6$ to a positive (five-fold) disclination, and $s = -2\pi/6$ to a negative (seven-fold) disclination. The other topological defects such as dislocations or grain boundaries can

be built from these elementary imperfections. Dislocations can be considered as a bound pair of disclinations with opposite charge and thus have a net charge $s = 0$. For spherical surfaces, one has $\chi_{\text{Euler}} = 2$. The topological constraint requires a minimum number of topological defects for a spherical membrane with crystalline, tilt or hexatic order: A triangular lattice with translational order must be interrupted by at least twelve five-fold disclination defects. Likewise, tilt order (bond-orientational order with two-fold rotation symmetry) necessarily generates two antipodal defects (vortices with charge 2π), and hexatic order leads to at least twelve vortices (five-fold disclinations with charge $s = 2\pi/6$). In general, the creation of disclinations involves quite high energies. Some elastic strain around such a defect can be reduced or screened by a deformation of the membrane which modifies the local Gaussian curvature [141]. These defects interact with each other in a long-range way [142].

As a consequence, unconstrained vesicles with in-plane order which can adjust to their optimal volume exhibit non-spherical equilibrium shapes. This is in contrast to fluid vesicles. Development of tilt order leads to ellipsoidal (prolate) or cylindrical shapes. Hexatic order is expected to induce a transition to an icosahedral morphology [143–148].

In the case of crystalline order on a small elastic shell, the equilibrium shape is believed to be a sphere where the disclination defects are located at the vertices of an inscribed icosahedron. If the size of the shell increases, the situation becomes more involved. For a flat plate, the elastic energy associated with the lattice distortion around an isolated disclination grows as a function of the area of the system. Therefore, for larger shell sizes the associated elastic energy becomes quite large and lots of strain is created. Above a certain shell size, the spherical shape becomes unstable and the excess strain is relieved by buckling of the membrane. Buckling is the consequence of energy minimisation of stretching and bending contributions near a disclination. For a spherical soft shell, it results in a morphological transition towards an icosahedron shape [149]. The instability of an elastic shell towards buckling might provide an explanation for the experimentally observed faceting of lecithin vesicles in a crystalline phase [150]. Furthermore, it may be relevant for the morphology of various virus capsids where larger viruses are found to be more faceted [149, 151]. The volume enclosed by the shell decreases during a buckling transition. Buckling therefore can only occur if the vesicle volume can change. If the geometry is fixed to be spherical, there is an alternative mechanism for lowering the strain energy. The buckling instability is replaced by an instability towards the formation of extra defects. This mechanism has been first investigated theoretically for a spherical crystal [152] and verified later on in experiments with colloidosomes [153]. Colloidosomes (named in analogy with liposomes) are spherical solid capsules which are formed by colloidal particles self-assembled on water droplets in oil. The analysis of the typical arrangement of the colloidal particles reveals that above a critical size of the colloidosome additional defects besides the defects required by topology are present [153]. One observes dislocations, tightly bound pairs of disclinations of opposite charge, which are aligned in strings to form grain boundaries or so-called scars. Since their net disclination charge is zero, these extra defects still satisfy Poincaré's theorem. Their function is to reduce the large stresses in the vicinity of a disclination. The drastic relief of elastic energy compensates the additional energies associated with the creation of dislocations. If one takes interactions between dislocations into account, one can show that the dislocations organise in grain boundaries to minimise the energy even further [152].

As an aside we may also mention that curvature-induced defect unbinding is not limited to crystalline order or spherical topologies. In [154] it is shown to occur with hexatic bond orientational order in toroidal geometries, for which $\chi_{\text{Euler}} = 0$.

4.3 Solid domains in fluid vesicles

Having touched some aspects on order-phenomena extending over the whole vesicle membrane, we turn to inhomogeneous vesicles where only parts of the vesicle membrane develop ordered structures. Such a situation occurs when the membrane is quenched into a phase-coexistence of two phases, an ordered solid (gel) phase (α) and a disordered fluid phase (β). Experimentally, this situation may be realised by a single-component membrane as well as a multi-component membrane made of a lipid mixture. Phase-coexistence is achieved for a single-component membrane by adapting the temperature and for a multi-component membrane by adjusting the temperature and composition, respectively. At the appropriate conditions, the vesicle membrane phase separates and domains of different phases form.

Since bilayer membranes consist of two monolayers, domain formation can occur, in principle, separately within both monolayers. One can have monolayer domains, which extend only across a single monolayer, or bilayer domains, which extend across both monolayers. Monolayer domains usually have a nonzero spontaneous curvature, whereas bilayer domains should be typically characterised by zero spontaneous curvature. Experimentally, for the solid-liquid coexistence in a mixture of DLPC/DPPC lipids all domains were found to be bilayer domains [74]. A strong coupling between domains in both monolayers is also indicated by coarse grained molecular dynamics simulation in lipid bilayers [155].

4.4 The model

In the following we restrict ourselves to the situation where the vesicle membrane is far from a phase transition [134, 135] and we assume that only bilayer domains form. In the so-called strong-segregation limit spatial variations of the in-plane membrane structure are restricted to the domain boundaries. Since the width of these boundaries is assumed to be much smaller than the size of the domains, the domains are considered to be separated by a sharp interface of vanishing thickness. We denote the area of the membrane which is covered by the solid phase (α) with $A^{(\alpha)}$, and the area of the fluid phase (β) with $A^{(\beta)}$. The total area of the vesicle is given by $A = A^{(\alpha)} + A^{(\beta)}$. It is useful to introduce the area fraction covered by the solid phase $\chi^{(\alpha)}$ as an additional degree of freedom

$$\chi^{(\alpha)} \equiv A^{(\alpha)}/A\,. \tag{4.1}$$

The area fraction $\chi^{(\beta)}$ of phase (β) is given by

$$\chi^{(\beta)} \equiv A^{(\beta)}/A = 1 - \chi^{(\alpha)}\,. \tag{4.2}$$

Energy contributions of the domains

To calculate the morphology of the phase separated vesicle, one has to identify the relevant energy contributions of the different phases. For the fluid phase (β), the energy is given by the Helfrich bending energy $\mathcal{H}_{\text{fluid}}$, Eq. (2.1). For the solid phase (α), the situation is more complex and a few clarifications are necessary. As explained in chapter 2, the generic low temperature phase of an unconstrained membrane is hexatic. This is because, above a certain size of the membrane, thermal fluctuations in combination with membrane undulations induce free dislocations. In vesicles, however, membrane undulations are suppressed by the geometry and further reduced by possible volume constraints. As a consequence, defects cannot

be formed so easily by out-of-plane bending. Therefore, only a small number of thermally induced dislocations should exist on average. We can assume that the correlation length for the translational order ξ_T is of the order or larger than the size of the solid domains. Accordingly, the elastic energy $\mathcal{H}_{\text{cryst}}$, Eq. (2.19), derived from the continuum elasticity theory of thin plates, can be employed for the solid domain. The energy $\mathcal{H}_{\text{cryst}}$ comprises bending and stretching contributions. Stretching energy penalises deviations from a preferred in-plane reference or ground state, which needs to be specified. We assume that the ground state (or reference metric) has a flat metric which is equivalent to saying that in the ground state defects are absent (cf. [156]).

To arrive at the full energy for the phase separated vesicle, the elastic energies have to be supplemented by the energy which arises at the interface between the different domains. This is incorporated by a line energy, which is proportional to the length of the domain boundary. The proportionality factor is the line tension $\lambda^{(\alpha,\beta)}$ [157, 158] which, for solid-like domains, is in principle anisotropic.

Combining these energies, we obtain the total energy of the phase separated vesicle

$$\mathcal{H} = \int_\alpha dA \mathcal{H}^{(\alpha)}_{\text{cryst}} + \int_\beta dA \mathcal{H}^{(\beta)}_{\text{fluid}} + \lambda^{(\alpha,\beta)} \int_\partial dl + \sigma^{(\alpha)} A^{(\alpha)} + \sigma^{(\beta)} A^{(\beta)} + pV \,. \tag{4.3}$$

It consists of the elastic energies for the solid and fluid membrane domain and an interface energy for the domain boundary. The first term describes the solid membrane and involves an integral of the elastic energy $\mathcal{H}^{(\alpha)}_{\text{cryst}}$ over the solid membrane area $A^{(\alpha)}$. The second term describes the fluid membrane domain and involves an integral of the elastic energy $\mathcal{H}^{(\beta)}_{\text{fluid}}$ over the fluid membrane area $A^{(\beta)}$. The third term is the energy of the domain boundary with line tension $\lambda^{(\alpha,\beta)}$ and contains an integral along the domain boundary ∂. In order to take the constraints on the domain area $A^{(\alpha)}$ and $A^{(\beta)}$ into account, two Lagrange multipliers, $\sigma^{(\alpha)}$ and $\sigma^{(\beta)}$, are introduced. The parameter p is the Lagrange parameter for possible constraints on the enclosed volume and corresponds physically to the pressure difference between the interior and exterior of the vesicle.

The constraint imposed by the topology of the vesicle on the minimum number of defects becomes ineffective for the solid domains. This constraint holds for the vesicle as a whole and is easily fulfilled by the unordered fluid membrane parts.

Relative importance of bending and stretching energy

If one starts from the energy expression, Eq. (4.3), and tries to determine the equilibrium configuration with minimum energy, for example by functional variation of Eq. (4.3), one faces severe difficulties in the general case. The energies $\mathcal{H}_{\text{fluid}}$ and $\mathcal{H}_{\text{cryst}}$ contain second order partial derivatives in the coordinate function parametrising the surface. Already, if one performs the first variation for these individual energies separately, one obtains partial differential equations of fourth order. For example, for the bending energy $\mathcal{H}_{\text{fluid}}$, this leads to the already familiar 'shape equation', Eq. (3.4) [120]. For the energy $\mathcal{H}_{\text{cryst}}$, which contains stretching and bending energy, one obtains the Föppl-von Kármán equations, which are highly nonlinear and "very complicated, and cannot be solved exactly, even in very simple cases [58]". We therefore have to narrow to some limiting cases.

To proceed, we keep in mind that the vesicle morphology is determined by a combination of bending energy of the fluid domain, bending and in-plane stretching energy of the solid domain and line tension contributions at the domain boundaries. In general, the different

energy contributions differ in orders of magnitude. In the following we focus on the relation between stretching and bending energy. The relative importance of stretching and bending deformations is given by the dimensionless Föppl-von Kármán number γ

$$\gamma \equiv \frac{k_{\mathrm{Y}} R_0^2}{\kappa}\,, \tag{4.4}$$

where k_{Y} is the two-dimensional Young's modulus, κ the bending rigidity and R_0 the size of the membrane.

In the limit of small γ the formation of solid domains has been addressed in the recent articles [136] and [137]. There, the authors studied solid domains on exactly spherical geometries. The fixed spherical geometry can be enforced by dominating bending energy or by other physical mechanism such as the interface tension between oil and water, as it is the case with two-dimensional colloidal crystals (colloidosome). In this specific case, the shape of the domain is determined by a competition between line tension and elastic stretching energy. For the spherical geometry, the stretching energy has been solved for certain given domain shapes, in the absence [136] and in the presence of defects (scars) [137]. Scars are expected to occur in larger stretched domains, since they considerable reduce strain, see section 4.2. Given the stretching energy for a set of different domain shapes, the equilibrium domain shapes have been calculated [136, 137]. It is found that as the line tension in decreased, the equilibrium domain shapes evolve from a single cap to several caps to stripes that become thinner. The authors conclude that their results are most relevant for domain patterns in colloidosomes.

Intermediate regimes of γ, where stretching and bending energies are comparable, received current research interest in [159]. In [159] it was shown that a high line tension in combination with spontaneous curvature leads to the budding of the crystalline domain. The budding mechanism is conjectured to be biologically relevant for the formation of clathrin cages [159].

Limit of large Föppl-von Kármán number

In this chapter, we address the limit of large γ, i.e. when the stretching energy is distinctly larger than the bending energy. In this limit, the membrane surface is considered unstretchable. This limit is relevant for solid (gel) phases of lipid bilayers because for a micrometer-size vesicle one finds $\gamma \simeq 10^{10}$. It naturally applies for a thin plate in the limit of vanishing thickness. For a thin plate, the ratio of stretching energy over bending energy is inverse proportional to the square of the plate thickness and hence diverges for an infinitesimal thin plate [58]. A familiar example of such a plate with a comparably small thickness is a sheet of paper, which easily bends but hardly stretches or shears. For these surfaces, only bending deformations are possible which do not cause in-plane stretching. This has implications for the geometry of the phase separated vesicle. When a solid domain which cannot be stretched forms on a vesicle, the vesicle cannot remain spherical but has to deform. Possible vesicle morphologies are proposed in [62] and are depicted in Fig. 4.1.

Membrane bending deformations which do not cause strain are deformations where the distance between nearby points in the membrane remains fixed, so-called isometric deformations. In the limit of large γ, it follows from a discussion of the general Föppl-von Kármán equations that the Gaussian curvature of the crystalline surface has to equal the disclination density [58].

If one assumes a disclination free ground state for the solid membrane, the solid membrane acquires a conformation where the Gaussian curvature vanishes everywhere. Geometrically,

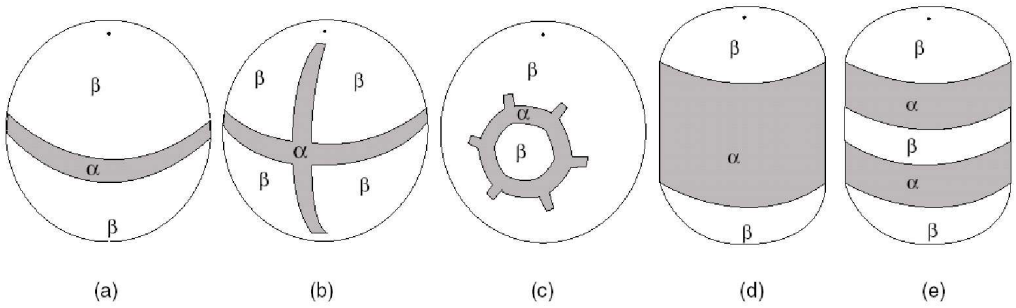

Figure 4.1: Proposed vesicle morphologies with stripe domains containing solid (α) and fluid (β) domains. All solid (α) domains (grey) have the shape of cylindrical segments with vanishing Gaussian curvature. If the vesicle is inflated and almost spherical, the solid phase can form narrow stripes as in (a)-(c). If the vesicle is deflated and prolate, the solid phase can form barrels as in (d) and (e). from [62]

such a surface is called a developable surface [160]. A developable surface is a surface that can be mapped isometrically (i.e. developed) onto a plane, i.e. be flattened onto a plane without distortion, or reversely, made by transforming a plane without distortions. From differential geometry it is known that locally there are only three types of developable surfaces in three-dimensional space: normal developable (cylindrical) surfaces, binormal developable (conical) surfaces and tangent developable surfaces (the tangent surface of a twisted curve [1]). Globally, developable surfaces can be a rather complicated composition of these three surface types.

In our approach, the different membrane domains are characterised as follows. The solid membrane domains cannot be stretched and they are flat in their ground state. Therefore, possible conformations are developable surfaces. The solid domains are characterised by the bending modulus $\kappa^{(\alpha)}$ and the spontaneous curvature $C_0^{(\alpha)}$. Fluid domains are governed by bending elasticity, with the material parameters bending modulus $\kappa^{(\beta)}$, Gaussian bending modulus $\kappa_G^{(\beta)}$ and spontaneous curvature $C_0^{(\beta)}$. The domain boundary is characterised by the line tension $\lambda^{(\alpha,\beta)}$. The vesicle morphology and the domain shape are governed by an interplay between the different bending energies and the line energy.

For simplicity, we neglect in the following the Gaussian bending modulus $\kappa_G^{(\beta)} = 0$ and restrict ourselves to zero spontaneous curvatures $C_0^{(\alpha)} = C_0^{(\beta)} = 0$. We use $\kappa^{(\beta)}$ as the reference energy. As relevant parameters there remain four dimensionless quantities, the ratio of the elastic moduli

$$\epsilon^{\kappa} \equiv \frac{\kappa^{(\alpha)}}{\kappa^{(\beta)}}\,, \tag{4.5}$$

the reduced line tension

$$\lambda \equiv \lambda^{(\alpha,\beta)} \frac{R_0}{\kappa^{(\beta)}}\,, \tag{4.6}$$

the solid area fraction $\chi^{(\alpha)}$ and the reduced volume v.

[1] in German called 'Torsen'

4.5 Equilibrium configurations

As the first step we consider configurations with minimum energy. This corresponds to $T = 0$. We start with a vesicle without volume constraints. We consider fluid vesicles with one solid domain, which may be round, a cylindrical ring or a conical ring, and fluid vesicles with two solid domains. These domain shapes are expected to be the relevant domain shapes for the investigated material parameters. Later on, we extend our analysis to vesicles with volume constraints. Thereby, as the vesicle geometry approaches a sphere it will become necessary to include vesicle configurations with more than two solid domains.

4.5.1 Vesicles without volume constraints

Isotropic line tension

Given our characterisation for the solid domains and an isotropic line tension, the equilibrium configuration for a solid domain on a free membrane is flat, simple-connected and has circular shape. For a solid domain on a fluid vesicle, this is not necessarily the case. Only if the domain size is small compared to the size of the vesicle, the solid domain is circular and remains flat. For a larger domain size, the shape of the domain is affected by the geometry of the vesicle. The solid membrane has to bend in order to adapt to the vesicle geometry. It may also deform its shape because a large circular domain involves high bending of the fluid membrane near the domain boundary. As a consequence, the shape of a comparably large solid domain becomes elongated and deviates from an exact circle. An example of a phase separated vesicle with one solid (α) and one fluid (β) domain is displayed in Fig. 4.2a (for the parameters $\chi^{(\alpha)} = 0.15$, $\lambda = 0.5$, $\epsilon^{\kappa} = 6$). This vesicle morphology is in the following referred to as I_1 [2].

On a closed object like a vesicle, the morphology with one domain in each phase is not always the equilibrium morphology. In particular for large area fraction of the solid membrane, one has to consider more complex domain shapes. In the following we consider vesicle shapes with one solid (α) and two fluid (β) domains. These are vesicle shapes where the solid domain is either a cylindrical ring, morphology I_{2a}, or a conical ring, morphology I_{2b}. Examples are shown in Fig. 4.2b and Fig. 4.2c, respectively. To characterise the ring domains, we use the parameter $\chi_{(\beta_1,\beta_2)}$, defined as the area ratio of the two fluid domains $A_1^{(\beta)}$ and $A_2^{(\beta)}$ (with $A_1^{(\beta)} < A_2^{(\beta)}$ and $A^{(\beta)} = A_1^{(\beta)} + A_2^{(\beta)}$),

$$\chi_{(\beta_1,\beta_2)} \equiv \frac{A_1^{(\beta)}}{A^{(\beta)}} \,. \tag{4.7}$$

As another possibility we consider vesicles where the solid domain is split into two domains, i.e. we consider vesicles with two solid (α) and one fluid (β) domains, referred to as morphology II_1. An example is depicted in Fig. 4.2d. The area ratio of the two solid domains $A_1^{(\alpha)}$ and $A_2^{(\alpha)}$ (with $A_1^{(\alpha)} < A_2^{(\alpha)}$ and $A^{(\alpha)} = A_1^{(\alpha)} + A_2^{(\alpha)}$) is characterised by

$$\chi_{(\alpha_1,\alpha_2)} \equiv \frac{A_1^{(\alpha)}}{A^{(\alpha)}} \,. \tag{4.8}$$

[2] Regarding notation: the Roman numerals denote the number of phase (α) domains, the subscripts with the Arabic numerals denote the number of phase (β) domains.

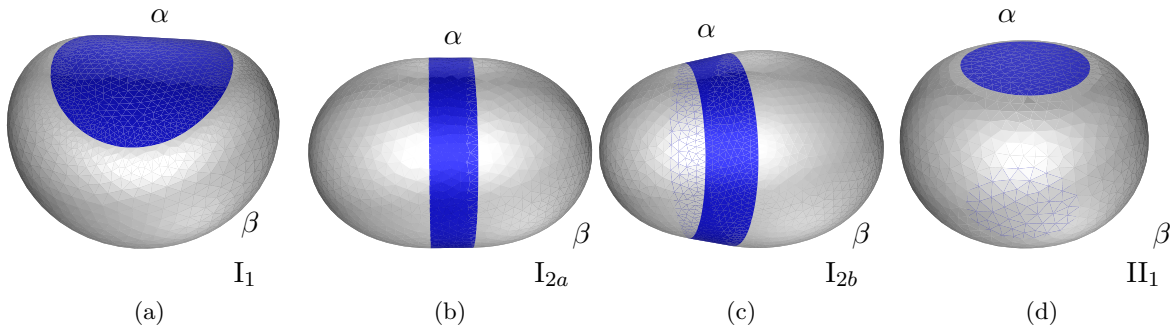

Figure 4.2: Equilibrium configurations of a vesicle with fluid (β) (white) and solid (α) (blue) membrane domains (solid area fraction $\chi^{(\alpha)} = 0.15$, reduced line tension $\lambda = 0.5$, and bending rigidity ratio $\epsilon^{\kappa} = 6$): a fluid vesicle with (a) a single round (α) domain (I_1), (b) a cylindrical ring (α) domain (I_{2a}), (c) a conical ring (α) domain (I_{2b}), and (d) two (α) domains (II_1) (The second (α) domain is hidden.).

In the following we determine and compare the ground state energies of these vesicles for different material parameters up to a solid area fraction $\chi^{(\alpha)} = 0.3$. As the subclass of possible solid domain forms we consider a simple-connected, round domain, type I_1, a cylindrical ring domain, type I_{2a}, a conical ring domain, type I_{2b} and two solid domains, type II_1. These domain shapes are expected to be the relevant domain topologies for the investigated material parameters. For simplicity, we restrict ourselves to a cylindrical ring with $\chi_{(\beta_1,\beta_2)} = 0.5$, a conical ring with $\chi_{(\beta_1,\beta_2)} = 0.25$ and two solid domains of the same size, $\chi_{(\alpha_1,\alpha_2)} = 0.5$. Our main interest is on the equilibrium shapes with minimum energy. Morphologies with a higher energy are metastable. We do not perform an explicit stability analysis of metastable states.

Minimisation method

The equilibrium shapes are determined numerically by direct minimisation of the energy functional with the help of the software package 'The Surface Evolver' [161] [3]. In this package, the surface of the vesicle is implemented as a discretised surface (i.e. a union of triangles, which, mathematically, corresponds to a simplicial complex). The surface evolves towards a minimum energy state via a gradient descent method. During the minimisation procedure, the triangulation of the surface is adapted, i.e. refined near regions of high curvature. The constraint of the solid domain – a developable surface with vanishing Gaussian curvature – is implemented via an auxiliary harmonic potential in the Gaussian curvature

$$H_{\text{aux}} = \bar{\kappa}_{\text{aux}} \int_{\alpha} dA K^2 \,. \tag{4.9}$$

By using a sufficiently high constant $\bar{\kappa}_{\text{aux}}$, any deviation from a flat metric is strongly penalised. This way a developable surface for the solid domain is achieved. The estimated numerical accuracy of the obtained energy values is about $\simeq 1\%$.

[3] This software package has been developed by Kenneth Brakke and is freely available at http://www.susqu.edu/facstaff/b/brakke/evolver/

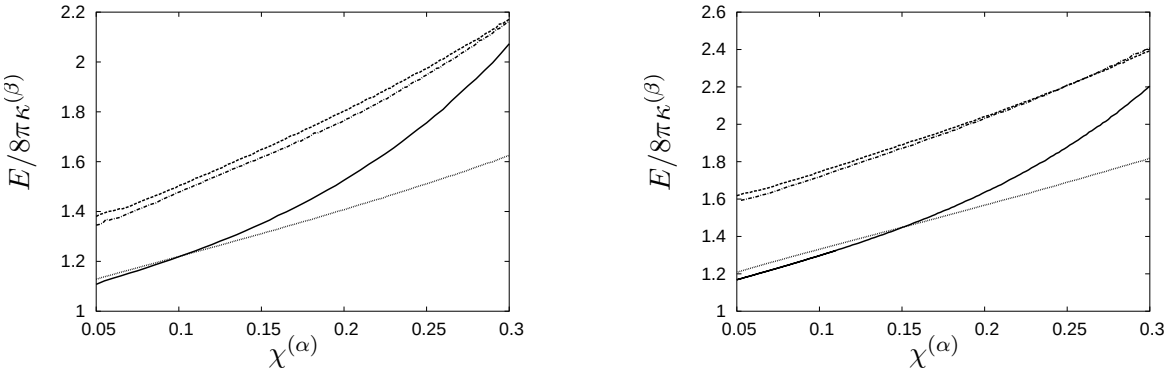

Figure 4.3: Ground state energy of a fluid vesicle with solid domains without volume constraints. The minimum energy E of a vesicle with a round solid domain (I_1) (solid line), a cylindrical ring, $\chi_{(\beta_1,\beta_2)} = 0.5$ (I_{2a}) (dashed line), a conical ring, $\chi_{(\beta_1,\beta_2)} = 0.5$ (I_{2b}) (alternating dots and dashes), and two solid domains, $\chi_{(\alpha_1,\alpha_2)} = 0.5$ (II_1) (dotted line) is plotted as a function of solid area fraction $\chi^{(\alpha)}$ for the bending rigidity ratio $\epsilon^{\kappa} = 10$ and reduced line tension (a) $\lambda = 0.5$ and (b) $\lambda = 1$.

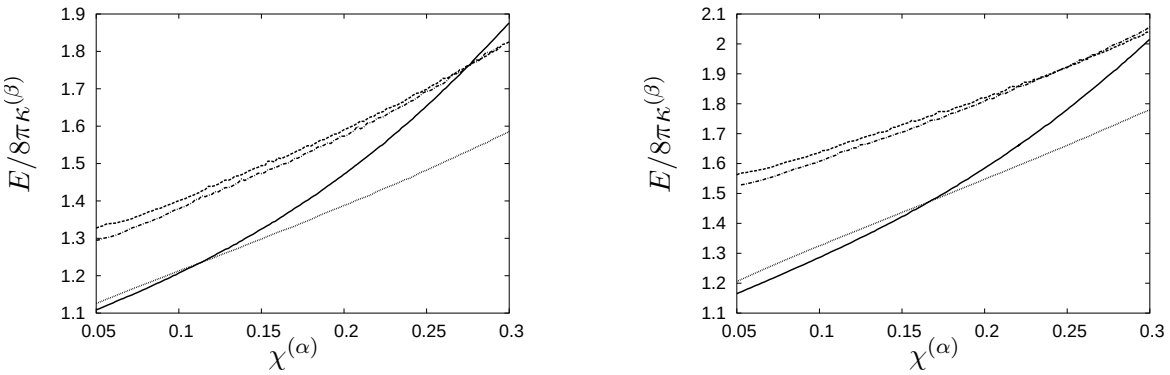

Figure 4.4: Ground state energy of a fluid vesicle with solid domains without volume constraints, same parameter values as in Fig. 4.3 but with bending rigidity ratio $\epsilon^{\kappa} = 6$. The minimum energy E of a vesicle with a round solid domain (I_1) (solid line), a cylindrical ring, $\chi_{(\beta_1,\beta_2)} = 0.5$ (I_{2a}) (dashed line), a conical ring, $\chi_{(\beta_1,\beta_2)} = 0.5$ (I_{2b}) (alternating dots and dashes), and two solid domains, $\chi_{(\alpha_1,\alpha_2)} = 0.5$ (II_1) (dotted line) is plotted as a function of solid area fraction $\chi^{(\alpha)}$ for reduced line tension (a) $\lambda = 0.5$ and (b) $\lambda = 1$.

Numerical results

In Fig. 4.3 - Fig. 4.5 the ground state energy of a vesicle with a round domain, morphology I_1, a cylindrical ring, morphology I_{2a}, a conical ring, morphology I_{2b}, and two solid domains, morphology II_1, is shown as a function of the solid area fraction $\chi^{(\alpha)}$ for different bending

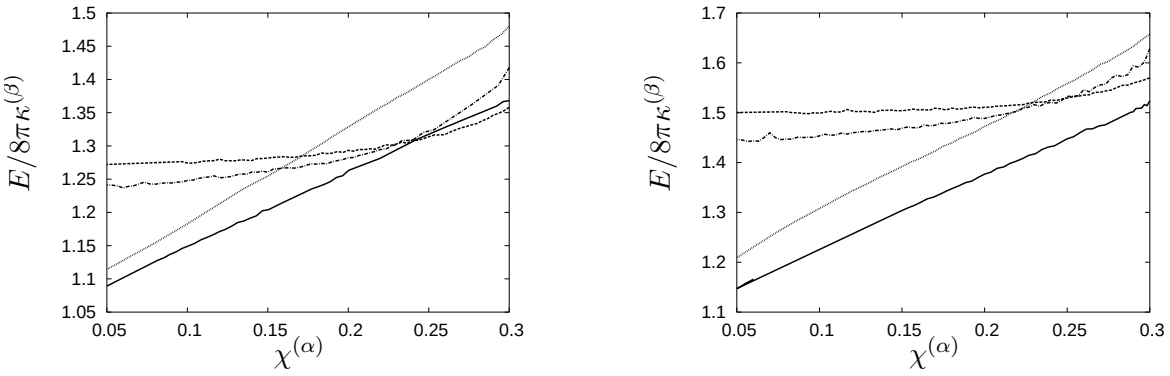

Figure 4.5: Ground state energy of a fluid vesicle with solid domains without volume constraints, same parameter values as in Fig. 4.3 but with bending rigidity ratio $\epsilon^\kappa = 1$. The minimum energy E of a vesicle with a round solid domain (I_1) (solid line), a cylindrical ring, $\chi_{(\beta_1,\beta_2)} = 0.5$ (I_{2a}) (dashed line), a conical ring, $\chi_{(\beta_1,\beta_2)} = 0.5$ (I_{2b}) (alternating dots and dashes), and two solid domains, $\chi_{(\alpha_1,\alpha_2)} = 0.5$ (II_1) (dotted line) is plotted as a function of solid area fraction $\chi^{(\alpha)}$ for the reduced line tension (a) $\lambda = 0.5$ and (b) $\lambda = 1$.

rigidity ratios and different reduced line tensions. For the typical condition that the solid membrane is about one order of magnitude stiffer than the fluid membrane [20], morphology I_1 is found to be the optimal conformation for small solid area fraction $\chi^{(\alpha)}$. For larger area fraction, morphology II_1 has the smallest energy. This is demonstrated in Fig. 4.3a and Fig. 4.3b where the minimum energy of the different vesicle morphologies is shown as a function of $\chi^{(\alpha)}$ for bending rigidity ratio $\epsilon^\kappa = 10$ and reduced line tension $\lambda = 0.5$ and $\lambda = 1$, respectively. The value of $\chi^{(\alpha)}$, where the crossover from one to two solid domains takes place, depends on λ. It is shifted towards a larger area fraction $\chi^{(\alpha)}$ as the line tension is increased. For $\epsilon^\kappa = 10$ and $\lambda = 0.5$, the transition occurs at about $\chi^{(\alpha)} \simeq 0.1$, while for $\lambda = 1$ it occurs at $\chi^{(\alpha)} \simeq 0.15$.

The diagrams in Fig. 4.3 also include the ground state energies of the ring-like solid domains morphologies, morphology I_{2a} and morphology I_{2b}. In general, the ground state energy of the cylindrical and conical ring is found to be comparable and considerably larger than the ground state energy of the vesicle with one, respectively two domains. The conical ring, morphology I_{2b}, has a slightly smaller energy than the cylindrical ring, morphology I_{2a}. Yet, as $\chi^{(\alpha)}$ increases, the energies of the ring-like domains become closer.

The situation changes slightly when the difference in the bending rigidity between solid and fluid membrane is less pronounced. As the data in Fig. 4.4 ($\epsilon^\kappa = 6$) shows, morphology I_1, respectively II_1, still remain the optimum configuration. Yet, as ϵ^κ decreases, the transition between morphology I_1 and II_1 occurs at a larger solid area fraction $\chi^{(\alpha)}$. In addition, for small values of λ, there is a crossover in the energy between the metastable morphology I_1 and the metastable morphologies I_{2a} and I_{2b}, see Fig. 4.4a.

The crossover towards the morphologies with a ring-like solid domain, morphology I_{2a} and I_{2b}, becomes relevant, if the bending rigidities of the solid and fluid membrane become similar and the reduced line tension λ is small. Fig. 4.5a shows the ground state energy for equal bending rigidity in the solid and fluid phase, $\epsilon^\kappa = 1$, and $\lambda = 0.5$. While for $\lambda = 0.5$

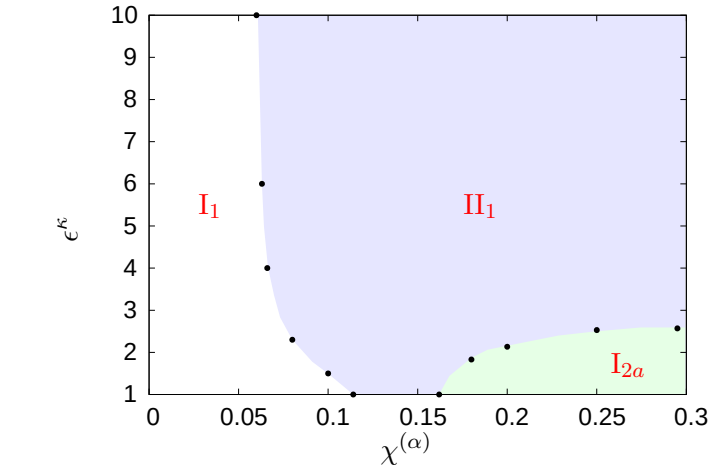

(a)

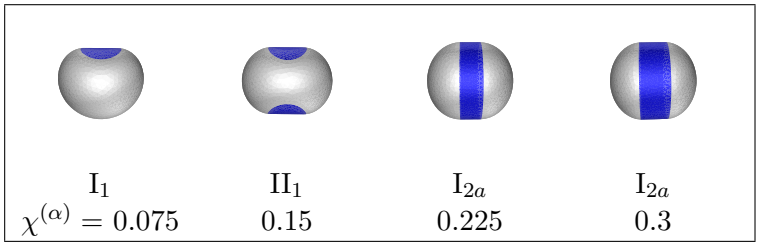

(b)

Figure 4.6: (a) Morphology diagram of an unconstrained fluid vesicle with solid membrane domains at temperature $T = 0$ as a function of the area fraction $\chi^{(\alpha)}$ and the bending rigidity ratio ϵ^κ for the reduced line tension $\lambda = 0.2$. (b) Corresponding shapes of minimum energy for $\epsilon^\kappa = 2$ and increasing area fraction $\chi^{(\alpha)}$.

morphology I_1 is optimal for $\chi^{(\alpha)} \lesssim 0.24$, one finds that above $\chi^{(\alpha)} \gtrsim 0.24$ morphology I_{2a} has the lowest ground state energy. This morphological transition does not occur for larger values of λ, see Fig. 4.5a for $\lambda = 1$. For $\lambda = 1$, morphology I_1 is optimal for $\chi^{(\alpha)} \leq 0.3$.

The full information as to which domain morphology has lowest energy at a given set of parameters is shown in the morphology diagrams of Fig. 4.6 - Fig. 4.8. These diagrams contain the main results of this subsection regarding unconstrained vesicles without volume constraints. The equilibrium morphology is displayed as a function of the bending rigidity ratio ϵ^κ and area fraction $\chi^{(\alpha)}$ for the reduced line tension $\lambda = 0.2$ (Fig. 4.6a), $\lambda = 0.5$ (Fig. 4.7a) and $\lambda = 1$ (Fig. 4.8a). We obtain the following picture: For a stiff solid membrane, morphology I_1 is the optimum configuration only at small solid area fraction. Above a certain value of $\chi^{(\alpha)}$, a transition towards morphology II_1 occurs. The value of $\chi^{(\alpha)}$ where the crossover towards a vesicle with two solid domains takes place depends on ϵ^κ and λ. It is shifted towards a larger solid area fraction, as the line tension λ increases and/or ϵ^κ decreases. For $\epsilon = 10$ and $\lambda = 0.2$, the transition occurs at $\chi^{(\alpha)} \simeq 0.06$, while for $\lambda = 1$ it occurs at $\chi^{(\alpha)} \simeq 0.15$. As ϵ^κ decreases, morphology I_1 becomes increasingly favourable. For $\epsilon = 1$ and $\lambda = 0.2$, the transition occurs at $\chi^{(\alpha)} \simeq 0.11$ (Fig. 4.6a), whereas for $\lambda = 1$ it does not occur any more in the range of the investigated solid area fraction (Fig. 4.8a).

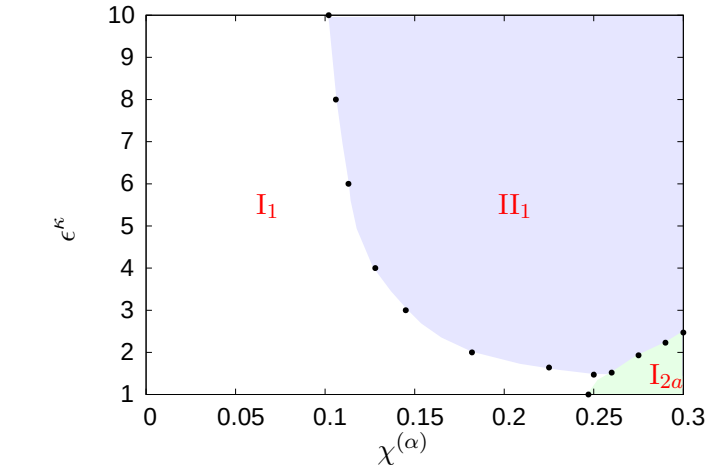

(a)

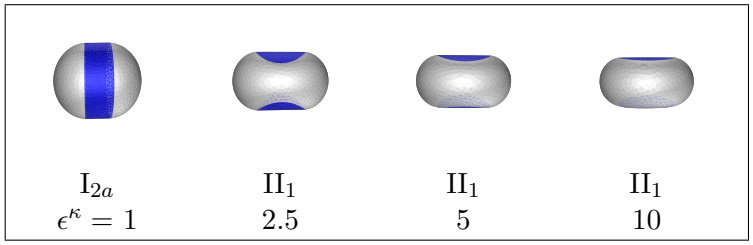

(b)

Figure 4.7: (a) Morphology diagram of an unconstrained fluid vesicle with solid membrane domains at temperature $T = 0$ as a function of the solid area fraction $\chi^{(\alpha)}$ and the bending rigidity ratio ϵ^κ for the reduced line tension $\lambda = 0.5$. (b) Corresponding shapes of minimum energy for area fraction $\chi^{(\alpha)} = 0.275$ and increasing bending rigidity ratio ϵ^κ.

For small line tension and similar bending rigidities of the fluid and solid membrane, there is a transition to morphology I_{2a}, as the solid area fraction $\chi^{(\alpha)}$ is increased and/or ϵ^κ decreases. The cylindrical domain shape, morphology I_{2a}, is found to have a slightly smaller ground state energy than the conical domain, morphology I_{2b} in regions where ring-like conformations become important. The value of $\chi^{(\alpha)}$, where the transition to morphology I_{2a} occurs, depends on ϵ^κ and λ. The transition occurs at larger $\chi^{(\alpha)}$, as the line tension increases. For $\epsilon = 1$ and $\lambda = 0.2$, it occurs at $\chi^{(\alpha)} \simeq 0.16$ (Fig. 4.6a), whereas for $\epsilon = 1$ and $\lambda = 0.5$ the transition takes place at about $\chi^{(\alpha)} \simeq 0.25$ (Fig. 4.7a). For $\epsilon = 1$ and $\lambda = 1$, this transition is not observed any more in the range of investigated solid area fraction $\chi^{(\alpha)}$ (Fig. 4.8a).

How can these results be understood qualitatively? First, line energy favours the vesicle with the round solid domain, morphology I_1, because the interface length of the round domain is the shortest for the investigated values of $\chi^{(\alpha)}$. This explains why the region in the morphology diagram where morphology I_1 has lowest energy enlarges when the line tension increases. Then, regarding bending energy, if the bending energy of the vesicle is dominated by the contribution of the stiffer solid membrane, the vesicle adapts a configuration where the solid membrane remains comparably flat. As the configurations in Fig. 4.8b show, the vesicle is deflated. This is possible because the vesicle can change its volume. Morphology I_1 is the equilibrium morphology only for small values of $\chi^{(\alpha)}$, because for larger area fraction the solid

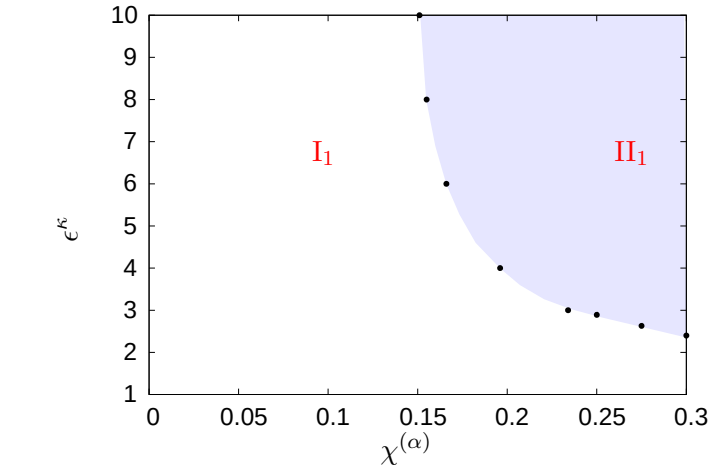

(a)

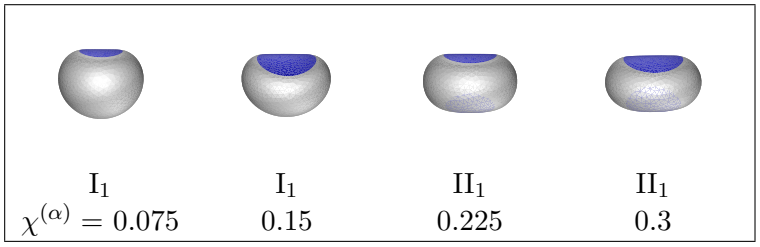

(b)

Figure 4.8: (a) Morphology diagram of an unconstrained fluid vesicle with solid membrane domains at temperature $T = 0$ as a function of the solid area fraction $\chi^{(\alpha)}$ and the bending rigidity ratio ϵ^κ for the reduced line tension $\lambda = 1$. (b) Corresponding shapes of minimum energy for $\epsilon^\kappa = 6$ and increasing area fraction $\chi^{(\alpha)}$.

membrane would have to bend considerably in order to adapt to the vesicle geometry. For large solid area fraction, the vesicle with two domains, type II_1, has the smallest energy. The higher line energy and slightly higher bending energy of the fluid membrane in morphology II_1 is compensated by the smaller bending deformation of the solid membrane. The contributions to the bending energy from the solid membrane become less relevant when the difference in the bending rigidities of the two membrane phases diminishes. This is why for smaller values of ϵ^κ the transition to the vesicle with two solid domains sets in at a larger value of $\chi^{(\alpha)}$.

Vesicles with a ring-like domain shape, morphology I_{2a} and I_{2b}, are unfavourable at large ϵ^κ for similar reasons. The solid membrane is bent around the vesicle which involves a high bending energy for the solid membrane. In addition, the ring-like domain shapes have a long domain interface and thus a high line energy. Yet, for large area fraction the cylindrical ring, morphology I_{2a}, causes less deformation of the fluid membrane than the other morphologies. The smaller bending energy of the fluid membrane becomes important for similar bending rigidities in both phases and small line tension. Therefore, a transition towards morphology I_{2a} occurs at small line tension, large solid area fraction and similar bending rigidities.

Regarding the different ring-like domain morphologies, for small solid area fraction the conical shape, morphology I_{2b}, is found to have a slightly smaller ground state energy than

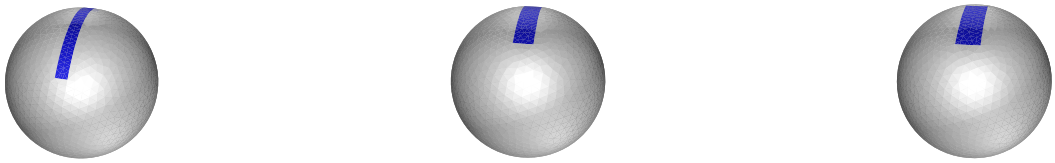

(a) (b) (c)

Figure 4.9: An anisotropic line tension gives rise to stripe-like domain shapes. Vesicle morphologies with (a) anisotropy of the line tension $\bar{\lambda} = 0.075$, (b) $\bar{\lambda} = 0.2$, and (c) $\bar{\lambda} = 0.3$.

the cylindrical ring, morphology I_{2a}. This is due to the smaller boundary length between the solid and fluid membrane domain. Morphology I_{2b}, however, causes in general larger bending deformation. If line energy becomes less relevant and the contributions from the bending of the solid and fluid membrane are more important, the morphology I_{2a} has a smaller ground state energy than the morphology I_{2b}. This applies for small λ and large $\chi^{(\alpha)}$, which is the case when the ring-like conformations become the equilibrium morphology.

Anisotropic line tension

So far, the solid membrane has been treated as an isotropic elastic material with isotropic bending and isotropic line energies. While this is a good approximation for many lipid phases such as the L_β phase, the approach neglects important properties of phases like the $L_{\beta'}$ and $P_{\beta'}$ ('rippled') phase where due to the tilting of the molecules or the corrugation of the membrane certain directions are distinguished. In order to describe such phases, anisotropic material parameters must be considered. In principle, one could think of introducing anisotropy in the bending energy [162] and in the line tension. In the following we include the effects of an anisotropic line tension. By this, we are able to demonstrate that an anisotropic line tension may give rise to stripe-like domain shapes as they are observed in the $P_{\beta'}$ phase.

In general, the equilibrium shape of a material is determined by the minimum of the interfacial (free) energy. In anisotropic media, the line tension $\lambda^{(\alpha,\beta)}$ is not a constant but depends on the orientation of the interface with respect to the symmetry axes such as the crystallographic axes in a solid crystal or the director in a nematic liquid crystal. If the interfacial energy $\lambda^{(\alpha,\beta)}(\mathbf{n})$ is known as a function of all orientations $\mathbf{n}$, the minimisation of the interfacial free energy can be performed by a construction proposed by Wulff long time ago [133, 163] [4].

In the limit of $T \to 0$, this procedure yields morphologies which consist of facets. As temperature increases, the faceting of the crystals progressively disappears. Thermal fluctuations start to smooth out the sharp edges, leaving planar facets which are connected by rounded surfaces. Above the so-called roughening temperature, the facets disappear and the complete crystal becomes rounded. It is, however, not spherical, since the surface tension remains

[4] Thereby, the equilibrium crystal shape is determined in a geometric way as follows: For each orientation $\mathbf{n}$ a ray is drawn from the origin with length proportional to $\lambda^{(\alpha,\beta)}(\mathbf{n})$. At the end of each ray the perpendicular plane is constructed. The crystal shape of minimum free energy is given by the inner envelope of these planes.

anisotropic. It turns out that for two-dimensional crystals (with underlying sufficiently short-ranged forces) the roughening temperature is zero and thus all crystal surfaces are smoothly curved for $T > 0$.

For the moment we are interested in shapes of minimum energy. Thus, we neglect entropic contributions and consider completely faceted crystal shapes. For simplicity we assume a rectangular domain shape which is specified by a line tension along the two sides of the rectangle, say $\lambda_{\mathrm{a}}^{(\alpha,\beta)}$ along side a and $\lambda_{\mathrm{b}}^{(\alpha,\beta)}$ along side b. The equilibrium shape of a planar crystal is then a rectangle with a length ratio of the a- and b- side of $\lambda_{\mathrm{b}}^{(\alpha,\beta)} : \lambda_{\mathrm{a}}^{(\alpha,\beta)}$. We denote the anisotropy of the line tension by $\bar{\lambda}$

$$\bar{\lambda} = \frac{\lambda_{\mathrm{b}}^{(\alpha,\beta)}}{\lambda_{\mathrm{a}}^{(\alpha,\beta)}} \,. \tag{4.10}$$

Stripe-like domain shapes can be achieved by a large anisotropy of the line tension $\bar{\lambda}$. This is demonstrated in Fig. 4.9 for different values of $\bar{\lambda}$. The obtained stripe-like domains agree well with the domain shapes observed experimentally in the $P_{\beta'}$ phase.

4.5.2 Vesicles with volume constraints

It is interesting to ask whether volume constraints have a significant impact on the domain shapes. For a fixed vesicle volume around $v \simeq 0.9$, the morphology diagram is expected to be qualitatively similar to the unconstrained case. This is because in the unconstrained case the vesicle deflates and acquires a reduced volume around this value.

A more interesting case to study is the situation of a vesicle geometry close to a sphere, i.e. $v \simeq 1$. Apparently, as the vesicle geometry approaches a sphere, it becomes increasingly difficult to adapt a single or two solid domains which cannot be stretched onto the vesicle geometry. Therefore, for a vesicle geometry close to a sphere, the phase separation will not lead to one or two domains but to several smaller domains which can more easily adjust to an almost spherical geometry.

In this section we investigate vesicles with volume constraints, focussing on reduced volumes close to one. For this geometry, the analysis needs to be extended to vesicles with a larger number of solid domains. In the following we determine and compare the equilibrium energy of vesicles with up to five solid domains, see Fig. 4.10. The morphologies are denoted with I_1, II_1, III_1, IV_1, and V_1, respectively. Ring-like solid domains are neglected because for the parameter values studied they do not play a role.

Minimisation Method

With the minimisation method used in the previous section numerical difficulties are encountered when it is applied to a larger number of domains. To circumvent problems, we resort to a Monte Carlo annealing technique for minimisation. This is a generalisation of the Metropolis Monte Carlo technique in which the temperature of the system is slowly decreased in a sequence of annealing steps so that in the end the configuration with minimal energy is obtained.

The vesicle conformation is represented by a triangulated surface according to the tether and bead model. To describe two different phases, the model has to be generalised to two different components A and B. Thereby, the information of the phase can be placed either on the surface triangles [164] or on the vertices [165]. With respect to resolution in the two

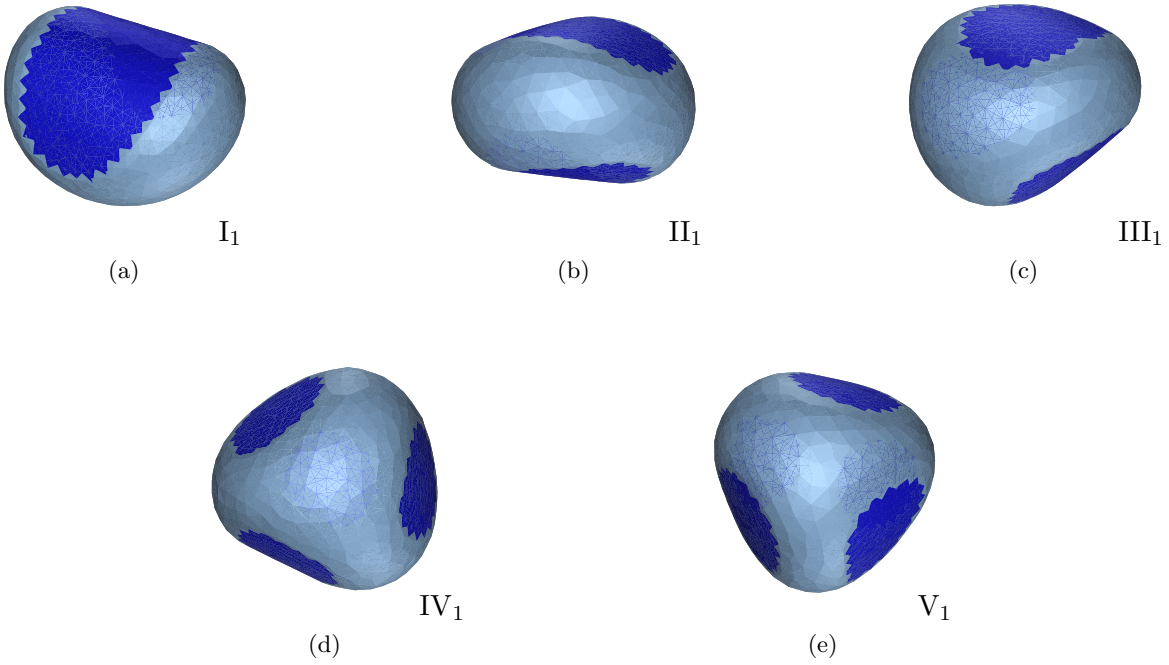

Figure 4.10: Equilibrium configurations for a vesicle with fluid (white) and several solid (blue) domains (with reduced volume $v = 0.96$, solid area fraction $\chi^{(\alpha)} = 0.3$, reduced line tension $\lambda = 1$, and bending rigidity ratio $\epsilon^{\kappa} = 6$): (a) single solid domain (I_1), (b) two solid domains (II_1), (c) three solid domains (III_1), (d) four solid domains (IV_1), and (d) five solid domains (V_1). The roughness of the domain boundaries reflects the discretisation of the vesicle surface.

components, it is advantageous to associate the component information onto the triangles as there are about twice as many triangles as vertices for the same triangulation. Yet for our calculation, the different phases have to be assigned to the vertices because the two phases differ (amongst others) in their properties regarding the Gaussian curvature, which is evaluated on a vertex. The line energy is calculated by

$$\mathcal{H}_{\text{line}} = \lambda \sum_{e_i} l_i \,, \tag{4.11}$$

where the summation extends over all edges e_i which connect vertices of different species A and B. The length l_i is the length of the edge in the dual lattice associated to e_i.

To obtain states with minimum energy, we proceed as follows. First, the vesicle is initialised with $N_v = 770$ beads and the desired domain topology. For simplicity, we assume that coexisting solid domains are approximately equal in size. During the minimisation process single vertices are displaced at random. Bond flips are performed to improve the triangulation. Besides, the type of beads is exchanged, taking care to conserve the domain topology and approximately the area of the individual domains. This rearrangement of the bead type optimises the shape and the distance between the different solid domains. A new configuration is accepted or rejected according to the Metropolis scheme. To find the energy minimum, the temperature is slowly decreased from $T = 0.1\,\kappa^{(\beta)}$ to $T = 0.005\,\kappa^{(\beta)}$, using about 20

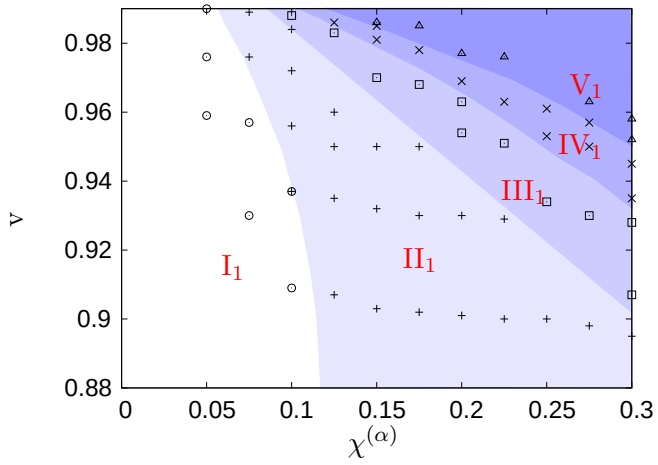

(a)

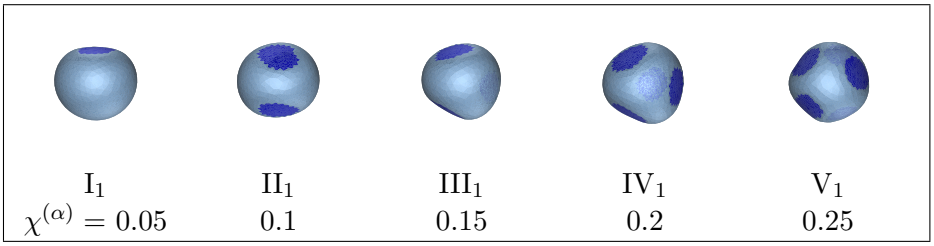

(b)

Figure 4.11: (a) Morphology diagram of a fluid vesicle with solid domains at temperature $T = 0$ with volume constraints. The equilibrium shape of a vesicle with bending stiffness ratio $\epsilon^\kappa = 10$ and reduced line tension $\lambda = 0.2$ is shown as a function of the solid area fraction $\chi^{(\alpha)}$ and the reduced volume v, focussing on v approaching one ($\circ$ 1 solid domain (I_1), $+$ 2 solid domains (II_1), $\boxdot$ 3 solid domains (III_1), $\times$ 4 solid domains (IV_1), $\triangle$ 5 solid domains (V_1)). (b) Corresponding shapes of minimum energy for $v = 0.97$ and increasing area fraction $\chi^{(\alpha)}$.

consecutive annealing steps, where in each step the system is allowed to equilibrate.

Numerical results

We focus on almost spherical vesicle geometries, i.e. v close to one. Fig. 4.11 - Fig. 4.13 display the morphology diagrams as a function of the solid area fraction $\chi^{(\alpha)}$ and the reduced volume v for different material parameters, bending stiffness ratio $\epsilon^\kappa = 10$ and $\epsilon^\kappa = 6$ and reduced line tension $\lambda = 0.2$, $\lambda = 0.5$ and $\lambda = 1$. These diagrams contain the main results for vesicles with fixed reduced volumes. We summarise the main findings:

First of all, as the vesicle geometry becomes more spherical, we observe morphological transitions from vesicles with a smaller number of solid domains to vesicles with an increasing number of solid domains. This is a general result and is seen in each of the diagrams in Fig. 4.11 - Fig. 4.13. For example, for $\epsilon^\kappa = 10$ and $\lambda = 0.2$ (Fig. 4.11), at $v \simeq 0.9$ the vesicle with one solid domain, morphology I_1, has the lowest ground state energy for $\chi^{(\alpha)} \lesssim 0.12$, followed by the vesicle with two solid domains, morphology II_1, for larger $\chi^{(\alpha)}$. As v approaches one, the transition between morphology I_1 and II_1 is shifted towards smaller values of $\chi^{(\alpha)}$. For

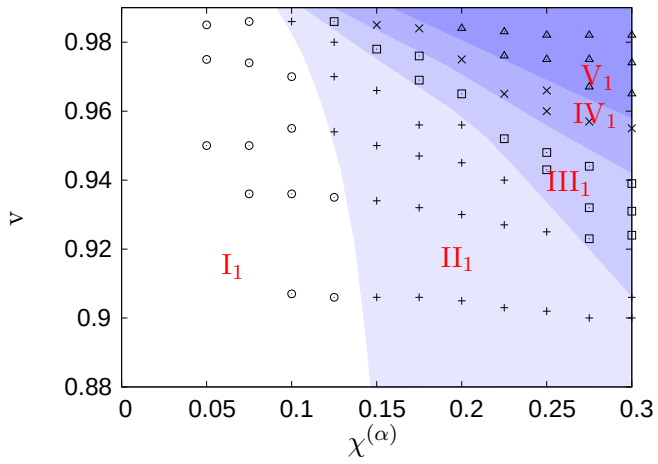

(a)

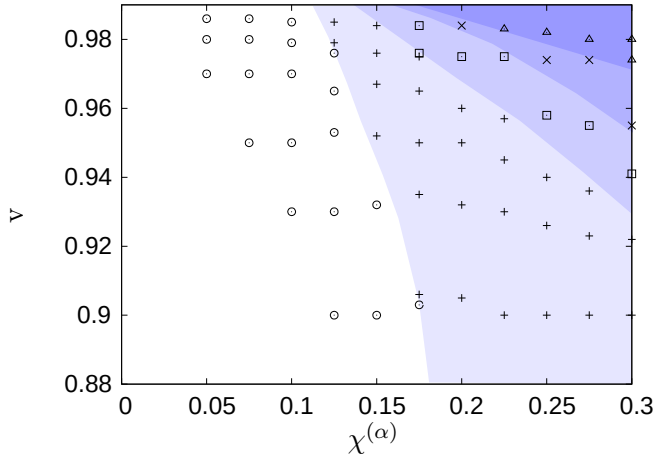

(b)

Figure 4.12: Morphology diagram of a fluid vesicle with solid domains at temperature $T = 0$ with volume constraints; same material parameters as in Fig. 4.11 (bending stiffness ratio $\epsilon^{\kappa} = 10$), but with different reduced line tension (a) $\lambda = 0.5$ and (b) $\lambda = 1$. The equilibrium shape of a vesicle is shown as a function of the solid area fraction $\chi^{(\alpha)}$ and the reduced volume v, focussing on v approaching one ($\circ$ 1 solid domain (I_1), $+$ 2 solid domains (II_1), $\boxdot$ 3 solid domains (III_1), $\times$ 4 solid domains (IV_1), $\triangle$ 5 solid domains (V_1)).

$v = 0.98$, it occurs at about $\chi^{(\alpha)} \simeq 0.07$. The effect is more pronounced for large solid area fraction $\chi^{(\alpha)}$. For $\chi^{(\alpha)} = 0.3$, morphology II_1 is found to be optimal for $v = 0.9$, while above $v \gtrsim 0.955$ the vesicle with five (or more – five is the largest number of solid domains considered) solid domains, morphology V_1, has the smallest energy.

Then, the number of solid domains is found to increase as the solid area fraction is increased. The effect is most striking for a reduced volume close to one. In the above example, for $v = 0.98$, there is a transition from morphology I_1 to morphology II_1 at $\chi^{(\alpha)} \simeq 0.07$, which is followed by a transition to morphology III_1 at about $\chi^{(\alpha)} \simeq 0.11$. At $\chi^{(\alpha)} \simeq 0.14$, morphology IV_1 becomes the equilibrium morphology and finally, above $\chi^{(\alpha)} \gtrsim 0.18$ morphology V_1 has the

smallest energy.

A higher line tension acts to favour a smaller number of domains. This is learnt by comparing the diagrams with different λ ($\lambda = 0.2, 0.5, 1$) in Fig. 4.11 and Fig. 4.12 (for $\epsilon^\kappa = 10$) and in Fig. 4.13 (for $\epsilon^\kappa = 6$), respectively. In general, the line tension is found to have a larger influence for the smaller bending rigidity ratio $\epsilon^\kappa = 6$, where the bending energy of the solid domain is less dominant.

To study the impact of a difference in the bending rigidity between the solid and fluid membrane, the corresponding diagrams in Fig. 4.11 and Fig. 4.12 ($\epsilon^\kappa = 10$) and Fig. 4.13 ($\epsilon^\kappa = 6$) with same λ have to be compared. The data shows that a stiffer solid membrane leads to vesicle morphologies with a larger number of solid domains. The effect is most pronounced for vesicles with an almost spherical geometry with a large solid area fraction.

Finally, we briefly comment on the arrangement of the solid domains in mechanical equilibrium. The discussion remains qualitatively. By inspection of the obtained equilibrium states we find that the domains typically tend to be separated from each other as far as possible. This holds especially for domains which have a comparably large size and thus affect the curvature of the fluid membrane. The effect indicates an effective repulsive interaction between the solid domains. The repulsion between the solid domains is induced by the deformation of the fluid membrane caused by the solid domains. A similar membrane mediated interaction is found between stiff inclusions of extended size on a vesicle [166, 167]. For small domain sizes which have a seemingly little impact on the curvature of the fluid domain such a repulsive interaction between the individual domains is not necessarily observed. It should also be noted that constraints of the vesicle geometry crucially affect the arrangement of the solid domains. This is seen by comparing the vesicle morphology II_1 in Fig. 4.7b and Fig. 4.12b.

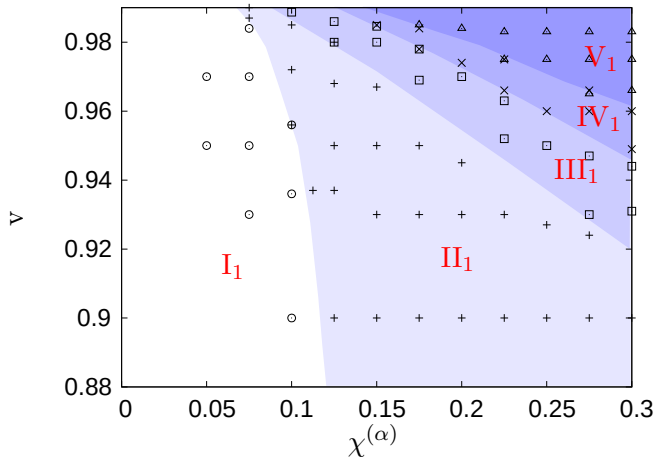

(a)

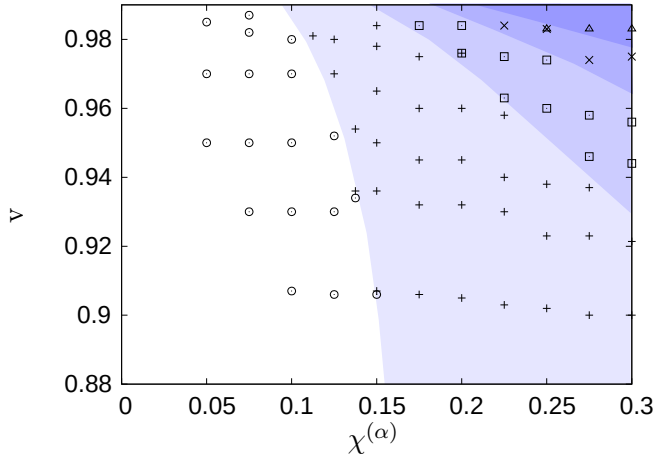

(b)

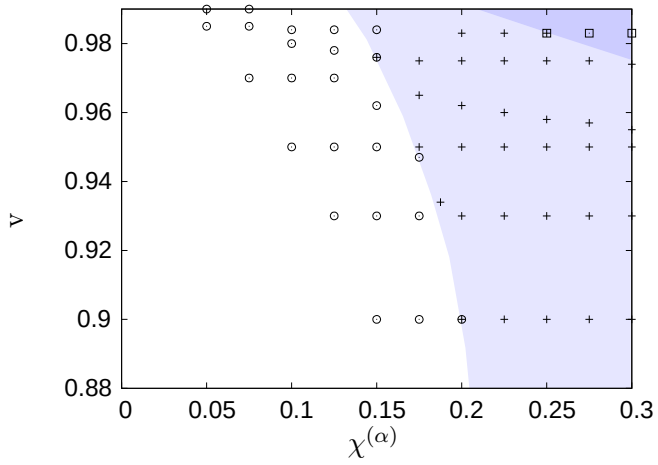

(c)

Figure 4.13: Morphology diagram of a fluid vesicle with solid domains at temperature $T = 0$ with volume constraints. The equilibrium shape of a vesicle is shown as a function of the solid area fraction $\chi^{(\alpha)}$ and the reduced volume v for the bending stiffness ratio $\epsilon^{\kappa} = 6$ and (a) reduced line tension $\lambda = 0.2$, (b) $\lambda = 0.5$, and (c) $\lambda = 1$ ($\circ$ 1 solid domain (I_1), $+$ 2 solid domains (II_1), $\boxdot$ 3 solid domains (III_1), $\times$ 4 solid domains (IV_1), $\triangle$ 5 solid domains (V_1)).

4.6 Thermal fluctuations

Up to now, the analysis was focused on equilibrium states with minimum energy, which formally corresponds to zero temperature. At finite temperature, entropic degrees of freedom have to be included. There are a number of effects from thermal fluctuations that influence the domain shapes in different ways. First, entropy favours a larger number of domains due to the larger translational and rotational in-plane degrees of freedom. Then, the different domain morphologies alter the membrane undulations in a distinct way. The undulation spectrum of fluctuating membranes is not only determined by the internal membrane structure, cf. chapter 2, but also modified by imposed boundary conditions. On a vesicle they are affected by the presence of domains. The specific arrangement of the solid domains restricts possible undulation modes of the fluid membrane in between. It is not obvious whether this favours a smaller or larger number of domains.

In addition, the modification of the possible fluctuation modes of the fluid membrane gives rise to Casimir-like forces between the domains. They are purely entropic in nature and have to be superimposed on the elastic interactions which are mediated by static membrane deformations. Whether these additional fluctuation-induced forces are attractive or repulsive is not clear, either. Solid domains are quite stiff and, in a first approximation, can be treated as rigid membrane inclusions. For completely stiff membrane inclusions, Casimir forces are shown to be attractive on almost planar membranes [37, 166, 168, 169].

4.6.1 Monte Carlo simulations

To quantify the impact of thermal fluctuations we perform Monte Carlo simulations on the triangulated surface with two membrane components. We determine and compare the thermal mean energy of vesicles with different domain shapes. The vesicle shapes with minimal thermal energy are arranged in morphology diagrams [5].

Simulation details

The vesicle is initialised with $N_v = 770$ beads and the desired domain topology, cf. subsection 4.5.2. For simplicity, the coexisting solid domains are assumed to be equal in size. During the simulation the domain topology and approximately the area of the individual domains is kept fixed. The following Monte Carlo moves are attempted in random order: single displacements of random vertices, bond flips and exchange of the type of phase between two beads. In one simulation we typically perform about $4.5 \cdot 10^6$ MC moves, about half of them are used for thermal averages. We neglect thermally excited defects, for the solid membrane only those bending deformations are allowed which remain isometric to a plane. This is assured with an auxiliary potential in the square of the Gaussian curvature, Eq. (4.9). Fig. 4.14 illustrates

[5] In principle, to include all effects of thermal fluctuations the free energy difference between vesicles with different domain topologies has to be calculated. However, with domain formation on vesicles one faces practical problems to determine free energy differences. For a system that in the course of a single simulation practically does not evolve into the different states of interest (as it is the case here with different domain shapes), free energy profile cannot be obtained directly by measuring relative frequencies. A possible alternative to compare the free energy of different states is to compute free energy differences via thermodynamic integration from a common reference state [170]. Applied to the vesicles, as the common reference state a homogeneous fluid vesicle can be chosen where the differences between the membrane phases diminish. In practice, however, thermodynamic integration was found computationally very expensive and it was not feasible to obtain sufficiently reliable statistics.

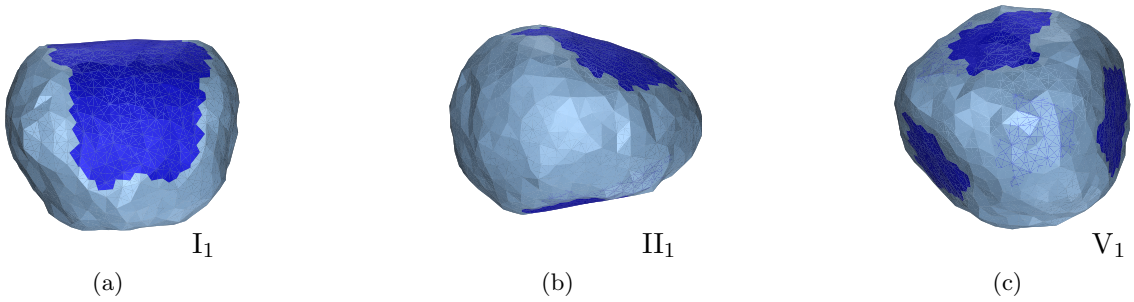

(a) (b) (c)

Figure 4.14: Snapshot of a fluctuating fluid vesicle with a (a) single solid domain (I_1), (b) two solid domains (II_1), and (c) five solid domains (V_1), reduced volume $v = 0.95$, bending rigidity ratio $\epsilon^\kappa = 10$, and reduced line tension $\lambda = 0.5$.

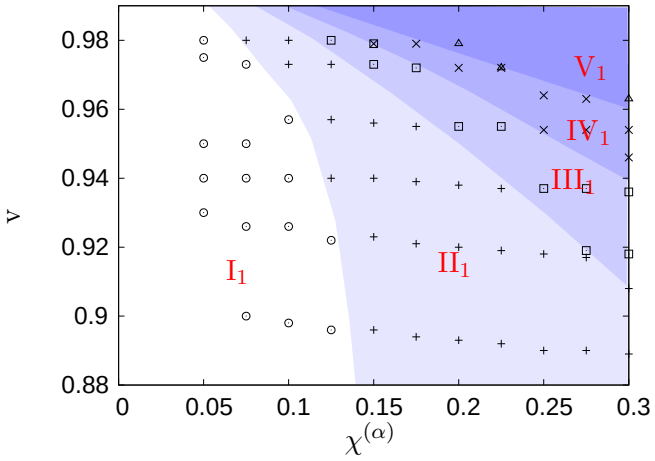

Figure 4.15: Morphology diagram of a fluid vesicle with solid domains at finite temperature $T = 0.1\,\kappa^{(\beta)}$ with volume constraints. The vesicle shape with minimum thermal mean energy is shown as a function of the solid area fraction $\chi^{(\alpha)}$ and the reduced volume v for the bending stiffness ratio $\epsilon^\kappa = 6$ and (a) reduced line tension $\lambda = 0.2$ ($\circ$ 1 solid domain (I_1), $+$ 2 solid domains (II_1), $\boxdot$ 3 solid domains (III_1), $\times$ 4 solid domains (IV_1), $\triangle$ 5 solid domains (V_1)).

typical vesicle configurations for domain topologies considered in the simulations.

Numerical results

Fig. 4.15 displays the morphology diagram for a vesicle with volume constraints as a function of $\chi^{(\alpha)}$ and v at $T = 0.1\,\kappa^{(\beta)}$ for $\epsilon^\kappa = 10$ and $\lambda = 0.5$. A comparison with the corresponding data at zero temperature, diagram Fig. 4.12a, shows that thermal fluctuations only have a minor influence on the domain morphologies. The data at finite temperature agrees qualitatively with the results for zero temperature. Only at vesicle geometries close to one, where morphologies with several domains exist, the crossover to more domains occurs at slightly smaller values of $\chi^{(\alpha)}$.

4.7 Discussion and conclusion

In this chapter we have investigated the geometry of fluid vesicles with solid membrane domains. Unconstrained vesicles and vesicles with volume constraints are studied. For the solid domains we have assumed that their in-plane elastic energies are exceedingly large so that they cannot be stretched, i.e. we address the limit of a large Föppl-von Kármán number γ. Since for a realistic vesicle of radius $10\mu m$ one has $\gamma \approx 10^{10}$, this limit is reasonable for solid domains on vesicles. Furthermore, we have assumed that the ground state of the solid domains is free of disclinations which implies that the conformations of the solid domains are restricted to developable surfaces.

The equilibrium morphology with minimum energy are summarised in morphology diagrams. Due to the restricted bending modes of the solid membrane and a competition between line energy and bending energy various morphological transitions between vesicles with different domain shapes are observed. For typical values of the bending rigidity, the vesicle with one round solid domain, morphology I_1, is found to be the equilibrium shape for small solid area fraction. As the area fraction of the solid membrane increases, vesicles with two or more solid domains are shown to be the equilibrium shape. The tendency to more solid domains is enforced on a constrained vesicle with almost spherical geometry. Thermal fluctuations are found to have only minor influence on the vesicle morphology. An anisotropic line tension is shown to lead to stripe-like solid domain shapes, as they are experimentally observed in the $P_{\beta'}$ phase.

Comparison with related work in literature

How do our results compare with the conclusions of the related work in the articles [136] and [137]? In [136] and [137] the authors consider the limit of small γ and study solid domain shapes on spherical geometries. The limit of small γ is relevant for domain shapes on colloidosomes. In this case, the domain shapes are determined by a competition between line tension and stretching energy. It is found that, analogous to our observation, at low solid area fraction and large line tension the preferred domain morphologies are round (cap-like on a sphere), with a tendency to an increasing number of caps as the area fraction increases. For large solid area fraction (and/or large Young modulus), a transition from several caps to a ribbon or ring-like structure is observed. Applied to a typical vesicle with radius $10\mu m$, the results for small γ would imply that the transition from cap-like domains to ring-like domain shapes occurs at comparably small solid area fraction $\chi^{(\alpha)}$, for $\lambda^{(\alpha,\beta)}R_0/(k_Y R_0^2) \simeq 10^7$ at about $\chi^{(\alpha)} \simeq 0.04$. In the limit of large γ, for typical bending moduli of the lipid membranes we do not observe a transition to stripe-like domains. Thus, stripe-like domain shapes in vesicles, as experimentally observed in the $P_{\beta'}$ phase, are most probably a consequence of the anisotropy of the solid membrane, either in the bending rigidity and/or the line tension.

Comparison with experiment

Our results propose that bending elasticity may play a role in limiting the size of solid domains on almost spherical vesicles. Whether the size limit indeed is related to the bending elasticity of the solid membrane can be checked experimentally. One would have to investigate whether and how the domain size depends on the vesicle radius. In contrast to other explanations such as for example electrostatic mechanisms, a size limitation caused by bending elasticity would imply that the size of the domains varies with the size of the vesicle and does

not favour an independent length scale. When evaluating the size dependence of the solid domains, one should keep in mind that the reduced line tension depends on the vesicle radius, see Eq. (4.6), which influences the results.

In this chapter we have determined the equilibrium configuration with minimum energy. In experiments the growth of crystals typically occurs under conditions that are far from equilibrium and the relaxation to the equilibrium configuration may be kinetically hindered due to slow diffusion. Crystal forms are then determined by growth kinetics rather than equilibrium considerations. Re-equilibration of a non-equilibrium mesoscopic crystal requires transport of material over larger distances and time scales that can be unrealistically long. In order to fully understand the experimentally observed solid domain shapes it seems promising to account for the non-equilibrium processes of growth. This is, however, beyond the scope of this thesis.

Of course, there are some caveat with our coarse grained approach. The basic assumption for the solid membrane was that the ground state of the solid membrane is flat and free of defects. This seems a sound approximation for solid membranes obtained by freezing a single-component lipid vesicle. Such vesicles are observed to exhibit locally flat patches which are separated with sharp edges [14, 150]. Caution is advised when this assumption is applied to domains formed in a multi-component membrane such as in a vesicle made of a mixture of different lipids and cholesterol. These vesicles do not always look facetted. Typically, phase separation and domain formation is initiated by cooling a fluid vesicle. During the freezing process the initial curvature of the membrane is frozen in and with it various defects. In this case, the solid membrane does not acquire a perfect flat conformation without defects. It should be noted that defects also occur naturally in the different gel phases due to the different packing constraints of the hydrocarbon chains and the lipid headgroups. Furthermore, defects may be excited by thermal fluctuations in combination with membrane undulations. While many features can already be seen from our approximation, it may be worthwhile to include certain aspects of defects in a future study.

The latest experiments indicate that the solid domain morphologies are strongly correlated with the molecular organisation of the lipids in the different phases [78]. In order to describe these effects theoretically, one has to go beyond a coarse-grained elasticity theory of the solid membrane. The theory has to be refined to include more details of the underlying crystal structure.

Chapter 5

Vesicles with fluid membrane domains

In this chapter we study the morphology of vesicles with coexisting fluid membrane domains. We determine the *equilibrium* shape of vesicles with simple and complex domain topologies. The emphasis is on vesicles with comparably small line tension. We investigate the impact of different bending rigidities and different Gaussian curvature moduli between the fluid phases. As the material parameters are varied, morphological transitions between vesicles with different domain shapes are observed.

5.1 Introduction

Vesicles with coexisting fluid membrane domains have been subject to increased attention in the recent years, both experimentally [67, 171] and theoretically [62, 134, 172–176]. The research on domain formation in fluid membranes is motivated by the recently refined picture of the cell membrane which claims that, despite the fluidity of the lipid bilayer, the different membrane lipids do not mix homogeneously but aggregate into small clusters or domains, so-called lipid 'rafts' [63]. Lipid rafts are small regions in the cell membrane with an estimated size between 20 and 700 nm which are enriched in cholesterol and sphingolipid and float like rafts in the sea of the other membrane lipids. The importance of rafts is related to their biological function. Rafts are believed to participate in many biological processes and to perform various tasks in intracellular transport and signalling.

Up to now, experimental evidence for domain formation *in vivo* is rather indirect and the existence of rafts in biological membranes is still a matter of current debate. In contrast, in *in vitro* systems fluid domains are observed clearly [67]. A well studied model system is given by vesicles made of a ternary mixture of a sterol (like cholesterol), a lipid with a high melting point (such as sphingomyelin) and a lipid with a lower melting point. This composition is supposed to roughly reproduce raft composition. At appropriate conditions, due to the interaction with cholesterol, the lipids separate into two fluid phases, a liquid-disordered phase, which is rich in the low-melting point lipid, and a liquid-ordered phase, enriched with cholesterol and the high-melting point lipid. The resulting fluid domains are of micron-size range and can be observed by optical means, for example with fluorescence imaging techniques.

The formation of fluid membrane domains gives rise to new phenomena on vesicles. In general, the shape of a vesicle with coexisting fluid membrane domains is determined by an

interplay between bending energy of the membrane and line energy at the domain interface. Fluid domains are different from solid domains because a fluid domain can rearrange easily and adapt its shape. No in-plane stretching energy is involved when the membrane deforms. As a consequence, fluid membrane domains are unstable against the formation of a bulge or bud if their size is sufficiently large [134]. The budding transition is caused by line tension at the domain interface which tends to shrink the length of the domain interface.

Although vesicles with more than two membrane domains are frequently observed in experiments (cf. Fig. 1.7), it is commonly believed that, at equilibrium, a vesicle with two coexisting fluid membrane phases has two domains, one for each phase. Such a vesicle has the shortest domain boundary. Vesicles with more than two domains are assumed to be metastable, albeit long-lived. This is because the fusion process of domains is kinetically impeded when they form a more pronounced bud [73]. Previous theoretical work therefore focused mainly on equilibrium shapes of membranes and vesicles with two coexisting domains, beginning with a circular domain in a nearly planar membrane [134], two domains in vesicles with axial symmetry [172, 173] or simple domain shapes in membranes with more complex topology [177]. Less attention has been paid to vesicles with more complex domain shapes, for example stripes or multiple domains on vesicles (these shapes have been analysed in [175] for a nearly flat membrane). Complexer domain shapes, however, become important when the line energy is comparably small and not the dominating factor. In this case, other material parameters such as the different bending moduli have an increasing influence on the shape of the domains. The aim of the present chapter is to show that in this case vesicles with one domain for each phase are not necessarily the equilibrium state. As line tension decreases, morphological transitions to vesicles with more complex domain shapes occur.

This chapter is organised as follows. We start with a brief discussion of the simplest vesicle shape, an axisymmetric vesicle with two domains, one domain in each fluid phase. This vesicle shape is relevant for large line tension. Then, we turn to vesicles with more than two domains. These are shown to be become relevant for small line tension. Morphological diagrams of these vesicles are determined as a function of domain sizes, line tension and ratio of bending moduli of the fluid phases. Vesicles with and without volume constraints are considered.

5.2 The model

Analogous to our treatment of solid domains, we study in the following two fluid phases which are well segregated and form homogeneous domains which are separated by a sharp phase boundary. In a bilayer, phase separation can occur separately within both monolayers. Thus, domains can form in each monolayer individually. Our model applies to the following types of domains: monolayer domains, which lead to an asymmetric bilayer and thus can be characterised by a spontaneous curvature, and bilayer domains, which extend over both monolayers. The case that two monolayer domains overlap only partially is, in principle, included since overlapping monolayer domains can be considered to be composed of subdomains of the above domain types. We do not further consider this possibility.

Due to the coupling between membrane composition and shape, it is possible to have composition-induced changes in shape (curvature) [178] and curvature-induced changes in composition [179]. Unless the curvature is of a molecular scale, it is generally expected that composition drives shape, i.e. shape changes do not affect the thermodynamics of the mixture. This is because the curvature energy per molecule is very small compared to $k_{\mathrm{B}}T_0$. A shift in

the chemical potential caused by changes of the local curvature is expected to be insufficient to cause a significant change in composition.

As a consequence, we can assume that the membrane area occupied by each phase is independent of the membrane curvature. We denote the area covered by the fluid phase (α) with $A^{(\alpha)}$, and the area covered by phase (β) with $A^{(\beta)}$. The areas $A^{(\alpha)}$ and $A^{(\beta)}$ add up to the total area $A = A^{(\alpha)} + A^{(\beta)}$. As with solid domains, it is useful to introduce the relative area of the fluid phases

$$\chi^{(\alpha)} \equiv A^{(\alpha)}/A \qquad \text{and} \qquad \chi^{(\beta)} \equiv A^{(\beta)}/A = 1 - \chi^{(\alpha)} . \tag{5.1}$$

The membrane domain is bounded by a domain boundary with line tension $\lambda^{(\alpha,\beta)}$. The line tension $\lambda^{(\alpha,\beta)}$ is based on two contributions [157, 158, 180]. There is a physical-chemical contribution to the line tension which arises from the compositional inhomogeneity across the domain boundary, and a mechanical line-tension which results from the thickness difference between coexisting domains. The latter leads to membrane compression and tilt at the domain boundary to avoid that hydrophobic parts of the lipids get unscreened. For lipid bilayers, line tension estimates are typically of the order 10^{-12} N at physiological temperature [171]. The value of the line tension varies with temperature and reduces to 0 at the critical point of mixing/demixing where the difference between coexisting phases vanishes.

Energy contributions of the domains

With these assumptions, the vesicle conformation is determined by the (free) energy functional

$$\mathcal{H} = \int_\alpha dA \mathcal{H}^{(\alpha)}_{\text{fluid}} + \int_\beta dA \mathcal{H}^{(\beta)}_{\text{fluid}} + \lambda^{(\alpha,\beta)} \int_\partial dl + \sigma^{(\alpha)} A^{(\alpha)} + \sigma^{(\beta)} A^{(\beta)} + pV . \tag{5.2}$$

It consists of the bending energy

$$\mathcal{H}^{(\alpha)}_{\text{fluid}} = \frac{\kappa^{(\alpha)}}{2}(2H - C_0^{(\alpha)})^2 + \kappa_G^{(\alpha)} K \tag{5.3}$$

and

$$\mathcal{H}^{(\beta)}_{\text{fluid}} = \frac{\kappa^{(\beta)}}{2}(2H - C_0^{(\beta)})^2 + \kappa_G^{(\beta)} K . \tag{5.4}$$

of the phase (α) and (β), respectively, and a line energy which is proportional to the length of the domain boundary. The two Lagrange multipliers, $\sigma^{(\alpha)}$ and $\sigma^{(\beta)}$, are introduced in order to take the constraints of fixed $A^{(\alpha)}$ and $A^{(\beta)}$ into account. The parameter p is the Lagrange parameter for the enclosed volume, or, alternatively, the pressure difference between the inside and the outside of the vesicle.

The morphology of the vesicle is determined by an interplay of bending energy and line energy. The competition between these energies and the fluidity of the bilayer opens the possibility for the formation of a bulge or bud. The line energy can be lowered when the membrane domain deforms into a bulge so that the domain boundary can shrink. If the bulge transforms into a complete bud, the line energy becomes essentially zero. The complete bud may leave the original vesicle or stay connected to the original vesicle via a small neck. The formation of a bump is opposed by an increase in bending energy. However, in contrast to line energy, which scales with the size of the bud, the bending energy is independent of the size of the bud. Thus, above a certain size of the domain the gain in line energy outweighs

the increase in bending energy and a bud is expected to form. The domain size above which this happens is given by the length scale where both energies become comparable. It is set by the ratio of the bending rigidity over the line tension. For typical lipids, this length scale is in the order of μm. The budding transition may be triggered by other mechanism than line tension, resulting in buds of different sizes. Budding is also induced by changes in temperature in homogeneous vesicles [181], by phase separation in the interior of the vesicle [182], by the adsorption of proteins [183], and by the structure of the membrane [184]. Examples for the last mechanismn are membrane domains with a chirality, leading to buds with a significantly smaller size $\sim 50nm$.

In the following we neglect spontaneous curvatures, i.e. $C_0^{(\alpha)} = C_0^{(\beta)} = 0$ and use $\kappa^{(\beta)}$ as the reference energy. The vesicle is then characterised by five dimensionless parameters, the ratio of the bending rigidities in phase (α) and (β)

$$\epsilon^{\kappa} \equiv \frac{\kappa^{(\alpha)}}{\kappa^{(\beta)}}\,, \tag{5.5}$$

the difference in the Gaussian bending moduli

$$\Delta\epsilon^{\kappa_G} \equiv \frac{\kappa_G^{(\alpha)} - \kappa_G^{(\beta)}}{\kappa^{(\beta)}}\,, \tag{5.6}$$

the reduced line tension

$$\lambda \equiv \lambda^{(\alpha,\beta)} \frac{R_0}{\kappa^{(\beta)}}\,, \tag{5.7}$$

the area fraction of phase (α) $\chi^{(\alpha)}$ and the reduced volume v.

In the next section we briefly review the results for a vesicle with large line tension. In this case, the equilibrium morphology is a vesicle with two coexisting membrane domains, one in each phase. Line tension causes the formation of a domain bud.

5.3 Vesicle with two coexisting fluid domains – Axisymmetric case

We start with the discussion of two coexisting fluid domains, one fluid domain with phase (α) and one domain with phase (β), type I_1 [173]. This case has been treated in detail in article [173], we briefly summarise the presentation and the main conclusions. We assume an axisymmetric vesicle conformation. The axisymmetric shape is parametrised by arclength along the meridian as illustrated in Fig. 5.1. It is practicable to describe the contour by the function $\psi(s)$ together with $R(s)$ and $Z(s)$, where s is the arclength of the contour, $R(s)$ the distance from the axis of rotational symmetry, $Z(s)$ the coordinate along this axis and $\psi(s)$ denotes the tilt angle of this contour [1]. The axisymmetric domain boundary is located at $s = s_1$. The domain (α) corresponds to the interval $s_0 = 0 < s < s_1$ and the domain (β) is described by the interval $s_1 < s < s_2$. In this parametrisation the energy functional Eq. (5.2) reads

$$\mathcal{H} = 2\pi \left(\int_{s_0}^{s_1} ds\mathcal{H}^{(\beta)} + \int_{s_1}^{s_2} ds\mathcal{H}^{(\alpha)} + \lambda^{(\alpha,\beta)} R(s_1) + \kappa_G^{(\alpha)} + \kappa_G^{(\beta)} + (\kappa_G^{(\alpha)} - \kappa_G^{(\beta)}) \cos\psi(s_1) \right) \tag{5.8}$$

[1] Note that these functions are not independent, but related via $\dot{Z}(s) = -\sin\psi(s)$ and $\dot{R}(s) = \cos\psi(s)$. The advantage using the parametrisation $\psi(s)$ compared to $R(Z)$ is that points with infinite derivative dR/dZ are regular in this parametrisation.

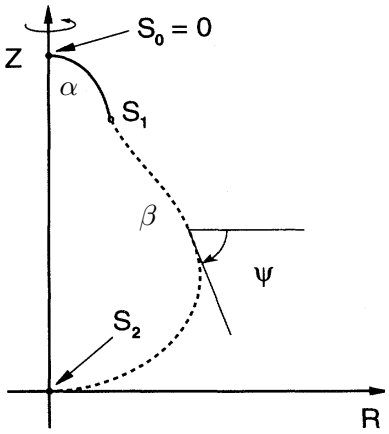

Figure 5.1: Contour of an axialsymmetric vesicle with two coexisting domains in the arclength parametrisation s, $Z(s)$ is the coordinate along this symmetry axis, $R(s)$ denotes the distance from this axis and $\psi(s)$ is the tangent angle of this contour. The domain boundary is located at $s = s_1$; adapted from [173].

with

$$\begin{aligned}\mathcal{H}^{(i)}(s) &= \frac{\kappa^{(i)}}{2}R(s)\left(\dot{\psi}(s)+\frac{\sin\psi(s)}{R(s)}-C_0^{(i)}\right)^2+\sigma^{(i)}R(s)\\ &\quad+\frac{p}{2}R(s)^2\sin\psi(s)+\gamma(s)\left(\dot{R}(s)-\cos\psi(s)\right). \end{aligned} \tag{5.9}$$

The overdots denote derivatives with respect to s. In order to fix the redundancy in the parametrisation, a Lagrange multiplier function $\gamma(s)$ needs to introduced.

5.3.1 Equilibrium configurations

Necessary conditions for a vesicle state being minimum are given by the Euler-Lagrange equations of the functional Eq. (5.8) [173]. The variation of Eq. (5.8) leads to the shape equations [2]

$$\ddot{\psi}(s) = \frac{\cos\psi(s)\sin\psi(s)}{R(s)^2}-\frac{\dot{\psi}(s)}{R(s)}\cos\psi(s)+\frac{p}{2\kappa^{(i)}}R(s)\cos\psi(s)+\frac{\gamma(s)}{\kappa^{(i)}R(s)}\sin\psi(s) \tag{5.10}$$

$$\dot{\gamma}(s) = \frac{\kappa^{(i)}}{2}(\dot{\psi}(s)-C_0^{(i)})^2-\kappa^{(i)}\frac{\sin^2\psi(s)}{2R(s)^2})+\sigma^{(i)}+pR(s)\sin\psi(s)\,, \tag{5.11}$$

$$\dot{R}(s) = \cos\psi(s)\,, \tag{5.12}$$

$$\dot{H}^{(i)}(s) = 0 \tag{5.13}$$

with

$$H^{(i)}(s)=\frac{\kappa^{(i)}}{2}R(s)\left(\dot{\psi}(s)^2-(\frac{\sin\psi(s)}{R(s)}-C_0^{(i)})^2\right)-\sigma^{(i)}R(s)-\frac{p}{2}R(s)^2\sin\psi(s)+\gamma(s)\cos\psi(s)\,. \tag{5.14}$$

[2] In order to perform the variation it is necessary to switch to an arbitrary parametrisation t with $s(t_0)=0$, $s(t_1)=s_1$ and $s(t_2)=s_2$ [173]. The result can then be reparametrised in the arclength parametrisation.

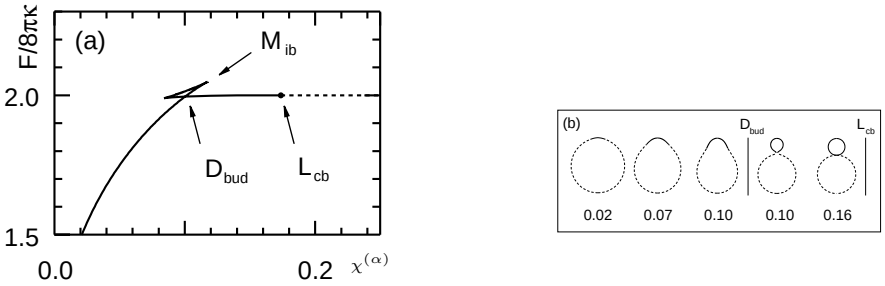

(a) (b)

Figure 5.2: Domain-induced budding. (a) The ground state energy F of an axisymmetric vesicle with two fluid domains is plotted as a function of the area fraction $\chi^{(\alpha)}$ for reduced line tension $\lambda = 7$, equal bending rigidities $\epsilon^\kappa = 1$, vanishing Gaussian bending rigidities $\Delta\epsilon^{\kappa_G} = 0$ and no constraints on the volume. With increasing domain size a discontinuous budding $D_{\rm bud}$ occurs. The incomplete bud becomes metastable at $D_{\rm bud}$ and unstable at $M_{\rm ib}$. At $L_{\rm cb}$ a singular limit shape occurs. (b) A sequence of corresponding shapes at different values of $\chi^{(\alpha)}$; from [173].

Within each domain these equations correspond to the shape equations for a vesicle with spherical topology. The equations are supplemented by boundary conditions at s_0 and s_1, $R(s_0) = R(s_2) = 0$, $\psi(s_0) = \psi(s_2) = \pi$, $\gamma(s_0) = \gamma(s_2) = 0$ and matching conditions connecting the bulk equations at the boundary between the different phases (ϵ is a positive, infinitesimally small number)

$$H^{(\alpha)} = H^{(\beta)} = 0\,, \tag{5.15}$$

$$\gamma(s_1+\epsilon) - \gamma(s_1-\epsilon) = \sigma\,, \tag{5.16}$$

$$\kappa^{(\alpha)}\dot{\psi}(s_1+\epsilon) - \kappa^{(\beta)}\dot{\psi}(s_1-\epsilon) = (\kappa^{(\beta)} - \kappa^{(\alpha)} + \kappa_G^{(\beta)} - \kappa_G^{(\alpha)})\frac{\sin\psi(s_1)}{R(s_1)} + \kappa^{(\alpha)}C_0^{(\alpha)} - \kappa^{(\beta)}C_0^{(\beta)}\,. \tag{5.17}$$

The variation of the functional Eq. (5.8) does not completely determine the conditions at $s = s_1$. To arrive at Eq. (5.16) and Eq. (5.17), continuity of $R(s)$ and $\psi(s)$ needs to be assumed. This is a reasonable assumption which can be justified more rigorously from a mechanical point of view. In mechanical terms, Eq. (5.15) - Eq. (5.17) can be interpreted as jump conditions for forces and moments. They follow from the balance equation for in-plane forces, out-of-plane forces and moments across the boundary [171].

It is worth to point out that the vesicle bulk equations do not contain any term involving κ_G. The Gaussian bending moduli enter through matching conditions at the domain boundaries. Only a difference in the Gaussian bending moduli gives a shape dependent contribution.

Stationary shapes are obtained by solving the shape equations, Eq. (5.10) - Eq. (5.13), together with the boundary and matching conditions, Eq. (5.15) - Eq. (5.17) [173].

Domain-induced budding

In the following we consider an unconstrained vesicle. We start with the most simple case of identical bending rigidities $\epsilon^\kappa = 1$, i.e. $\kappa^{(\alpha)} = \kappa^{(\beta)}$, vanishing spontaneous curvatures

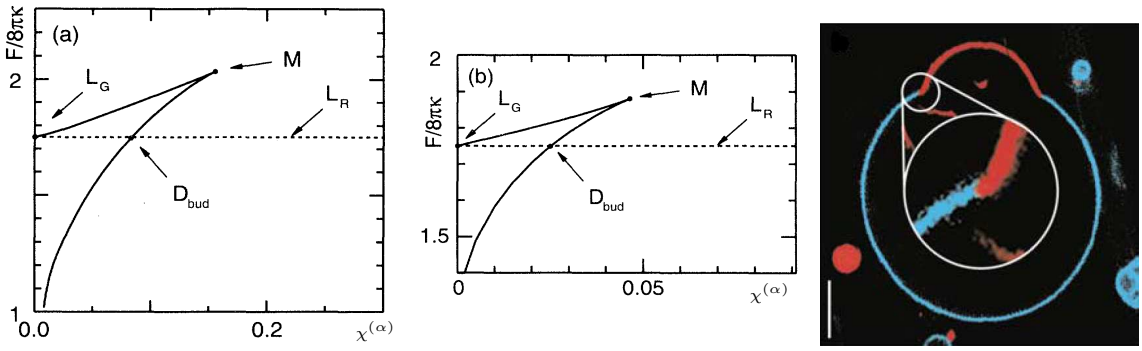

(a) (b) (c)

Figure 5.3: Influence of a difference in the Gaussian curvature moduli on the shape of an axisymmetric vesicle with two coexisting fluid domains. Fig. (a) and Fig. (b) show the minimum energy of the vesicle as a function of the area fraction $\chi^{(\alpha)}$ with line tension $\lambda = 7$, no constraints on the volume and (a) $\Delta\epsilon^{\kappa_G} = 1$, (b) $\Delta\epsilon^{\kappa_G} = -1$; from [173]. Two-photon microscopy image of an axially symmetric vesicle with liquid-disordered (red) and liquid-ordered (blue) phase coexistence. The inset shows the enlarged neck region at the domain boundary which demonstrates the influence of a difference in the Gaussian curvature moduli of both phases. The liquid-disordered membrane bends towards the liquid-disordered membrane and forms the neck due to its higher Gaussian bending modulus; scale bars $5\mu m$; from [67].

$C_0^{(\alpha)} = C_0^{(\beta)} = 0$ and neglect Gaussian bending rigidities $\Delta\epsilon^{\kappa_G} = 0$. Fig. 5.2 depicts a sequence of stationary shapes and the corresponding energy diagram for $\lambda = 7$ [173]. As the area fraction of phase (α) increases, the membrane in phase (α) develops a bulge or incomplete bud. The growing bud becomes metastable at D_{bud} and unstable above M_{IB} towards the formation of a complete bud. At D_{bud} a transition from the incomplete bud to a complete bud occurs. The budding transition is discontinuous. At L_{CB} the contour turns into a singular limit shape which consists of two spheres that are connected by an infinitesimal neck.

It should be noted that for vesicles with fixed volume the bud formation may be hindered by the constraint imposed by the enclosed volume [173]. Apparently, a bud cannot develop in a geometry close to a sphere. For sufficiently large line tension, budding may be induced by a decrease in v at constant $\chi^{(\alpha)}$. Experimentally, this is realisable through osmotic deflation of the vesicle.

Influence of Gaussian bending rigidity

So far, contributions from the Gaussian bending energy of the two phases have been neglected. For a homogeneous vesicle, this is justified because, unless fusion or fission processes of vesicles are considered, this term yields a constant independent of the size or shape of the vesicle. The Gaussian elastic modulus is associated with the energy cost of deformations that change topology of the membrane and thus can be regarded as a chemical potential for the formation of handles. For homogeneous vesicles, theoretical considerations on the stability of the vesicle require $-2 < \kappa_G/\kappa < 0$ [20] or, according to [185], $-1 < \kappa_G/\kappa < 0$. This is because, on the one hand, for $\kappa_G > 0$ the fluid membrane becomes instable to the formation

of a membrane torus with high topological genus, while on the other hand, for $\kappa_G < -\kappa$ ($\kappa_G < -2\kappa$) the membrane would fission into many small vesicles. Recent measurements yield a value $\kappa_G \sim -0.8\kappa$ for a monolayer of N-mono-methylated dioleoyl-phosphatidylethanolomine (DOPE-Me) [59].

For an inhomogeneous vesicle, in the Gaussian elastic moduli of the domains does matter. In general, a the difference in the Gaussian elastic moduli yields a shape dependent contribution the Gaussian bending energy. By virtue of the Gauss-Bonnet theorem, the Gaussian bending energy can be reformulated as an integral over the domain boundary (see appendix A.1). Yet, the Gaussian bending energy is not proportional to the length of the domain boundary and thus cannot be reduced to an effective line energy. This is evident by the fact that the Gaussian bending modulus has the dimension of an energy and not the dimension of a line tension. For a vesicle with liquid-ordered/liquid-disordered membrane domains, the difference between the Gaussian bending moduli of both fluid phases was determined experimentally and estimated to be in the same order of magnitude as the elastic bending modulus [171, 186].

The Gaussian curvature has the following impact on the shape of the phase separated vesicle with two domains. For $\Delta\epsilon^{\kappa_G} < 0$ ($\kappa_G^{(\alpha)} < \kappa_G^{(\beta)}$), the budding transition of the domain (α) occurs for smaller values of $\chi^{(\alpha)}$ than for $\Delta\epsilon^{\kappa_G} > 0$ ($\kappa_G^{(\alpha)} > \kappa_G^{(\beta)}$). This is seen in Fig. 5.3, where the equilibrium energy is shown as a function of the area fraction $\chi^{(\alpha)}$ for $\Delta\epsilon^{\kappa_G} = 1$ (Fig. 5.3-a) and $\Delta\epsilon^{\kappa_G} = -1$ (Fig. 5.3b). In general, a membrane domain with phase (i) forms a bud more easily if its Gaussian bending modulus $\kappa_G^{(i)}$ is smaller than that of the other membrane. Furthermore, a difference in the Gaussian bending moduli leads to a more pronounced Gibbs loop with a higher energy difference between the metastable incomplete bud and the completely budded vesicle.

In addition, a difference in the Gaussian bending moduli significantly affects the geometry of the neck. In the neck region, the Gaussian curvature of the membrane surface is high and negative. For $\Delta\epsilon^{\kappa_G} = 0$, the domain boundary is located at the smallest diameter of the neck. This is a consequence of the minimisation of the boundary length. For $\Delta\epsilon^{\kappa_G} \neq 0$, the domain boundary is shifted away from the smallest diameter in the neck. The neck is formed by the domain with the larger $\kappa_G^{(i)}$, which is the smaller in magnitude since $\kappa_G^{(i)}$ is negative for mechanically stable bilayers [3]. Qualitatively, this can be understood easily, when one considers a completely budded vesicle with an infinitesimal neck. The contribution to the Gaussian bending energy of an infinitesimal neck formed by a membrane with Gaussian bending rigidity κ_G yields $\simeq -4\pi\kappa_G$. Thus, the vesicle can gain more energy if the neck is formed by the domain with the larger κ_G. This effect has been first theoretically predicted some years ago [172, 173] and recently demonstrated experimentally [67]. The image of a vesicle experimentally demonstrating this is shown in Fig. 5.3c.

In conclusion, line tension, a difference in bending moduli, and a difference in the Gaussian bending moduli each affect vesicle shapes in a characteristically different way. By fitting experimental vesicle shapes to numerically determined vesicle geometries it is possible to obtain estimates of bending moduli of the different phases, line tension and differences in the Gaussian curvature [171].

[3] The text in [173] contains a misprint in the main text in subsection C.

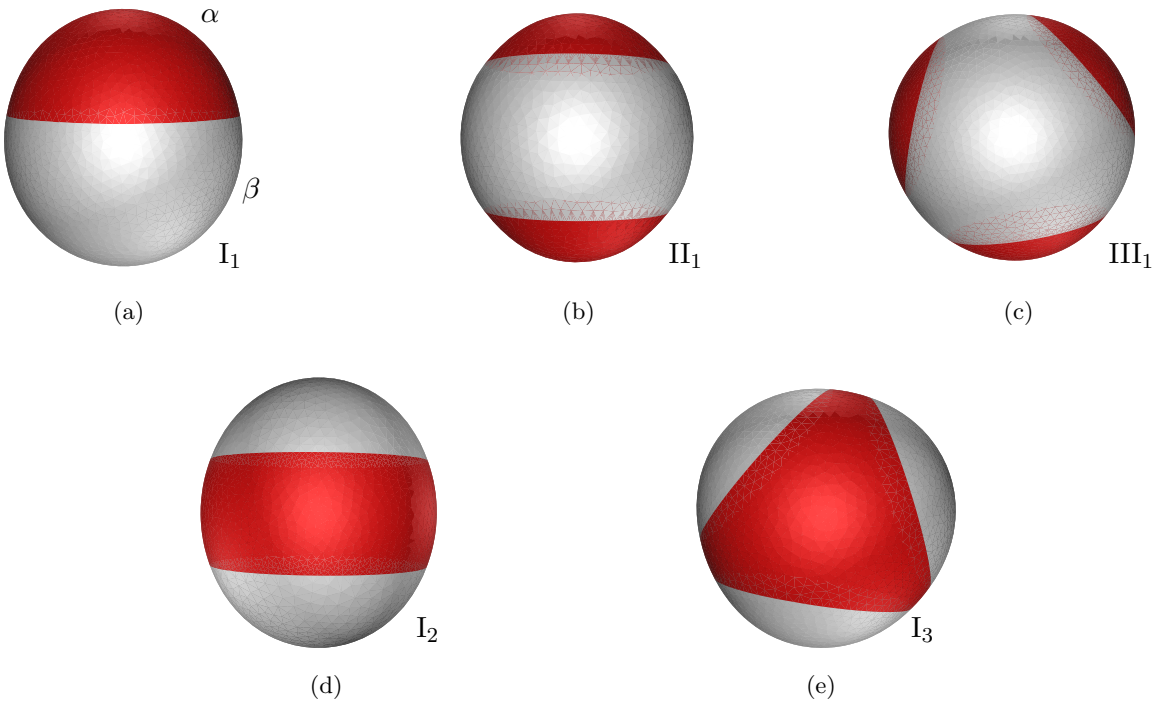

Figure 5.4: Vesicles with coexisting fluid membrane domains (membrane phase (α) red area, membrane phase (β) white area): (a) one (α) and one (β) domain (I_1), (b) two (α) and one (β) domains (II_1), (c) three (α) and one (β) domains (III_1), (d) one (α) and two (β) domains (I_2), and (e) one (α) and three (β) domains (I_3); material parameters bending rigidity ratio $\epsilon^\kappa = 1$, reduced line tension $\lambda = 1$, and equal Gaussian curvature moduli $\Delta\epsilon^{\kappa_G} = 0$.

5.4 Vesicles with several coexisting fluid domains

In the preceding section, we have discussed the geometry of an axisymmetric vesicle morphology I_1 with two coexisting fluid domains, one in each phase. Vesicles with two domains are the equilibrium configuration when line energy plays a large or dominant role because in this configuration the domain boundary is shortest. A sufficiently large line tension leads to a transition of the vesicle shape such as budding. In this section we address the opposite case where contributions from line energy are small compared to the bending energy. In this case, the axisymmetric vesicle shape with two fluid domains is not necessarily the shape of minimum energy anymore. We will show in the following that for comparably small line tension morphological transitions to vesicle shapes with more complex domain shapes occur.

A measure of the relative importance of line energy and bending energy is given by the reduced line tension λ. The reduced line tension λ is proportional to the physical line tension $\lambda^{(\alpha,\beta)}$ and scales linearly with the radius of the vesicle, R_0. Its value can vary in orders of magnitude as vesicles of different size or vesicles with a membrane composition close to the critical point of phase separation, where $\lambda^{(\alpha,\beta)}$ vanishes, are considered. The results in this section are therefore relevant for comparably small vesicles and/or membrane compositions with small $\lambda^{(\alpha,\beta)}$.

We include vesicles with five different domain topologies in our analysis, see Fig. 5.4: a

vesicle with one phase (α) domain and one phase (β) domain (I_1), a vesicle with two phase (α) domains and one phase (β) domain (II_1), a vesicle with three phase (α) domains and one phase (β) domain (III_1), a vesicle with one phase (α) domain and two phase (β) domains (I_2), and a vesicle with one phase (α) domain and three phase (β) domains (I_3) [4]. For simplicity, it is assumed that for morphology III_1 and I_3 the three domains each have the same size.

Our interest is in the equilibrium shape with minimum energy. We determine and compare the minimum energy for the different vesicle morphologies. Vesicle conformations which are found to have higher energy are metastable. As in chapter 4, we do not perform an explicit stability analysis for metastable states. The equilibrium morphologies are obtained by direct numerical minimisation of a triangulated vesicle surface with the help of the 'Surface Evolver' [161]. The estimated numerical accuracy of the obtained energy values is about $\simeq 1\%$. We investigate vesicles with and without volume constraints.

5.4.1 Vesicles without volume constraints – Equilibrium configurations

Influence of bending rigidity

We start with vesicles without volume constraints and investigate first the influence of different bending moduli in the fluid membrane phases. Without loss of generality, we assume $\epsilon^\kappa \geq 1$. The results for $\epsilon^\kappa < 1$ follow from renaming the phases (α) and (β). In Fig. 5.5a the minimum energy of the different domain morphologies is displayed as a function of the bending rigidity ratio ϵ^κ for area fraction $\chi^{(\alpha)} = 0.6$, reduced line tension $\lambda = 0.2$ and equal Gaussian bending moduli $\Delta\epsilon^{\kappa_G} = 0$. As one expects, for vesicles with a similar bending rigidity in both fluid phases (ϵ^κ close to one), the vesicle with two fluid domains, morphology I_1, has lowest energy. As the bending rigidity ratio ϵ^κ increases, one observes transitions to other domain morphologies. For $\chi^{(\alpha)} = 0.6$, at about $\epsilon^\kappa \simeq 1.55$ morphology I_2 with an (α) ring domain is optimal. Above $\epsilon^\kappa = 1.75$, a vesicle with two fluid (α) domains, morphology II_1, becomes the configuration with lowest energy. Morphologies III_1 and I_3 (their energies are not shown in Fig. 5.5a) have always higher energies. Judging from the data in Fig. 5.5a, it seems that the transitions are discontinuous.

The full information as to which domain morphology has the lowest energy for given $\chi^{(\alpha)}$ and ϵ^κ is shown in the morphology diagram Fig. 5.5b. Morphology I_1 is the equilibrium morphology for similar bending rigidity (ϵ^κ close to one) and small, respectively large, area fraction $\chi^{(\alpha)}$. In a large region of the morphology diagram, in particular with high bending rigidity ratio ϵ^κ, morphology II_1 has lowest energy. For large area fraction $\chi^{(\alpha)}$, the ring domain morphology, morphology I_2, is found in between morphology I_1 and II_1. The morphology I_2 occurs for intermediate bending rigidity ratios ϵ^κ and area fractions, depending on the line tension, in the range of $0.4 \gtrsim \chi^{(\alpha)} \gtrsim 0.9$.

In general, the obtained equilibrium morphologies exhibit a rotational symmetry. Typically, the shapes II_1 and I_2 are found to have an additional top-bottom symmetry. This means that the domains located at the poles (top and bottom) of the vesicle, i.e. (α) domains for morphology II_1 and (β) domains for morphology I_2, have the same size. We characterise the

[4] The property of the vesicle does not depend upon which of the two fluid phases is named (α) or (β), respectively. Apparently, Eq. (5.2) is invariant when phases (α) and (β) are renamed, i.e. when $\chi^{(\alpha)}$ is transformed into $\chi^{(\beta)} = 1 - \chi^{(\alpha)}$ and at the same time the material parameters of phase (α), $\kappa^{(\alpha)}$, $\kappa_G^{(\alpha)}$, and $C_0^{(\alpha)}$ are exchanged with material parameters of phase (β), $\kappa^{(\beta)}$, $\kappa_G^{(\beta)}$, and $C_0^{(\beta)}$, respectively. It should be noted that upon such a renaming of the phases, morphology I_1 remains type I_1, while morphologies II_1 and III_1 are transformed into I_2 and I_3, respectively.

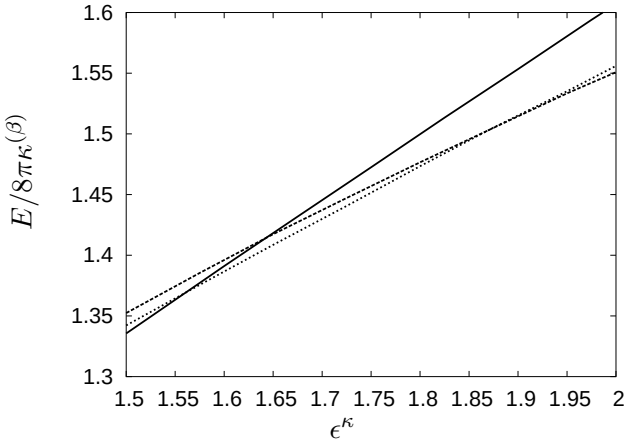

(a)

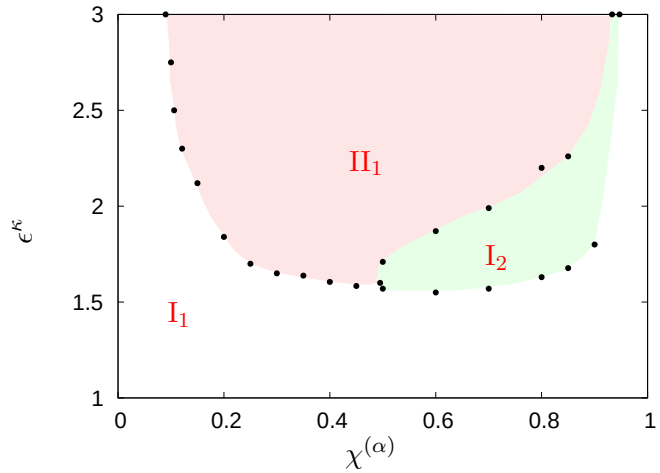

(b)

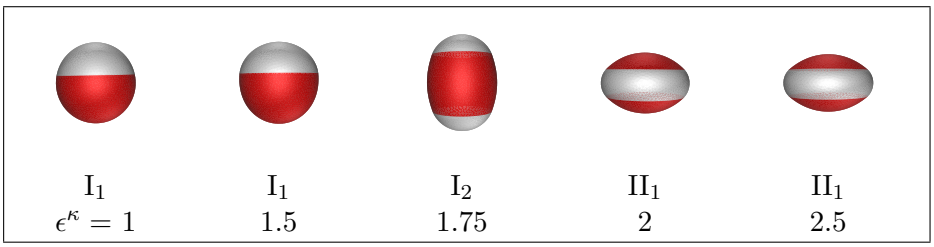

(c)

Figure 5.5: Vesicle with fluid membrane domains without volume constraints - Influence of a difference in the elastic bending moduli. (a) The minimum energy E of a vesicle with domain shape type I_1 (solid line), type II_1 (dashed line) and type I_2 (dotted line) as a function of the bending rigidity ratio ϵ^{κ} for the area fraction $\chi^{(\alpha)} = 0.6$, reduced line tension $\lambda = 0.2$, and equal Gaussian curvature moduli $\Delta\epsilon^{\kappa_G} = 0$. (b) Morphology diagram of this vesicle as a function of $\chi^{(\alpha)}$ and ϵ^{κ}. (c) Corresponding shapes of minimum energy for $\chi^{(\alpha)} = 0.6$ and increasing ϵ^{κ}.

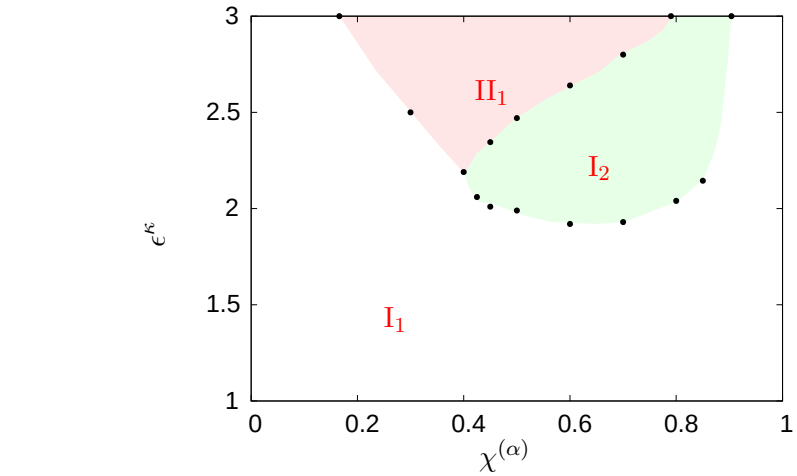

(a)

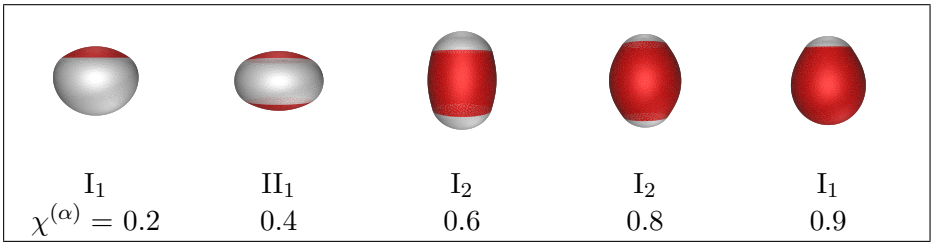

(b)

Figure 5.6: Vesicle with fluid membrane domains without volume constraints - Influence of a difference in the elastic bending moduli, the same as Fig. 5.5 before but with reduced line tension $\lambda = 0.5$. (a) Morphology diagram as a function of the area fraction $\chi^{(\alpha)}$ and the bending rigidity ratio ϵ^κ. (b) Corresponding shapes of minimum energy for $\epsilon^\kappa = 2.3$ and increasing area fraction $\chi^{(\alpha)}$.

area ratio of the domains in morphology II_1 with $\chi_{(\alpha_1,\alpha_2)}$, defined in Eq. (4.8), and analogously with $\chi_{(\beta_1,\beta_2)}$, defined in Eq. (4.7), for morphology I_2. Equal domain areas at the pole of the vesicle corresponds to $\chi_{(\alpha_1,\alpha_2)} = 0.5$ and $\chi_{(\beta_1,\beta_2)} = 0.5$, respectively. Vesicles with top-bottom symmetry, $\chi_{(\alpha_1,\alpha_2)} = 0.5$, are favoured by bending energy, yet they have a slightly higher line energy than vesicles where this symmetry is broken, $\chi_{(\alpha_1,\alpha_2)} \neq 0.5$. Whether the top-bottom symmetry holds for all equilibrium vesicle shapes II_1 and I_2, could not be fully clarified. Close to the transition between morphology I_1 and II_1, for small area fraction $\chi^{(\alpha)}$ and small ϵ^κ, vesicle morphologies II_1 with a slightly asymmetric area ratio, $\chi_{(\alpha_1,\alpha_2)}$ in the range of $0.4 \simeq \chi_{(\alpha_1,\alpha_2)} \lesssim 0.5$ are found to have fairly equivalent energy (within numerical accuracy) as the symmetric shape, $\chi_{(\alpha_1,\alpha_2)} = 0.5$.

The overall picture does not change qualitatively when the line tension is increased. This is illustrated in Fig. 5.6a where the morphology diagram for vesicles with $\lambda = 0.5$ is shown. In general, the transition from morphology I_1 to morphologies II_1 and I_2 occurs at larger values of ϵ^κ as the line tension increases.

The results are understood by inspection of the vesicle configurations in Fig. 5.5c and Fig. 5.6b. The membrane phase with the higher bending rigidity avoids conformations with large mean curvature. For small area fraction $\chi^{(\alpha)}$, the vesicle with one domain in each

phase, morphology I_1, has lowest energy because it exhibits the shortest domain boundary. For a small domain size, the slightly stiffer membrane can easily acquire a comparably flat conformation without deforming the rest of the vesicle too much. As the area fraction $\chi^{(\alpha)}$ increases (Fig. 5.6b), morphology I_1 becomes less favourable because the stiffer membrane domain would have to bend more strongly in order to fit onto the vesicle geometry. There is a transition towards morphology II_1. The stiffer membrane domain splits into two domains which are bent less and which are located at the poles of the vesicle. The gain in elastic bending energy compensates for the higher line energy due to the larger length of the domain boundary. For even larger area fraction $\chi(\alpha)$, morphology II_1 is less optimal than vesicle I_2. This is partly due to bending energy since two large, slightly stiffer (α) domains in morphology II_1 lead to a stronger deformation of the rest of the vesicle than a ring (α) domain in morphology I_2. It is also due to the contributions from line energy, as for $\chi(\alpha) \gtrsim 0.5$ the domain boundary of the ring morphology I_2 starts to be shorter than that of morphology II_1. The smaller line energy of morphology I_2 (compared to morphology II_1) explains why the parameter region with optimal I_2 morphology gets larger if the line tension increases, compare Fig. 5.5b with Fig. 5.6a. There is a transition from morphology I_2 to morphology II_1 if the difference in the bending rigidities of the two membrane phases becomes more pronounced, see Fig. 5.5c. This morphological transition is explained by the fact that in this case the bending energy of the stiffer membrane which is lowest for morphology II_1 becomes more important than the line energy or the bending energy of the other membrane domain.

Influence of Gaussian bending rigidity

Next we investigate the influence of different values of the Gaussian bending moduli. Some aspects of the impact of Gaussian curvature on domain formation has been pointed out in the preceding section for a vesicle with two domains. In general, since κ_G is negative, membrane patches with positive Gaussian curvature (such as a spherical cap in a bud) yield a negative contribution to the vesicle energy. Membrane patches with a negative Gaussian curvature (such as the neck region) result in a positive term. In a homogeneous vesicle with constant κ_G the Gaussian bending energy sums up to a topological constant, independent of the vesicle shape. This is, however, not the case for a phase separated vesicle with different Gaussian moduli of the membrane domains. While the integral over the Gaussian curvature is a topological invariant, the energy associated with the Gaussian curvature depends on the shape. The vesicle can gain energy if the membrane part with the lower Gaussian bending modulus adapts a configuration with a more positive (Gaussian) curvature (i.e. forms a bulge) while the membrane with the higher Gaussian bending modulus forms a configuration which is curved more negatively (i.e. for example forms a neck).

The bending of the membrane is opposed by the elastic bending rigidity. For a vesicle with liquid-ordered/liquid-disordered membrane domains, the difference between the Gaussian bending moduli of both fluid phases was estimated to be in the same order of magnitude as the elastic bending modulus [171, 186]. Therefore, the contribution from the Gaussian bending energy is in the same order of magnitude as the bending energy. It is independent of the number of domains. For certain material parameters, the gain in Gaussian curvature energy can outweigh the cost of bending the membrane.

In the following we investigate the effect of different Gaussian bending moduli, $\Delta\epsilon^{\kappa_G} \neq 0$, in detail. We first consider a vesicle with equal bending rigidities, $\epsilon = 1$, which implies that the two membrane phases are identical besides their Gaussian bending moduli. Fig. 5.7a

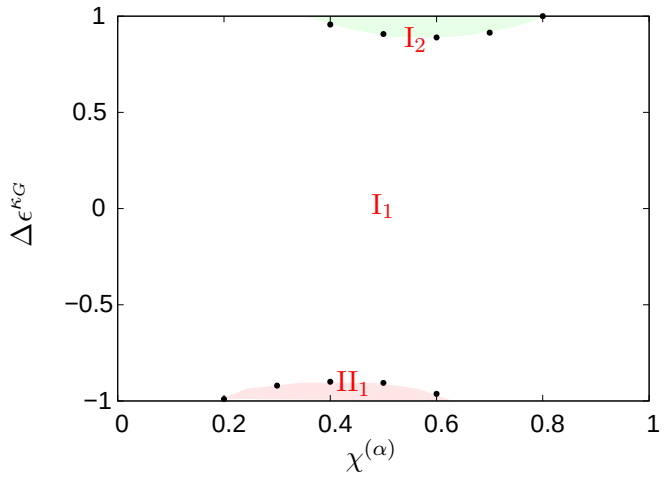

(a)

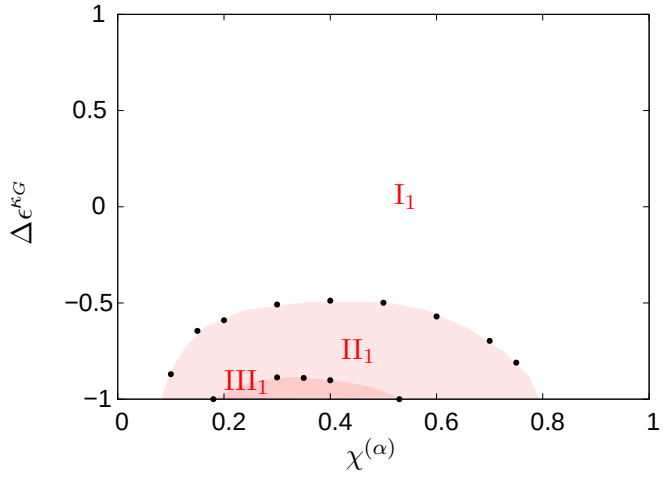

(b)

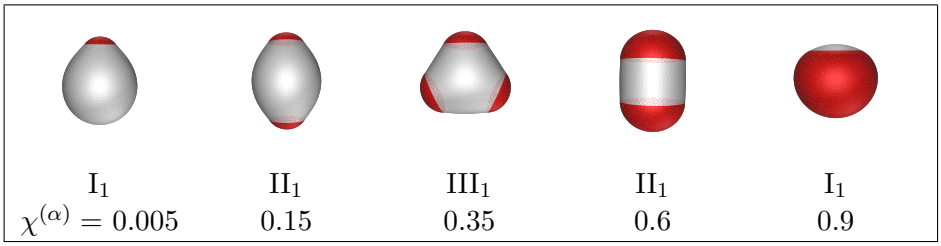

(c)

Figure 5.7: Vesicle with fluid membrane domains without volume constraints - Influence of a difference in the Gaussian bending moduli. (a) Morphology diagram of a vesicle with fluid domains without volume constraints as a function of the area fraction $\chi^{(\alpha)}$ and the ratio of the Gaussian bending rigidities $\Delta\epsilon^{\kappa_G}$ for reduced line tension $\lambda = 0.2$ and bending rigidity ratio (a) $\epsilon^{\kappa} = 1$ and (b) $\epsilon^{\kappa} = 0.8$. (c) Corresponding shapes of minimum energy for $\Delta\epsilon^{\kappa_G} = -1$, $\epsilon^{\kappa_G} = 0.8$ and increasing area fraction $\chi^{(\alpha)}$.

depicts the morphology diagram of this vesicle as a function of the area fraction $\chi^{(\alpha)}$ and the reduced Gaussian bending modulus $\Delta\epsilon^{\kappa_G}$ for $\lambda = 0.2$. The diagram is symmetric when $\chi^{(\alpha)}$ is exchanged into $\chi^{(\beta)} = 1 - \chi^{(\alpha)}$, $\Delta\epsilon^{\kappa_G}$ changes sign, and morphology II_1 is transformed into morphology I_2. This is because the two membrane phases differ only in their Gaussian bending moduli. The symmetry (redundancy) in the diagram corresponds to a renaming of phase (α) with (β). For equal bending rigidity, $\epsilon^{\kappa} = 1$, one finds that the morphology I_1 is the equilibrium configuration unless $\kappa_G^{(\alpha)}$ and $\kappa_G^{(\beta)}$ differ considerable, $|\Delta\epsilon^{\kappa_G}| \gtrsim 0.9$, and the area fraction of the phase $\chi^{(i)}$ with the smaller Gaussian bending modulus $\kappa_G^{(i)}$ is around $0.2 \lesssim \chi^{(\alpha)} \lesssim 0.6$. Otherwise, the membrane with the smaller Gaussian bending modulus forms two domain caps located at the pole of the vesicle. Morphology II_1, respectively I_2, become the equilibrium conformation. The reason for this morphological transition is that for this area fraction the two domains can form a more pronounced bud, which accumulates Gaussian curvature in the phase with the smaller Gaussian curvature modulus, so that the overall energy of the vesicle reduces.

The impact of a different bending rigidity ratio, $\epsilon^{\kappa} \neq 1$, can be seen from Fig. 5.7b. We assume that the membrane in phase (α) is softer and easier to bend, i.e. $\epsilon^{\kappa} < 1$. Fig. 5.7b displays the morphology diagram for $\epsilon^{\kappa} = 0.8$. The two membrane phases have different bending moduli and therefore the diagram is not symmetric any more with respect to the exchange of the sign of $\Delta\epsilon^{\kappa_G}$. We find that for $\Delta\epsilon^{\kappa_G} > 0$ the formation of buds and domains is suppressed while for $\Delta\epsilon^{\kappa_G} < 0$ the vesicle has a larger propensity to form buds. For $\Delta\epsilon^{\kappa_G} < 0$ ($\kappa_G^{(\alpha)} < \kappa_G^{(\beta)}$), the area in the morphology diagram where a vesicle with two (α) domains, morphology II_1, has minimum energy increases significantly. In a small region of the morphology diagram there is even a morphological transition towards a vesicle with three (α) domains, III_1.

In conclusion, we find a stronger tendency of the vesicle to form domains with a pronounced bulge if the membrane which forms the bud has a smaller bending modulus and a smaller Gaussian bending modulus. In this case, the Gaussian bending energy and the elastic bending energy support the formation of more domains. In the other case, for a membrane domain with larger bending modulus and smaller Gaussian bending modulus, the bending energies compete and the formation of buds and more domains is suppressed.

Influence of line tension

Finally, we investigate the impact of the reduced line tension. To quantify the value of λ below which morphological transitions are predicted to take place we analyse a vesicle with typical material parameters taken from experiments. For a phase separated vesicle with liquid-ordered/liquid-disordered membrane domains recent experiments yield the material parameters $\epsilon = 4$ and $\Delta\epsilon^{\kappa_G} = -1.5$ [186]. Fig. 5.8 depicts the morphology diagram for a vesicle with these parameter values as a function of the area fraction $\chi^{(\alpha)}$ and reduced line tension λ. As a major result we find that above $\lambda \gtrsim 1.68$ the morphology I_1 has minimum energy for all $\chi^{(\alpha)}$. For $\lambda \lesssim 1.68$, morphology I_1 is found for large and small $\chi^{(\alpha)}$ while for $\chi^{(\alpha)}$ around $\chi^{(\alpha)} \simeq 0.5$ morphology II_1 is favoured. In the range of $\chi^{(\alpha)} \simeq 0.8$ a region exists where I_2 has the lowest energy.

The reduced line tension λ depends on the size of the vesicle R_0 and the physical line tension $\lambda^{(\alpha,\beta)}$, Eq. (5.7). If a value for the line tension $\lambda^{(\alpha,\beta)}$ is given, one can estimate the size of the vesicle R_0^* below which the morphological transition is predicted to occur. Or vice

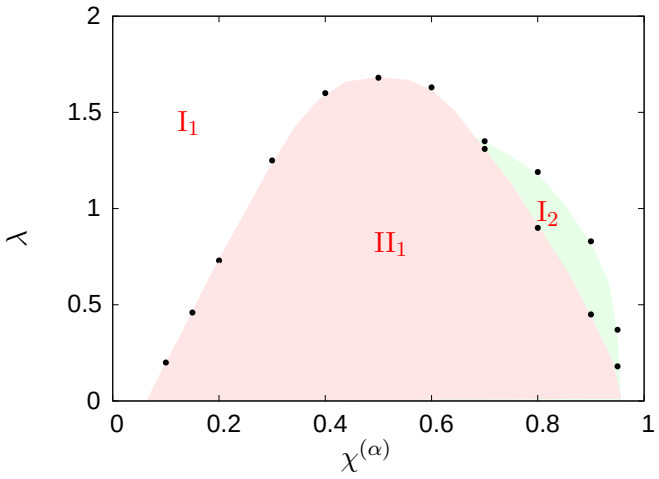

(a)

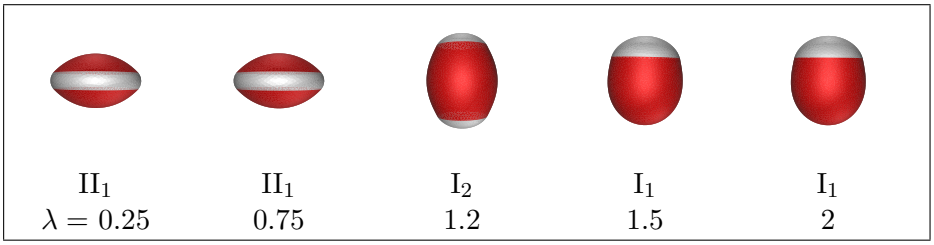

(b)

Figure 5.8: Vesicle with fluid membrane domains without volume constraints - Influence of the reduced line tension λ. (a) Morphology diagram of the vesicle as a function of the area fraction $\chi^{(\alpha)}$ and λ for bending rigidity ratio $\epsilon^{\kappa} = 4$ and ratio of Gaussian bending moduli difference $\Delta\epsilon^{\kappa G} = -1.5$. (b) Corresponding shapes of minimum energy for $\chi^{(\alpha)} = 0.75$ and increasing λ.

versa, if a size for the vesicle is assumed, one can determine the critical line tension below the transition takes place. In [186], a typical value for $\lambda^{(\alpha,\beta)}$ is given as $\lambda^{(\alpha,\beta)} \simeq 1.2pN$ (at $T = 293\,K$). Then, together with $\kappa^{(\beta)} \simeq 2 \cdot 10^{-19} J$ the critical size of the vesicle R_0^* can be estimated. For the vesicle with above material parameters we obtain for R_0^*

$$R_0^* \leq \kappa^{(\beta)} \frac{\lambda}{\lambda^{(\alpha,\beta)}} \lesssim 0.28\,\mu m\,, \tag{5.18}$$

where $\lambda \lesssim 1.68$ has been considered. The critical size of the vesicle R_0^* is expected to become larger as the temperature increases. Upon an increase in the temperature, the line tension $\lambda^{(\alpha,\beta)}$ is decreased significantly while the bending rigidity is only affected modestly.

5.4.2 Vesicles with volume constraints – Equilibrium configurations

So far, vesicles which can freely adapt their volume have been analysed. In this section we extend the analysis to vesicles which are subject to volume constraints. In general, additional constraints such as a volume constraint lead to the existence of new morphologies which would otherwise not be stable. Examples were encountered in chapter 4, where in the case of an almost spherical geometry the fixed vesicle volume leads to a larger number of solid domains.

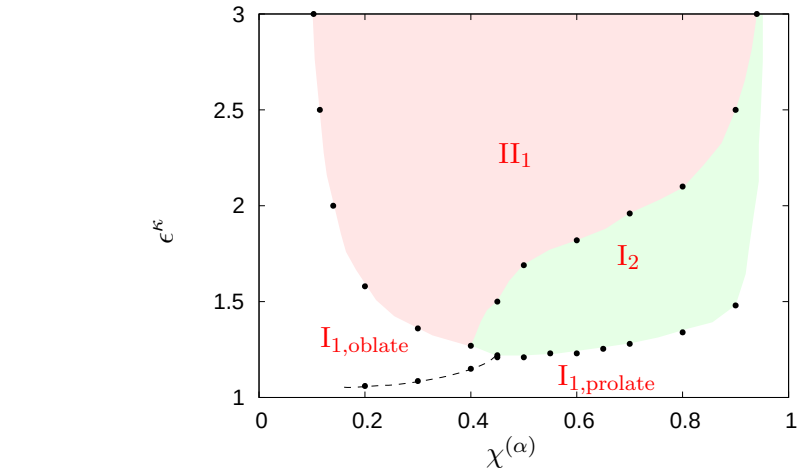

(a)

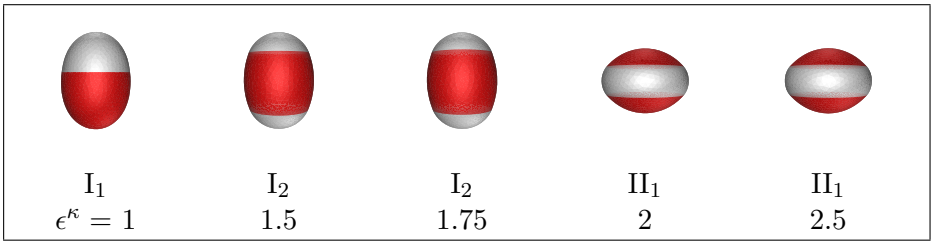

(b)

Figure 5.9: Vesicle with fluid membrane domains with volume constraints - Influence of a difference in the elastic bending moduli. (a) Morphology diagram of the vesicle at reduced volume $v = 0.97$ as a function of the area fraction $\chi^{(\alpha)}$ and the bending rigidity ratio ϵ^κ for the reduced line tension $\lambda = 0.2$ and vanishing Gaussian curvature $\Delta\epsilon^{\kappa_G}$. (b) Corresponding shapes of minimum energy for $\chi^{(\alpha)} = 0.6$ and increasing ϵ^κ.

We analyse the vesicle with the reduced line tension $\lambda = 0.2$ and equal Gaussian bending moduli $\Delta\epsilon^{\kappa_G} = 0$ for the reduced volume $v = 0.97$, which has been studied in section 5.4.1 in the unconstrained case. Fig. 5.9 depicts the morphology diagram with equilibrium shapes. Qualitatively, it looks similar to the diagram without volume constraints. However, the transition from morphology I_1 occurs at a slightly smaller bending rigidity ratio ϵ^κ. This is because, for small differences in the bending rigidities, the unconstrained vesicle I_1 prefers an almost spherical shape, $v \simeq 0.99$. Thus, for reduced volume $v = 0.97$, it is forced to acquire a smaller volume than in the unconstrained case which implies a slightly higher energy. For $v = 0.97$, morphology II_1 and I_2 are less affected by the constraint on the volume because they acquire an equilibrium shape which differs from the sphere already in the unconstrained case.

Domain-induced transition between prolate and oblate morphology

Regarding vesicle morphology I_1, there is an interesting effect not present for unconstrained vesicles. For vesicle morphology I_1, the formation of the domain can induce a morphological transition between an oblate and a prolate shape. We start with axisymmetric shapes. Fig. 5.10a depicts the equilibrium energy of an axisymmetric prolate and an axisymmetric

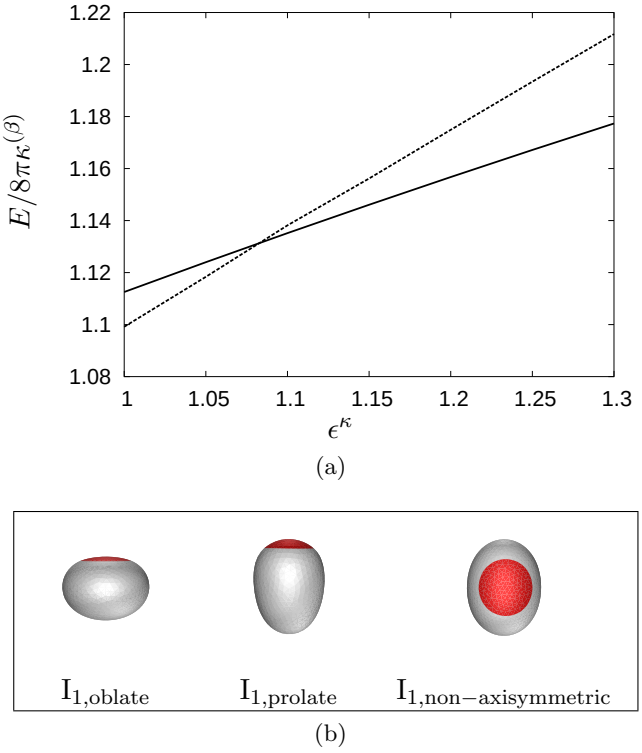

Figure 5.10: Domain-induced transition between a prolate and an oblate vesicle. (a) The minimum energy E of an axisymmetric prolate, morphology $I_{1,prolate}$ (dashed line), and an axisymmetric oblate vesicle, morphology $I_{1,oblate}$ (solid line), as a function of the bending rigidity ratio ϵ^{κ} for the area fraction $\chi^{(\alpha)} = 0.3$, reduced line tension $\lambda = 0.2$, equal Gaussian curvature moduli $\Delta\epsilon^{\kappa_G} = 0$ and fixed reduced volume $v = 0.97$. (b) Different vesicle morphologies: the axisymmetric oblate, morphology $I_{1,oblate}$, the axisymmetric prolate, morphology $I_{1,prolate}$ and an example of a non-axisymmetric shape, morphology $I_{1,non-axisymmetric}$.

oblate morphology as a function of the bending rigidity ratio ϵ^{κ} for area fraction $\chi^{(\alpha)} = 0.3$. For $\epsilon^{\kappa} \lesssim 1.08$, the prolate $I_{1,prolate}$ has minimum energy, while for $\epsilon^{\kappa} \gtrsim 1.08$ the oblate morphology $I_{1,oblate}$ is optimum. At $v = 0.97$, the equilibrium morphology of a homogeneous vesicle is a prolate. Accordingly, for a phase separated vesicle at low line tension, for $\epsilon^{\kappa} = 1$ the equilibrium state is an axisymmetric prolate with a 'cap domain' on its pole. This domain configuration provides shortest domain boundary. As the bending rigidity ratio ϵ^{κ} increases, there is a transition to an oblate morphology $I_{1,oblate}$. The transition occurs for area fraction $\chi^{(\alpha)} < 0.5$ and bending rigidities slightly above $\epsilon^{\kappa} = 1$ and is shown in Fig. 5.10 as a dashed line.

If non-axisymmetric shapes are included, it is possible that the transition between the prolate and the oblate vesicle is not discontinuous but proceeds in a continuous manner via a sequence of intermediate non-axisymmetric shapes, see Fig. 5.10b. These are biaxial shapes where the domain is not located at the pole of the vesicle, but shifted away. For small reduced line tension, the energy difference between the different morphologies is small and beyond the numerical accuracy of our calculations.

For small values of $\chi^{(\alpha)}$, the situation is even less clear. As the area fraction decreases,

the energies of the different vesicle morphologies become more similar. It seems that the region where non-axisymmetric biaxial shapes exist becomes larger. This would imply that the transition line between $\mathrm{I}_{1,\mathrm{prolate}}$ and $\mathrm{I}_{1,\mathrm{prolate}}$ would be smeared further and end at some point. It should be noted that in the limit $\chi^{(\alpha)} \approx 0$, the prolate morphology is recovered. In the limit $\epsilon^{\kappa} \approx 1$, the equilibrium shape is a prolate with a domain cap at the pole of the vesicle.

5.5 Discussion and conclusion

It was the goal of this chapter to investigate vesicle morphologies with coexisting fluid domains. The shape of these vesicles is governed by an interplay of line energy and different bending energies. Line tension causes shape transformations of the vesicle such as the budding transition. In this chapter the focus was on phenomena when effects from line tension are less relevant. It was shown that morphological transitions can be induced upon a change of the bending and/or Gaussian bending rigidity. It was argued that for a comparable low line tension also vesicles with more than two domains are stable configurations. We have given an estimate for the size of a typical vesicle below which these morphological transitions should occur.

Both, unconstrained vesicles and vesicles at fixed volume have been considered. For fixed volume, we have observed for the vesicle with two domains a morphological transition which between prolate and oblate conformation.

In our analysis we have determined the morphology diagrams for zero temperature. We expect that, analogously to solid domains, the morphology diagrams will not be seriously affected by thermal fluctuations.

Chapter 6

General conclusions and outlook

Vesicles are fascinating due to their biological implications and the wide spectrum of biotechnological applications, and also as a challenging topic for fundamental research. In this thesis, several important aspects regarding the morphology of vesicles have been addressed. Morphological transitions between different vesicle shapes were encountered which were either induced by thermal fluctuations, as it is the case between prolate and oblate vesicles, covered in chapter 3, or by membrane domains – lateral inhomogeneities in the membrane compositions – which was the subject of chapter 4 (vesicles with coexisting solid and fluid membrane domains) and 5 (vesicles with coexisting fluid membrane domains).

The main results of the investigations presented here are summarised as follows:

In chapter 3 the statistical mechanics of fluid vesicles is studied. While vesicles without volume constraints acquire an exact spherical shape at zero temperature, their configurations undergo transitions between prolate and oblate morphologies at finite temperatures. We determined the free energy profile of this shape transition, revealing that the transition proceeds continuous and there is no free energy barrier involved.

Domain formation on closed surfaces such as vesicles exhibits a rich behaviour, compared to flat membranes. Chapter 4 considers the morphology of fluid vesicles with solid membrane domains. Morphology diagrams for the domain shapes with minimum energy have been determined for vesicles with and without volume constraints for different material parameters. For typical membrane properties, a single round solid domain is found to have the lowest energy at small domain sizes, while a vesicle with two solid domains is optimal when the solid area fraction increases. An almost spherical geometry of the vesicle was shown to lead to an increasing number of solid domains as the area fraction of the solid membrane increases.

Finally, in chapter 5 vesicles with coexisting fluid domains were investigated. Vesicles with two domains, thus with the smallest interface length between the domains, are the optimal configurations if line tension plays a major role. In this chapter it was shown that when the line energy is comparably small, at appropriate conditions the vesicle will not necessarily acquire shapes with two domains. Upon a variation of the bending moduli and Gaussian bending moduli of the different membranes, morphological transitions to vesicle geometries with more complex domain shapes occur.

There are several (research) directions into which the work in this thesis may be extended. The section on solid domains starts from the assumption that the solid membrane is flat and free of any defects. Although many features can already be seen from this approximation, it

may be worthwhile (and challenging) to work out the implications of defects in the membrane, as they are can be observed in the experiments, in a future study.

In our analysis of domains we have determined morphology diagrams which give information about the equilibrium configuration with minimum energy and the location of morphological transitions between them (corresponding to the binodal in a phase diagram). For an understanding of the kinetics of shape transformations in addition information about the order of the transition, the stability of metastable states (spinodal) and knowledge of the free energy barrier between the metastable state and the equilibrium configuration is necessary. This barrier has to be overcome by thermal fluctuations when the vesicle undergoes a transition. The Monte Carlo algorithm implemented in this thesis can serve as a starting point to address these questions.

Appendix

Appendix A

A.1 Differential geometry and topology of surfaces

In this section we briefly review the differential geometry and topology of surfaces, thus providing the necessary tools which are used in this thesis to describe the geometry of membranes and vesicles. A more comprehensive introduction of this classical field of mathematics can be found in textbooks [140, 187, 188].

A.1.1 Basic definitions

A surface S is defined as a two-dimensional, smooth object (submanifold) embedded into three-dimensional Euclidean space $\mathbb{R}^3$. Let the variables ξ^1 and ξ^2 denote the internal coordinates of the surface. The configuration of the surface is then given by the vector function $\mathbf{X}(\xi^1, \xi^2)$

$$\mathbf{X} : \begin{cases} U \subset \mathbb{R}^2 & \rightarrow & \mathbb{R}^3 \\ (\xi^1, \xi^2) & \mapsto & \mathbf{X}(\xi^1, \xi^2) \end{cases} . \tag{A.1}$$

Provided that this mapping is sufficiently smooth (i.e. $\mathbf{X}(\xi_1, \xi_2)$ differentiable), one can assign to each point p of this submanifold its tangent space T_pS, which is a vector space spanned by the two tangential vectors given by

$$\mathbf{e}_\mu|_p \equiv \partial_\mu \mathbf{X}|_p := \left. \frac{\partial \mathbf{X}}{\partial \xi^\mu} \right|_p , \tag{A.2}$$

where $\mu = 1, 2$. This basis of T_pS is denoted as the coordinate basis $\{\mathbf{e}_\mu\} = \{\partial_\mu\}$. The normal space at p, $T_p^\perp S$, is defined as the orthogonal complement of T_pS in $\mathbb{R}^3$ with the basis

$$\mathbf{n} \equiv \frac{\partial_1 \mathbf{X} \times \partial_2 \mathbf{X}}{|\partial_1 \mathbf{X} \times \partial_2 \mathbf{X}|} , \tag{A.3}$$

where the symbol $\times$ denotes the conventional cross-product in $\mathbb{R}^3$. The sign of the vector $\mathbf{n}$ depends on the choice of an orientation of the surface. The so-called cotangent space T_p^*S is defined as the dual space of T_pS at p, $T_p^*S = (T_pS)^*$, its elements are linear functionals on T_pS. Vectors in T_pS are called contravariant vectors, its components are written with superscript ("upper") indices; vectors in T_p^*S are called covariant vectors and are denoted by subscripts ("lower" indices).

Once the tangent space and cotangent space are defined, one can introduce vector fields (and one-forms) which assign in a smooth manner to every point of the manifold an element,

a vector (or covector) from the tangent (cotangent) space at that point. Tensor fields are multi-linear forms which provide for every point of the manifold a map from a collection of vectors and covectors to an element of $\mathbb{R}$. The map varies smoothly from point to point on the manifold and fulfils the well known transformation properties under passing to a new coordinate system.

In order to perform calculus on surfaces or other manifolds one has to compare elements from infinitesimally close, but different tangent spaces. For this purpose one needs an extra structure called (affine) connection which provides the mapping between different tangent spaces and describes how vectors (or covectors) are parallel-transported along a curve. It is defined via the connection coefficients $\Gamma^{\mu}_{\nu\lambda}$, which specify how the basis vector coefficients change when they are parallel-transported in a certain direction. The covariant derivative of a vector function $\mathbf{v} = v^{\nu}\mathbf{e}_{\nu}$ along the direction $\mathbf{e}_{\mu}$ is defined as [1]

$$D_{\mu}v^{\nu} \equiv \partial_{\mu}v^{\nu} + v^{\lambda}\Gamma^{\nu}_{\lambda\mu}\,. \tag{A.4}$$

The covariant derivative of a tensor field yields a tensor quantity again. The parallel-transport of a vector between two points along a curve is fixed by demanding that the covariant derivative of the vector vanishes along the curve. In general, the result of parallel-transport is path-dependent, i.e. it depends on the specific curve chosen between the two endpoints of the curve. We will come back to this fact when we talk about (intrinsic) curvature and torsion further below in the text.

The local geometry of the surface can be characterised by two tensors, the first fundamental form (or metric tensor) and second fundamental form (the extrinsic curvature).

A.1.2 First fundamental form

A surface is the simplest object that has an own intrinsic geometry. The intrinsic properties of the surface are described by the first fundamental form (or metric) $g_{\mu\nu}$. The metric tensor is a symmetric second-rank tensor (a positive-definite quadratic form on the manifold's tangent spaces) defined by

$$g_{\mu\nu} \equiv \partial_{\mu}\mathbf{X}\cdot\partial_{\nu}\mathbf{X}\,, \tag{A.5}$$

where the dot is the conventional scalar product in $\mathbb{R}^3$. Its dual tensor is denoted as $g^{\mu\nu}$, so that one has

$$g^{\mu\nu}g_{\nu\lambda} = \delta^{\mu}_{\lambda}, \tag{A.6}$$

where δ^{μ}_{λ} is the Kronecker delta. The metric provides a natural isomorphism between the tangent space and the cotangent space. Together with its inverse, it can be used to raise and lower Greek indices in tensor quantities.

The determinant of the first fundamental form is given by

$$g \equiv \det\mathbf{g} = \frac{1}{2}\epsilon^{\mu\nu}\epsilon^{\lambda\omega}g_{\mu\lambda}g_{\nu\omega}, \tag{A.7}$$

where $\epsilon^{\mu\nu}$ is the two-dimensional antisymmetric Levi-Civita symbol

$$\epsilon^{\mu\nu} = \delta^{\mu}_{1}\delta^{\nu}_{2} - \delta^{\nu}_{1}\delta^{\mu}_{2}, \qquad \epsilon_{\mu\nu} = \epsilon^{\mu\nu}. \tag{A.8}$$

[1] Repeated Greek superscript-subscript indices imply summation following the Einstein summation convention.

We also need the antisymmetric tensor density $\gamma_{\mu\nu}$. Its covariant expression is defined by

$$\gamma_{\mu\nu} = \mathbf{n} \cdot (\mathbf{e}_\mu \times \mathbf{e}_\nu) = \sqrt{g}\epsilon_{\mu\nu} \,, \tag{A.9}$$

and its contravariant counterpart by $\gamma^{\mu\nu} = g^{\mu\lambda}g^{\nu\omega}\gamma_{\lambda\omega}$. The mixed quantity $\gamma^\mu_\nu = g^{\mu\lambda}\gamma_{\lambda\nu}$ acts on vectors of the tangent plane by rotating them by $\pi/2$.

The metric tensor is an important geometric quantity which, as the name indicates, allows to measure distances along the surface. The area of a local differential element of the surface is given by

$$dA = \sqrt{g}\, d\xi^1 d\xi^2 \,, \tag{A.10}$$

an expression which will be repeatedly used in surface integrals.

The metric induces a unique (symmetric and torsion free) affine connection, the so-called Levi-Civita connection. The connection coefficients are the Christoffel symbols which are derived from the metric by

$$\Gamma^\lambda_{\mu\nu} = \frac{1}{2} g^{\lambda\omega} \left(\partial_\nu g_{\omega\mu} + \partial_\mu g_{\omega\nu} - \partial_\omega g_{\mu\nu}\right) \tag{A.11}$$

with $\Gamma^\lambda_{\mu\nu} = \Gamma^\lambda_{\nu\mu}$.

Up to now, the coordinate basis $\{\mathbf{e}_\mu\} = \{\partial_\mu\}$ has been used as a basis for the tangent space T_pS. Sometimes it is favourable to work in a non-coordinate, orthonormal basis with orthonormal basis vectors $\{\mathbf{e}_a\}$ $(a = 1, 2)$ for the tangent space T_pS [2]. Orthonormality implies that $\mathbf{e}_a \cdot \mathbf{e}_b = \delta_{ab}$. Such a basis is achieved by introducing a zweibein e^μ_a, compatible with the metric $g_{\mu\nu}$

$$g_{\mu\nu} e^\mu_a e^\nu_b = \delta_{ab} \,, \qquad e^\mu_a e^\nu_b \delta^{ab} = g^{\mu\nu} \,. \tag{A.12}$$

The zweibein e^μ_a provides the transition from the coordinate basis $\{\mathbf{e}_\mu\}$ of T_pS to an orthonormal basis $\{e_a\}$ of T_pS

$$\mathbf{e}_a \equiv e^\mu_a \mathbf{e}_\mu \,. \tag{A.13}$$

A connection formulated with respect to the orthonormal basis $\{\mathbf{e}_a\}$ is commonly called spin connection. The covariant derivative of a vector $\mathbf{u} = u^a \mathbf{e}_a$ along the direction $\mathbf{e}_\mu$ reads

$$D_\mu u^a = \partial_\mu u^a + u^b \omega^a_{b\mu} \,, \tag{A.14}$$

where $\omega^a_{b\mu}$ denotes the coefficients of the spin connection. Metric-compatibility requires $\omega^a_{b\mu} = -\omega^b_{a\mu}$, in two dimension this simplifies to $\omega^a_{b\mu} = \epsilon_{ab} A_\mu$. The parallel-transport of a vector should not depend on the choice of the basis of the tangent space, i.e. whether a coordinate basis $\{\mathbf{e}_\mu\}$ or a non-coordinate basis $\{\mathbf{e}_a\}$ is used. From this requirement, relations between the (affine) connection coefficients and the spin connection coefficients can be derived [140].

[2] Hereafter, in order to distinguish between these two different basis, we use Greek indices for the coordinate basis and letters of the Latin alphabet when we work in a non-coordinate basis.

A.1.3 Second fundamental form

While the first fundamental form is concerned with intrinsic geometric properties of the surface, the second fundamental form provides information on extrinsic geometric properties, i.e. the embedding of the surface. The second fundamental form or extrinsic curvature tensor $h_{\mu\nu}$ is a symmetric second-rank tensor and measures the local deviation of the surface from its tangent plane. It is defined via

$$\partial_\mu \partial_\nu \mathbf{X} \equiv \Gamma^\lambda_{\mu\nu} \mathbf{e}_\lambda + h_{\mu\nu} \mathbf{n} \,. \tag{A.15}$$

From the extrinsic curvature tensor one can extract two scalar invariants, the scalar mean curvature H and the Gaussian curvature K:

$$H \equiv \frac{1}{2} \mathrm{Tr}\,(g^{\mu\nu} h_{\nu\lambda}) = \frac{1}{2} g^{\mu\nu} h_{\nu\mu} = \frac{1}{2}(C_1 + C_2) \tag{A.16}$$

$$K \equiv \det\,(g^{\mu\nu} h_{\nu\lambda}) = C_1\, C_2 \,. \tag{A.17}$$

The eigenvalues of $g^{\mu\nu} h_{\nu\lambda}$, C_1 and C_2, are called principal curvatures. The sign of the mean curvature H depends on the choice of an orientation $\mathbf{n}$ on the surface. The Gaussian curvature does not have a sign ambiguity. The Gaussian curvature is positive for convex or concave regions of the surface and negative for saddle like regions.

The first and second fundamental form of a surface are not independent of each other. In order to describe a surface they have to satisfy certain integrability equations which are called Gauss-Mainardi-Codazzi equations [140].

Here, the first and second fundamental forms have been formulated with tensor notation. They can be cast in the compact notion of differential forms, see [189] for applications to membranes and vesicles.

Intrinsic curvature and torsion

The Gaussian curvature, though here it is defined with the help of the extrinsic curvature tensor, is an intrinsic property of the surface, i.e. it depends only on the first fundamental form (Gauss' theorema egregium [3]). This is quite remarkable.

The observation that it is possible to study intrinsic curvature properties of a manifold itself and not only the curvature of a submanifold's embedding can be generalised to higher dimensional manifolds and leads to Riemannian geometry. Riemannian manifolds are defined as manifolds equipped with a metric and a connection that is compatible with the metric.

There are two important intrinsic quantities that characterise Riemannian manifolds: the curvature tensor $R^\lambda_{\omega\mu\nu}$ and the torsion tensor $T^\lambda_{\mu\nu}$. The curvature tensor $R^\lambda_{\omega\mu\nu}$ is defined via the noncommutativity of the covariant derivative along two coordinate lines, in components

$$(D_\mu D_\nu - D_\nu D_\mu)\, v^\lambda i \equiv R^\lambda_{\omega\mu\nu} v^\omega \,. \tag{A.18}$$

Geometrically, the Riemannian curvature measures the change of a vector when parallel-transported along an infinitesimal closed loop on the manifold. The group that is generated by parallel-transport of vectors along arbitrary closed loops is called holonomy group. For surfaces, the Gaussian curvature K determines all components of $R^\lambda_{\omega\mu\nu}$. One arrives at the simple relation

$$R^\lambda_{\omega\mu\nu} = g_{\omega\pi} \gamma^{\lambda\pi} \gamma_{\mu\nu} K \,. \tag{A.19}$$

[3] Latin: excellent theorem

The coefficients of the torsion tensor are defined as the anti-symmetric parts of the connection coefficients

$$T^{\lambda}_{\mu\nu} \equiv \Gamma^{\lambda}_{\mu\nu} - \Gamma^{\lambda}_{\nu\mu} \,. \tag{A.20}$$

Geometrically, the main feature of a connection with non-vanishing torsion is that two infinitesimal vectors fail to close when transported parallel along each other.

An important second order differential operator on manifolds is given by the Laplace operator. Although the general definition is conceptually independent of a connection, for surfaces or general Riemannian manifolds it is natural to define the Laplace-Beltrami operator as the trace of the covariant derivative

$$\Delta \equiv \nabla^2 \equiv g^{\mu\nu}\nabla_\mu\nabla_\nu = g^{\mu\nu}D_\mu D_\nu = D^\nu D_\nu \,. \tag{A.21}$$

The Laplacian of a scalar function $\phi(\xi^\nu)$ simplifies to

$$\Delta\phi = \frac{1}{\sqrt{g}}\frac{\partial}{\partial\phi^\mu}\left(\sqrt{g}g^{\mu\nu}\frac{\partial\phi}{\partial\xi^\nu}\right) . \tag{A.22}$$

We now turn from local properties of a surface to global properties. There is a remarkable relation between local and global quantities, as evidenced by the theorem of Gauss-Bonnet.

A.1.4 The theorem of Gauss-Bonnet

Topological methods allow to investigate manifolds according to their global properties. For surfaces in general a complete topological classification has been achieved. In the following we restrict to compact, orientable, connected surfaces, i.e. closed surfaces (without boundary) and open surfaces (with boundaries). These surfaces are uniquely classified (up to homeomorphism) by the genus g and the number of boundary components b of the surface. The genus of a surface (number of 'holes') is defined as the maximum number of nonintersecting, distinct closed curves that can be drawn on the surface without separating it. For closed surfaces, the topologically different surfaces are given by the g-fold tori, which are obtained from the sphere by attaching g handles. From these tori, open surfaces are obtained by creating the corresponding number of boundaries b.

An important topological invariant is given by the Euler-Poincaré characteristic χ_{Euler}. It is defined as the alternating sum of the n^{th} Betti number b_n (b_n is the rank of the n^{th} homology group). For orientable surfaces, the Euler-Poincaré characteristic can be computed according to

$$\chi_{\text{Euler}} = 2 - 2g - b \,. \tag{A.23}$$

On a surface discretised with triangles one finds alternatively

$$\chi_{\text{Euler}} = N_v - N_e + N_f \,, \tag{A.24}$$

where N_v is the number of vertices, N_e the number of edges and N_f the number of triangles. The Euler-Poincaré characteristic χ_{Euler} does not depend on the specific discretisation of the surface.

With the previous notions we can formulate the theorem of Gauss-Bonnet. This theorem states that the integral over the Gaussian curvature is a topological invariant. For a closed surface S, it reads

$$\int_S dA\, K = 2\pi\chi_{\text{Euler}}\,. \tag{A.25}$$

For an open surface with b closed boundary curves, it has to be corrected by boundary contributions

$$\int_S dA\, K = 2\pi\chi_{\text{Euler}} - \sum_{i=1}^{b} \oint_{\partial S_i} c_g dl_i\,, \tag{A.26}$$

where dl_i denotes the line integral along the boundary line ∂S_i and c_g is the geodesic curvature of the boundary line. The geodesic curvature c_g is a measure for the curvature of a line in a metric space. Let $\mathbf{R}(l) \equiv \mathbf{R}(\xi^1(l), \xi^2(l))$ parametrise a curve on a surface via the arc length l (with $|d\mathbf{R}/dl| = 1$). The curvature of this line can be split into an orthogonal and a tangential part to the surface

$$\frac{d^2\mathbf{R}}{dl^2} \equiv c_n\,\mathbf{n} + c_g\left(\mathbf{n} \times \frac{d\mathbf{R}}{dl}\right)\,, \tag{A.27}$$

where c_n is the normal curvature of the line. Thus, c_g is given by

$$c_g = \left(\mathbf{n} \times \frac{d\mathbf{R}}{dl}\right) \cdot \frac{d^2\mathbf{R}}{dl^2}\,. \tag{A.28}$$

The geodesic curvature is a measure for the intrinsic curvature of a line on a surface and does not depend on how the surface is embedded in space. It quantifies the deviation of the curve from following the geodesic line, which is the natural generalisation of the 'straight' line in a curved manifold. Obviously, for the geodesic line the geodesic curvature vanishes everywhere.

The Gauss-Bonnet theorem is the simplest example of an index theorem. Index theorems connect certain local, differential properties of a manifold to global properties of the manifold. To be more precise, they link the analytical index of certain differential operators (which is closely related to the dimension of the space of solutions of the differential operator on a manifold) to a topological index of the manifold [190].

A.2 Discretisation of surfaces

In order to perform numerical calculations or simulations the smooth surface has to be discretised, for example by triangulation, in which the surface is approximated by triangular mesh cells. The smooth surface is recovered in the continuum limit of infinitesimally small triangles. Mathematically, a triangulation $\mathcal{T}_{N_v}$ is defined as a two-dimensional set of simplices (a simplical complex) consisting of N_f triangles (2-simplices), N_e edges (1-simplices) and N_v vertices (0-simplices). The simplices are combined such that the intersection of any two simplices is either empty or a shared simplex of lower dimensionality. The numbers N_f, N_e and N_v fulfil $\chi_{\text{Euler}} = N_v - N_e + N_f$, where χ_{Euler} is the Euler-Poincaré characteristic. In the following individual triangles are denoted with f_i, edges with e_i, and vertices with v_i.

Once the surface has been triangulated, the differential geometric quantities like mean or Gaussian curvature have to be extended onto the discretised surface. This task turns out to be difficult. An obvious requirement which a suitable generalisation has to meet is that, as the triangulation is refined, the discretised version approaches continuously the corresponding

quantities of the smooth surface. Unfortunately, for an arbitrary triangulation a practicable definition which assigns a discretised differential geometric quantity to a vertices and converges locally does not exist in general. What can be found instead are quantities which convergence in the sense of (integral) measures [191]. These are given by the $(d+1)$ Minkowski functionals (in d dimensions). Minkowski functionals are integral geometric measures (quermass measures), which are constructed to be motion-invariant, continuous and additive. In three dimensions, these functionals correspond to the (local) integrated volume, the integrated area, integrated mean curvature and integrated Gaussian curvature. Because of the continuity of these integral measures, the values calculated on a polyeder converge for a sequence of refined triangulations to the correct values of the smooth surface.

The area of the total surface or parts of it is given by the sum of the areas of the individual triangles

$$\int dA = \sum_{f_i} A_i \,, \tag{A.29}$$

where A_i is the area of triangle f_i.

The volume enclosed by the triangles f_i can be calculated by

$$\int dV = \sum_{f_i} V_i \,, \tag{A.30}$$

where

$$V_i = \frac{1}{3}(\mathbf{n}_i \cdot \mathbf{X}_i) A_i \tag{A.31}$$

denotes the volume of a pyramid defined by its base triangle f_i and its top vertex which lies in the coordinate origin ($\mathbf{n}_i$ is the normal vector of the triangle f_i and $\mathbf{X}_i$ the position vector to one of the vertices of the triangle).

The (local) integral over the mean curvature is obtained by the sum over edges e_i

$$\int dA\, H = \sum_{e_i} \frac{1}{2}\, l_i \phi_i \tag{A.32}$$

where l_i is the length of the edge e_i and is ϕ_i the tilting angle between the neighbouring triangles f_j and f_k adjacent to e_i, $\cos\phi_i = \mathbf{n}_j \cdot \mathbf{n}_k$.

The integral over the Gaussian curvature is computed as a sum over vertices v_i

$$\int dA\, K = \sum_{v_i} \left(2\pi - \sum_j \alpha_j \right)_i \,, \tag{A.33}$$

where α_j is the angle of the triangle f_j incident to the vertex v_i. $(2\pi - \sum_j \alpha_j)_i$ measures the deficit angle of vertex v_i to 2π.

In 1957 Hadwiger showed that the Minkowski functionals are the only scalar functionals which are motion-invariant, continuous and additive [192]. This implies that for other integrals like $\int dAH^2$ or $\int dAK^2$ an appropriate discrete version does not exist on a polytope. Hence we will have to resort to some approximations.

In our simulations we apply for the integral over the squared mean curvature the approximation proposed in [105]. It is based on the square of the local average of the discretised

integrated mean curvature around a vertex. In this way, certain shortcomings are avoided which are encountered in other discretisation approaches, see [104] for a detailed discussion. Following Eq. (A.32), we can calculate the averaged integrated mean curvature around the vertex v_i

$$(H\bar{A}_i)_i = \frac{1}{2}\left(\sum_{e_j}\frac{1}{2}\,l_j\phi_j\right)_i\,, \tag{A.34}$$

where the sum extends over all edges e_j which share the vertex v_i. The factor $\frac{1}{2}$ arises because only half of the contribution of an edge should be assigned to a single vertex. The area associated to a vertex v_i, when shared equally between the vertices, is given by

$$\bar{A}_i = \left(\sum_{f_j}\frac{1}{3}A_j\right)_i\,, \tag{A.35}$$

where A_j is the area of the adjacent triangle f_j. The discretised Helfrich Hamiltonian can be expressed as

$$\frac{1}{2}\int dA(2H)^2 \simeq 2\sum_{v_i}\frac{(H\bar{A}_i)_i^2}{\bar{A}_i}\,. \tag{A.36}$$

For the Gaussian curvature, the situation is slightly different because it is an intrinsic geometric quantity. Nevertheless, appropriate measures for the discretised Gaussian curvature that converge pointwise around a vertex can only be found for very special triangulations, for example for regular meshes with valency six [193]). In general, a measure for the Gaussian curvature associated with a vertex v_i can be inferred from the angular defect of v_i [194]. The angle deficit has to be multiplied by a factor with dimension $[\text{length}]^{-2}$. The natural quantity to divide the angular defect with is the area of the incident triangles, thus

$$K_i \simeq \left(\frac{2\pi - \sum_j \alpha_j}{\bar{A}_i}\right)_i\,. \tag{A.37}$$

It has to be noticed, however, that this formula is justified only for triangulations which are based on geodesic triangles of the surface [106]. Therefore, this formula is of little help from a practical point of view as the knowledge of the geodesics is required. For arbitrary triangulations, it is advantageous to correct the angle deficit with the so-called module of the mesh. As a local estimate for the Gaussian curvature we use [106]

$$K_i \simeq \left(\frac{2\pi - \sum_j \alpha_j}{\frac{3}{2}\bar{A}_i - \frac{1}{8}\sum_j \operatorname{cotg}(\alpha_j)\bar{l}_j^2}\right)_i\,, \tag{A.38}$$

where $\bar{l}_j$ is the length of the triangle f_j edge opposed to the angle α_j. From this result expressions for the integrated square of the Gaussian curvature can be derived.

Appendix B

B.1 On the integral measure for fluid membranes

Thermal equilibrium properties of fluid membranes are encoded in the partition function, Eq. (2.3),

$$\mathcal{Z}(T) = \int \mathcal{D}\{\mathbf{X}(\xi)\}\, e^{-\mathcal{H}_{\rm fluid}(\mathbf{X}(\xi))/T}\,. \tag{B.1}$$

It is written as a functional integral which extends over all possible, physically different embeddings of the membrane. When evaluating this functional integral, one has to be careful because of the reparametrisation symmetry of the integrand. The Hamiltonian $\mathcal{H}_{\rm fluid}(\mathbf{X}(\xi))$ is invariant under changes of the coordinate system parametrising the surface, $\xi^a \to \xi'^a(\xi^1, \xi^2)$. This reparametrisation symmetry reflects the fluidity of the membrane.

Apparently, when calculating the partition function, B.1, the result must not depend on the chosen parametrisation. The measure $\mathcal{D}\{\mathbf{X}(\xi)\}$ has to guarantee that each physical configuration is counted only once and redundant (unphysical) degrees of freedom arising from the ambiguity in the parametrisation are eliminated. Infinitesimal reparametrisations are generated by the vector fields $\epsilon^a(\xi)$, $\xi^a \to \xi'^a = \xi^a + \epsilon^a(\xi)$, which act on $\mathbf{X}(\xi)$ as

$$\mathbf{X}(\xi) \to \mathbf{X}_\epsilon(\xi) = \mathbf{X}(\xi) + \epsilon^a(\xi)\frac{\partial}{\partial \xi^a}\mathbf{X}(\xi)\,. \tag{B.2}$$

Since $\mathbf{X}(\xi)$ and $\mathbf{X}_\epsilon(\xi)$ describe the same membrane conformation, they should only give a single contribution to the functional integral. One way to overcome this problem is to extend the integral in Eq. (2.3) with an integral over the metric tensor $g_{\mu\nu}(\xi)$, which is treated as an independent field [1]

$$\begin{aligned}\mathcal{Z}(T) &= \int \mathcal{D}\{\mathbf{X}(\xi)\}\, e^{-\mathcal{H}_{\rm fluid}(\mathbf{X}(\xi))/T} = \\ &= \int \mathcal{D}\{\mathbf{X}(\xi)\}\mathcal{D}\{g_{\mu\nu}(\xi)\}\, \delta\left(\partial_\mu \mathbf{X}(\xi)\cdot\partial_\nu \mathbf{X}(\xi) - g_{\mu\nu}(\xi)\right)\, e^{-\mathcal{H}_{\rm fluid}(\mathbf{X}(\xi), g_{\mu\nu}(\xi))/T}\,.\end{aligned} \tag{B.3}$$

The δ-functional relates the embedding functions with the fluctuating metric, and guarantees that this is an identity transformation. The two redundant degrees of freedom in the parametrisation can be removed by fixing two local degrees of freedom of the metric. A convenient choice of gauge is given by the conformal metric

$$g_{\mu\nu}(\xi) = \rho(\xi)\delta_{\mu\nu}\,. \tag{B.4}$$

[1] This has been proposed originally by Polyakov in a different context [195].

That means that one finds local coordinates in which the metric is a spatially dependent conformal factor times the trivial metric. Conformal gauge is the two dimensional analogue of arc-length parametrisation of a curve in space and contains one (physical) degree of freedom $\rho(\xi)$ over which remains to be integrated. Thus, one ends up with

$$\mathcal{Z}(T) = \int \mathcal{D}\{\mathbf{X}(\xi)\}\mathcal{D}\{\rho(\xi)\}\,\delta(\partial_\mu \mathbf{X}(\xi)\cdot\partial_\nu \mathbf{X}(\xi) - \rho(\xi)\delta_{\mu\nu})\,e^{-\mathcal{H}_{\text{fluid}}(\xi)(\mathbf{X}(\xi),\rho(\xi))/T}\,. \tag{B.5}$$

The δ-functional leads to important measure corrections, so-called Faddeev-Popov terms [96].

Eq. (B.5), which is mostly a reformulation of Eq. (2.3), achieves the non trivial task of taking the underlying symmetries into account in a rigorous manner. In this form, it can be evaluated in a perturbative manner via the renormalisation procedure [96, 195].

Appendix C

C.1 On the elastic energy for hexatic membranes

Hexatic membranes are membranes with short translational and QLR orientational order. Orientational order means that there exists a preferred direction within the tangent plane at each point $\mathbf{X}(\xi)$ on the membrane. It can be expressed by the local bond order parameter

$$\mathbf{m}(\xi) = \cos\Theta(\xi)\mathbf{e}_1 + \sin\Theta(\xi)\mathbf{e}_2 = m^a(\xi)\mathbf{e}_a \tag{C.1}$$

where $\{\mathbf{e}_a\}$ $(a = 1, 2)$ forms an orthonormal basis of the tangent plane. Hexatic order implies that $\Theta(\xi)$ has six-fold symmetry, i.e. rotations of $\mathbf{m}(\xi)$ by $2p\pi/6$ (p is an integer) lead to physically equivalent states.

The free energy of hexatic membranes $\mathcal{H}_{\text{hex}}$ consists of a Helfrich-type bending energy and in-plane elastic energies $\mathcal{H}_{\text{hex, elast}}$

$$\mathcal{H}_{\text{hex}}(\mathbf{X}(\xi)) = \int d^2\xi\sqrt{g}\left(\frac{\kappa}{2}\left(2H - C_0\right)^2 + \kappa_G K\right) + \mathcal{H}_{\text{hex, elast}}(\mathbf{X}(\xi))\,. \tag{C.2}$$

The lowest non-trivial contribution to the in-plane elastic energy for orientational order can be written as [196]

$$\mathcal{H}_{\text{hex, elast}} = \frac{1}{2}k_A\int d^2\xi\sqrt{g}\, D_\mu m^a D^\mu m_a\,. \tag{C.3}$$

The coupling constant or hexatic stiffness k_A measures the strength of the coupling between the orientations of neighbouring bonds. In C.3, $D_\mu u^a = \partial_\mu u^a + u^b\omega^a_{b\mu}$ is the covariant derivative of the vector $\mathbf{u} = u^a\mathbf{e}_a$, $\omega^a_{b\mu}$ denotes the coefficients of the spin connection. The spin connection can be expressed as $\omega^a_{b\mu} = \epsilon_{ab}A_\mu$ with the antisymmetric Levi-Civita symbol ϵ_{ab} and the 'vector potential' A_μ. A_μ measures the frustration of the angular order parameter when it is parallel transported along an infinitesimal closed path on a curved surface [1]. The source field (curl) of

[1] In general, the parallel transport of a vector between two points on a curved surface depends on the chosen path. This implies that the bond angle at an arbitrary point on a curved surface has no path-independent meaning and thus is ambiguous. This is the case for the standard choice of connection (Levi-Civita connection), where the bond angle at some point reached by two distinct paths from a reference point depends on the intrinsic curvature (Gaussian curvature) enclosed by the paths. The problems of a path dependent order parameter can be circumvented by introducing a different connection which is tuned curvature free so that parallel transport of a vector is path independent, as desired. This is achieved by the connection $\omega^a_{b\mu}$ which involves a new degree of freedom, a geometric quantity called torsion. The curvature of the connection with torsion has the physical meaning as being proportional to the density of disclinations. In the presence of a high density of disclinations, when the hexatic melts into a fluid, the parallel transported bond angle becomes ambiguous, which is equivalent to saying that order in the bond angles does not exist in an isotropic fluid phase [197].

A_μ is given by the Gaussian curvature $K(\xi)$

$$\gamma^{\mu\nu} D_\mu A_\nu = K(\xi) \tag{C.4}$$

with $\gamma^{\mu\nu} = \epsilon^{\mu\nu}/\sqrt{g}$. A possible solution for Eq. (C.4) is

$$A_\mu = g^{\lambda\nu}\gamma_{\nu\mu} D_\lambda \int d^2\xi' \sqrt{g(\xi')}\, \widetilde{\Gamma}(\xi,\xi') K(\xi')\,. \tag{C.5}$$

Here, $\widetilde{\Gamma}(\xi,\xi') = 1/\Delta$ is the Green's function for the Laplacian Δ, i.e. $\Delta\widetilde{\Gamma}(\xi,\xi') = 1/\sqrt{g}\delta(\xi-\xi')$.

To proceed, it is instructive to rewrite the elastic energy Eq. (C.3) in terms of the angle variable $\Theta(\xi)$

$$\mathcal{H}_{\text{hex, elast}} = \frac{1}{2} k_A \int d^2\xi \sqrt{g} g^{\mu\nu} (\partial_\mu \Theta - A_\mu)(\partial_\nu \Theta - A_\nu)\,. \tag{C.6}$$

The free energy is invariant under local transformations $\Theta(\xi) \to \Theta(\xi) + \epsilon(\xi)$

$$A_\alpha(\xi) \to A_\alpha(\xi) + \partial_\alpha \epsilon(\xi)\,, \tag{C.7}$$

which corresponds to a local rotation of the reference frame $\{\mathbf{e}_a\}$.

To provide a more intuitive picture of this energy, we divide the field Θ into a regular part Θ^{reg} and a singular part Θ^{sing}. The regular part Θ^{reg} fulfils $D_\mu\partial_\nu\Theta^{\text{reg}} = D_\nu\partial_\mu\Theta^{\text{reg}}$. The singular part Θ^{sing} is related to the disclination density $s(\xi) = 1/\sqrt{g}\sum_i s_i\delta(\xi-\xi_i)$ (s_i denotes the charge of disclination i) by

$$\gamma^{\mu\nu} D_\mu \partial_\nu \Theta^{\text{sing}} = s(\xi). \tag{C.8}$$

Thus, one has

$$\partial_\mu \Theta^{\text{sing}} = g^{\lambda\nu}\gamma_{\nu\mu} D_\lambda \int d^2\xi' \sqrt{g(\xi')}\, \widetilde{\Gamma}(\xi,\xi') s(\xi')\,, \tag{C.9}$$

where $\widetilde{\Gamma}(\xi,\xi')$ is the same Green's function as above. By this, one finally can express Eq. (C.6) as

$$\mathcal{H}_{\text{hex, elast}} = \frac{1}{2} k_A \int d^2\xi \sqrt{g(\xi)} \int d^2\xi' \sqrt{g(\xi')} (K(\xi) - s(\xi)) \widetilde{\Gamma}(\xi,\xi') (K(\xi') - s(\xi'))\,. \tag{C.10}$$

Eq. (C.10) describes the in-plane stretching energy of a hexatic membrane, taking into account possible disclinations. A few things should be pointed out. First, the relevant quantity is not the disclination density or the Gaussian curvature separately, but the difference between them [2]. The disclination density can be screened by the development of Gaussian curvature (and vice versa). The in-plane elastic energy of hexatic membranes is smaller than the energy for crystalline membranes, Eq. (2.25). This is due to the presence of free dislocations in the hexatic. These act to reduce the strain caused by a non-isometric membrane deformation.

Geometric methods are an elegant and quite common approach in the modern description of topological defects [197, 198]. The proper geometric framework to describe a medium with a continuous distribution of dislocations and disclinations is provided by manifolds with non-vanishing intrinsic curvature and torsion (see appendix A.1). It is natural to assign torsion to a system with a high density of dislocations, such as in the hexatic, since torsion measures the nonclosure of the parallel transport of a vector. In an analogous manner, the density of free disclinations acts as a source for intrinsic curvature.

[2] The in-plane elastic energy in Eq. (2.25) is formulated for a crystalline membrane with a flat ground state without disclinations. In principle, for the general case of an arbitrary groundstate with disclinations, one would also have as the relevant quantity the difference between the Gaussian curvature and the disclination density.

Appendix D

D.1 Monte Carlo simulations

This section provides a brief introduction to computer simulations based on Monte Carlo methods. The reader is referred to the textbooks [199, 200] for a more detailed analysis on Monte Carlo techniques and computer simulations in general.

D.1.1 Basic principles

Monte Carlo methods have become an indispensable numerical tool for studying problems in statistical mechanics. As their name indicates (Monte Carlo is a reference to the casino in Monaco), these methods are stochastic techniques, meaning they are based on the repetitive use of random numbers to investigate problems. Historically, the first large scale Monte Carlo work carried out dates back to the middle of the 20^{th} century. Stanislav Ulam, John von Neumann and Enrico Fermi were the first who proposed and applied the Monte Carlo method as a numerical technique. The earliest published work on Monte Carlo is probably the paper by Metropolis and Ulam from 1949 [201].

Monte Carlo methods are especially useful for the numerical evaluation of high-dimensional integrals. Such integrals inevitably occur in the statistical treatment of systems with many degrees of freedom. A typical task in equilibrium statistical mechanics is to compute thermal averages of macroscopic observables of the system. The expectation value of an observable $A(x)$ is given by the integral over the (high-dimensional) phase space,

$$\langle A(x)\rangle = \int dx\, A(x) p_{\mathrm{eq}}(x)\,, \tag{D.1}$$

where x stands for the degrees of freedom $x = (x^1, x^2, x^3, \ldots, x^N)$. The probability density $p_{\mathrm{eq}}(x)$ describes the probability with which the configuration x occurs in thermal equilibrium. For the canonical ensemble, $p_{\mathrm{eq}}(x)$ is given by the normalised Boltzmann factor

$$p_{\mathrm{eq}}(x) = \frac{1}{\mathcal{Z}} e^{-\mathcal{H}(x)/T}\,. \tag{D.2}$$

Its normalisation constant is the canonical partition function $\mathcal{Z}$

$$\mathcal{Z} = \int dx\, e^{-\mathcal{H}(x)/T}\,. \tag{D.3}$$

Conventional methods of numerical integration operate by taking a number of evenly spaced samples x_i from the integration interval, estimating the integral by the sum

$$\langle A(x)\rangle \simeq \sum_{x_i} A(x_i)p_{\mathrm{eq}}(x_i)\,. \tag{D.4}$$

The number of computations required for these integration methods increases exponentially with the dimension of the integral. Hence, they become impracticable for higher-dimensional integrals. A solution is provided by Monte Carlo methods. There, instead of summing over a regular array of sampling points, one averages over a random sample of points. In the simplest variant these are distributed uniformly over the integration interval. This is called simple sampling. The statistical error is independent of the dimensionality of the integral, its accuracy increases with the square root of the sample size. Since the convergence towards the true value may be rather slow, simple sampling is not a real improvement. This is the case for sharply peaked integrals as they occur in statistical mechanics. The efficiency of the sampling routine can however be significantly enhanced if one does not sample configurations with a constant probability, but chooses preferentially those regions of phase space which contribute most to the integral. This is the basic principle lying behind importance sampling techniques. Apparently, the averages estimated by employing importance sampling are statistically much more reliable than those calculated by simple sampling.

Importance sampling

At first sight, determining a proper probability distribution that is similar to the integrand, seems to be just as difficult as solving the integrand itself. Nevertheless, there are powerful algorithms available that generate sampling states according to the desired distribution. These are based on stochastic processes which have the desired distribution function as their unique stationary distribution. In practice, the most frequently used are Markov processes. A Markov process is a stochastic process which generates a sequence of microstates. The transition probability from a present state x to the state x' depends only on the state x and x' and not on any other other state the chain has passed through before getting to x. The probability of the system going from microstate x to x' is denoted with $\rho(x, x')$. We assume that $\rho(x, x')$ is time-independent and preserves the normalisation of the probability distribution $p_{\mathrm{eq}}(x)$, i.e. $\rho(x, x')$ fulfils $\int dx'\,\rho(x, x') = 1$. We further require that $\rho(x, x')$ is irreducible or ergodic, meaning that it must be possible for the system, starting from any state, to reach any other state of its configuration in a finite time.

We discuss the conditions under which the probability distribution undergoing a Markov process converges towards a desired distribution $p_{\mathrm{eq}}(x)$. Let $p^{(t)}(x)$ indicate the probability density that the system is in the state x at time t. After one time step along the Markov chain, the probability $p^{(t+1)}(x')$ of being in state x' at time $(t + 1)$ is given by

$$p^{(t+1)}(x') = \int dx\,\rho(x, x')p^{(t)}(x)\,. \tag{D.5}$$

The equilibrium distribution $p_{\mathrm{eq}}(x)$ is reached when

$$p_{\mathrm{eq}}(x') = \int dx\,\rho(x, x')p_{\mathrm{eq}}(x)\,. \tag{D.6}$$

An important property of a Markov chain is that, as long as the transition matrix is ergodic, the sampled distribution converges for any choice of initial state towards $p_{\text{eq}}(x)$ in the long time limit. Eq. (D.6) can be reformulated by noting that at the kinetic equilibrium the system transition rates into and out of any state x must be equal. This can be expressed as

$$\int dx'\, \rho(x,x')p_{\text{eq}}(x) = \int dx'\, \rho(x',x)p_{\text{eq}}(x')\,. \tag{D.7}$$

In practice one usually imposes a stronger condition

$$\rho(x,x')p_{\text{eq}}(x) = \rho(x',x)p_{\text{eq}}(x')\,. \tag{D.8}$$

This is the condition of detailed balance and is a sufficient, though not necessary condition for a stationary distribution $p_{\text{eq}}(x)$.

For obvious reason, Monte Carlo estimates are always associated with some statistical error. First, before taking the average over samples one has to assure that the Markov process has reached equilibrium. One has to take into account in the error analysis that the data generated via a Markov process are correlated. The usual square root $N^{-1/2}$ behaviour of the variance for sample size N obtained by employing the central limit theorem does not hold. It has to be corrected by the the correlation time it takes that a microstate becomes uncorrelated to its initial state, see [202].

Metropolis algorithm

There is some freedom in choosing the transition probabilities $\rho(x,x')$. Here we will present the procedure proposed by Metropolis et al. [203], which in the literature is commonly referred to as the 'Metropolis algorithm'. Notwithstanding its age, it is still the basis of most Monte Carlo work done in statistical physics. The Metropolis algorithm allows to calculate expectation values of observables in the canonical ensemble. To proceed, we split the transition probability $\rho(x,x')$ into two parts, $\rho(x,x') = g(x,x')\,p_{\text{acc}}(x,x')$: a selection probability $g(x,x')$ and an acceptance probability $p_{\text{acc}}(x,x')$. The selection probability $g(x,x')$ defines the conditional probability that a new 'trial' state x' is proposed given that the current state is x. The acceptance probability $p_{\text{acc}}(x,x')$ gives the conditional probability that the proposed move is accepted. In the Metropolis algorithm the acceptance probability is chosen as the

$$p_{\text{acc}}(x,x') = \min[1, \frac{g(x,x')}{g(x',x)} e^{-(E(x')-E(x))/T}]\,. \tag{D.9}$$

It is easy to see that $\rho(x,x')$ satisfies detailed balance. In practice, $g(x,x')$ is often chosen to be symmetric in x and x', so $p_{\text{acc}}(x,x')$ reduces to

$$p_{\text{acc}}(x,x') = \min[1, e^{-(E(x')-E(x))/T}]\,. \tag{D.10}$$

A single move in a Metropolis Monte Carlo trajectory is obtained by the following steps

(i) Starting from the initial state x of the system, a new trial state x' is chosen according to the selection probability $g(x,x')$ and the energy difference $\Delta E(x,x') = E(x') - E(x)$ computed.

(ii) If $\Delta E(x, x') \leq 0$ the new state x' is accepted.

If $\Delta E(x, x') > 0$ a random number ρ_{rand} is drawn, which is uniformly distributed in the interval $[0, 1)$. The new state x' is accepted if the random number is smaller than $\rho_{\text{rand}} \leq e^{-\Delta E(x,x')/T}$, otherwise rejected.

The trajectory generated with this algorithm samples configurations according to the Boltzmann distribution. An important aspect for the implementation of a Metropolis algorithm is the choice of the selection rules $g(x, x')$. This has to be adapted to the individual problem in order to obtain an efficient sampling of the relevant microstates in phase space.

Pseudo-random numbers

Monte Carlo simulations require a huge amount of random numbers. The statistical reliability of the estimates depends on the quality of the random numbers used. The randomness (or complexity) of a sequence of numbers is well defined and can be quantified to a certain extent within the framework of algorithmic information theory [204]. However, formally it is impossible to proof that a given specific sequence of numbers is indeed random. This is due to an incompleteness theorem [204]. A list of numbers can be considered random, if (and only if) it is generated by a physical process such as radioactive decay which, according to present day theories, is believed to involve some intrinsic randomness. In Monte Carlo simulations one usually employs random numbers obtained by a software generator. These are pseudo random numbers, which are generated by a deterministic algorithm and thus are predictable and reproducible. One has to guarantee that they approximate 'true' random numbers in some sense, that they are not biased, appear uncorrelated, and are distributed uniformly in the range zero to one.

Acknowledgements - Danksagung

This dissertation was written in the 'Department of Theory and Bio-Systems' at the Max-Planck-Institute of Colloids and Interfaces. I would like to thank everyone who contributed, in whatever manner, to the success of this work.

An erster Stelle gilt mein Dank Prof. Reinhard Lipowsky, der als Leiter dieser Abteilung die Schirmherrschaft über diese Arbeit innehatte. Ich bedanke mich, einen fundierten Einblick in die aktuelle Forschung in einem lebendigen und vielfältigen Forschungsgebiet erhalten zu haben, sowohl durch das umfangreiche Lehr- und Seminarangebot am Institut als auch durch die Teilnahme an Konferenzen – darunter eine aufregende Sommerschule über weiche und biologische Materie in Zanjan (Iran) im Juni 2004.

Weiters danke ich meinem unmittelbaren Betreuer Thomas Gruhn für eine kritische Durchsicht und Korrektur des Manuskripts.

Ein herzliches Danke an Jan Kierfeld für anregende und hilfreiche Diskussionen über einzelne Themen in dieser Arbeit und, ebenso wie Prof. Ken Brakke, für Hilfestellung bei der Benützung des Softwareprogramms 'The Surface Evolver'.

Last, but not least grüße ich meine Eltern und bedanke mich für Unterstützung über all die Jahre hinweg.

List of symbols

A	vesicle area
A_j	area of triangle f_j
$\bar{A}_i$	area associated to vertex v_i
$A^{(i)}$	membrane area of phase (i)
α	asphericity
c_0	reduced spontaneous curvature
C_0	spontaneous curvature
$C_0^{(i)}$	spontaneous curvature of phase (i)
χ_{Euler}	Euler-Poincaré characteristic
$\chi^{(i)}$	area fraction of phase (i)
$\chi^{(i_1,i_2)}$	area fraction of domains in phase (i)
δ	shape anisotropy
Δ	Laplace operator
$\Delta\epsilon^{\kappa_G}$	difference of Gaussian bending rigidities
e_j	edge j
E	energy
ϵ^{κ}	ratio of bending rigidities
f_j	triangle j
F	free energy
F_a	free energy as a function of the order parameter a
$g(x,x')$	selection probability
$g_{\mu\nu}$	metric tensor
$g^0_{\mu\nu}$	reference metric tensor
γ	Föppl-von Kármán number
$h(x)$	out-of-plane deformation
H	mean curvature
$\mathcal{H}_{\text{ADE}}$	Area-difference-elasticity energy
$\mathcal{H}_{\text{CH}}$	Canham-Helfrich energy
$\mathcal{H}_{\text{cryst}}$	energy of the crystalline membrane
$\mathcal{H}_{\text{fluid}}$	energy of the fluid membrane
k_a, k_b	Lamè coefficients
k_{B}	Boltzmann constant
k_Y	Young's modulus
K	Gaussian curvature

κ	bending rigidity
$\kappa^{(i)}$	bending rigidity of phase (i)
κ_G	Gaussian bending rigidity
$\kappa_G^{(i)}$	Gaussian bending rigidity of phase (i)
l_0	maximum tether length
l_j	length of edge e_j
λ	reduced line tension
$\lambda^{(\alpha,\beta)}$	line tension
λ_i	eigenvalues of $\mathbf{Q}$
$\bar{\lambda}$	average eigenvalue of $\mathbf{Q}$
m	reduced integrated mean curvature
m_0	reference reduced integrated mean curvature
M	integrated mean curvature
$\mathbf{n}$	normal to the membrane surface
N_v	number of vertices
p	pressure difference between inside and outside of the vesicle
$p(x)$	probability density
p_a	probability density as a function of the order parameter a
$p_{\mathrm{acc}}(x, x')$	acceptance probability
$\mathbf{Q}$	shape tensor
$\hat{\mathbf{Q}}$	traceless shape tensor
R_0	vesicle radius
$\rho(x, x')$	transition probability
s	charge of disclination
σ	membrane tension
$\sigma^{(i)}$	membrane tension in phase (i)
T	temperature
T_0	room temperature
$\mathcal{T}_{N_v}$	triangulation of membrane surface with N_v vertices
$\mathbf{u}(\xi)$	displacement vector field
$u_a(x)$	phonon displacement
$u_{\mu\nu}$	strain tensor
v	reduced volume
v_i	vertex i
V	vesicle volume
$\mathbf{X}_k$	coordinates of vertex k
$\mathbf{X}(\xi)$	membrane coordinates
$\bar{\mathbf{X}}$	centre of mass coordinates
ξ	membrane parametrisation
ξ_p	persistence length
ξ_T	translational correlation length
ζ	roughness exponent
$\mathcal{Z}$	partition function

Bibliography

Bibliography

[1] P.G. de Gennes. Soft matter. *Rev. Mod. Phys.*, 64:645, 1992.

[2] T.A. Witten. Insights from soft condensed matter. *Rev. Mod. Phys.*, 71:S367, 1999.

[3] R.A.L. Jones. *Soft Condensed Matter*. Oxford University Press, 2002.

[4] D. Frenkel. Soft condensed matter. *Physica A*, 313:1, 2002.

[5] J.L. Barrat and J.P. Hansen. *Basic Concepts for Simple and Complex Liquids*. Cambridge University Press, 2003.

[6] W. Poon, T. McLeish, and A. Donald. Soft condensed matter: where physics meets biology. *Physics World*, May 2001, 2001.

[7] G. Gompper, U. Kaupp, J. Dhont, D. Richter, and R. Winkler. *Physics meets Biology. From Soft Matter to Cell Biology. 35th Spring School of the Department of Solid State Research*. Schriften des Forschungszentrums Jülich. Reihe Materie und Material/Matter and Materials, 19, 2004.

[8] R. Lipowsky. The conformation of membranes. *Nature*, 349:475, 1991.

[9] U. Seifert. Configurations of fluid membranes and vesicles. *Adv. Phys.*, 46:13, 1997.

[10] P.L.L. Luisi and P. Walde, editors. *Giant Vesicles*. John Wiley & Sons Ltd, 2000.

[11] R. Lipowsky, M. Brinkmann, R. Dimova, C. Haluska, J. Kierfeld, and J. Shillcock. Wetting, budding, and fusion - morphological transitions of soft surfaces. *J. Phys.: Condens. Matter*, 17:S2885, 2005.

[12] H.-G. Döbereiner. *On the Curvature of Membranes*. Habilitation thesis, Universität Potsdam, 1999.

[13] M. Bloom, E. Evans, and O.G. Mouritsen. Physical properties of the fluid lipid-bilayer component of cell membranes: a perspective. *Quarterly Reviews of Biophysics*, 24:293, 1991.

[14] R. Lipowsky and E. Sackmann, editors. *Handbook of Biological Physics. Structure and Dynamics of Membranes*. Elsevier, 1995.

[15] R. Lipowsky. *Vesicles and Biomembranes*. in G.L. Trigg (editor): Encyclopedia of Applied Physics Bd. 23, Weinheim: Wiley-VCH, 1998.

[16] D. Boal. *Mechanics of the Cell*. Cambridge University Press, 2002.

[17] R. Dimova, S. Aranda, N. Bezlyepkina, V. Nikolov, K.A. Riske, and R. Lipowsky. A practical guide to giant vesicles. Probing the membrane nanoregime via optical microscopy. *J. Phys. Cond. Mat.*, 18:S1151, 2006.

[18] J. Israelachvili. *Intermolecular and Surface Forces: With Applications to Colloidal and Biological Systems*. Academic Press Inc., 1991.

[19] W.M. Gelbart, A. Ben-Shaul, and D. Roux, editors. *Micelles, Membranes, Microemulsions, and Monolayers*. Springer-Verlag, 1995.

[20] J. Meunier, D. Langevin, and N. Boccara, editors. *Physics of Amphiphilic Layers*. Springer Verlag, 1987.

[21] D.E. Discher and A. Eisenberg. Polymer vesicles. *Science*, 297:967, 2002.

[22] O.G. Mouritsen. *Life - as a Matter of Fat*. Springer, 2005.

[23] B. Alberts, D. Bray, J. Lewis, M. Raff, K. Roberts, and J.D. Watson. *Molecular Biology of the Cell*. Garland Publishing, Inc, 1994.

[24] D.D. Voet and J.G. Voet. *Biochemistry*. John Wiley & Sons Ltd, 1995.

[25] S.J. Singer and G. L. Nicolson. The fluid mosaic model of the structure of cell membranes. *Science*, 175:720, 1972.

[26] D.D. Lasic. *Liposomes: from Physics to Applications*. Elsevier, 1993.

[27] V. Noireaux and A. Libchaber. A vesicle bioreactor as a step toward an artificial cell assembly. *Proc. Natl. Acad. Sci. (USA)*, 101:17669, 2004.

[28] M. Hase, A. Yamada, T. Hamada, D. Baigl, and K. Yoshikawa. Manipulation of cell-sized phospholipid-coated microdroplets and their use as biochemical microreactors. *Langmuir*, 23:348, 2007.

[29] K. Berndl, J. Käs, R. Lipowsky, E. Sackmann, and U. Seifert. Shape transformations of giant vesicles: Extreme sensitivity to bilayer asymmetry. *Europhys. Lett.*, 13:659, 1990.

[30] J. Käs and E. Sackmann. Shape transitions and shape stability of giant phospholipid vesicles in pure water induced by area-to-volume changes. *Biophys. J.*, 60:825, 1991.

[31] H.-G. Döbereiner, E. Evans, M. Kraus, U. Seifert, and M. Wortis. Mapping vesicle shapes into the phase diagram: A comparison of experiment and theory. *Phys. Rev. E*, 55:4458, 1997.

[32] I. Tsafrir, Y. Caspi, M.-A. Guedeau-Boudeville, T. Arzi, and J. Stavans. Budding and tubulation in highly oblate vesicles by anchored amphiphilic molecules. *Phys. Rev. Lett.*, 91:138102, 2003.

[33] R. Lipowsky. Bending of membranes by anchored polymers. *Europhys. Lett.*, 30:197, 1995.

[34] M. Breidenich, R.R. Netz, and R. Lipowsky. The influence of non-anchored polymers on the curvature of vesicles. *Molecular Physics*, 103:3169, 2005.

[35] J. Wang, K. Guo, F. Qiu, H. Zhang, and Y. Yang. Predicting shapes of polymer-chain-anchored fluid vesicles. *Phys. Rev. E*, 71:041908, 2005.

[36] R. Golestanian, M. Goulian, and M. Kardar. Fluctuation-induced interactions between rods on membranes and interfaces. *Europhys. Lett.*, 33:241, 1996.

[37] R.R. Netz. Inclusions in fluctuating membranes: Exact results. *J. Phys. I France*, 7:833, 1997.

[38] U. Seifert and R. Lipowsky. Adhesion of vesicles. *Phys. Rev. A*, 42:4768, 1990.

[39] T. Gruhn and R. Lipowsky. Temperature dependence of vesicle adhesion. *Phys. Rev. E*, 71:011903, 2005.

[40] P. Ziherl and S. Svetina. Flat and sigmoidally curved contact zones in vesicle-vesicle adhesion. *Proc. Natl. Acad. Sci. (USA)*, 104:761, 2007.

[41] C.K. Haluska, K.A. Riske, V. Marchi-Artzner, J.-M. Lehn, R. Lipowsky, and R. Dimova. Timescales of membrane fusion revealed by direct imaging of vesicle fusion with high temporal resolution. *Proc. Natl. Acad. Sci. (USA)*, 103:15841, 2006.

[42] M. Kraus, U. Seifert, and R. Lipowsky. Gravity-induced shape transformations of vesicles. *Europhys. Lett.*, 32:431, 1995.

[43] K.A. Riske and R. Dimova. Electro-deformation and poration of giant vesicles viewed with high temporal resolution. *Biophys. J.*, 88:1143, 2005.

[44] M. Kraus, W. Wintz, U. Seifert, and R. Lipowsky. Fluid vesicles in shear flow. *Phys. Rev. Lett.*, 77:3685, 1996.

[45] H. Noguchi and G. Gompper. Shape transitions of fluid vesicles and red blood cells in capillary flows. *Proc. Natl. Acad. Sci. (USA)*, 102:14159, 2005.

[46] J.-B. Manneville, P. Bassereau, D. Lévy, and J. Prost. Activity of transmembrane proteins induces magnification of shape fluctuations of lipid membranes. *Phys. Rev. Lett.*, 82:4356, 1999.

[47] S. Ramaswamy and M. Rao. The physics of active membranes. *C. R. Acad. Sci., Paris Series IV*, 2:817, 2001.

[48] N. Gov. Membrane undulations driven by force fluctuations of active proteins. *Phys. Rev. Lett.*, 93:268104, 2004.

[49] G. Lim, M. Wortis, and R. Mukhopadhyay. Stomatocyte-discocyte-echinocyte sequence of the human red blood cell: evidence for the bilayer-couple hypothesis from membrane mechanics. *Proc. Natl. Acad. Sci. (USA)*, 99:16766, 2002.

[50] P. Ziherl and S. Svetina. Nonaxisymmetric phospholipid vesicles: Rackets, boomerangs, and starfish. *Europhys. Lett.*, 70:690, 2005.

[51] F. Jülicher, U. Seifert, and R. Lipowsky. Conformal degeneracy and conformal diffusion of vesicles. *Phys. Rev. Lett.*, 71:452, 1993.

[52] X. Michalet and D. Bensimon. Observation of stable shapes and conformal diffusion in genus 2 vesicles. *Science*, 269:666, 1995.

[53] A.D. Alexandrov. Uniqueness theorems for surfaces in the large I. *Vestnik Leningrad Univ. Math.*, 11:5, 1956.

[54] H. Wente. Counterexample of a conjecture of H. Hopf. *Pacific J. Math.*, 121:193, 1986.

[55] P.B. Canham. The minimum energy of bending as a possible explanation of the biconcave shape of the human red blood cell. *J. Theoret. Biol.*, 26:61, 1970.

[56] W. Helfrich. Elastic properties of lipid bilayers: Theory and possible experiments. *Z. Naturforsch. C*, 28:693, 1973.

[57] E. Evans. Bending resistance and chemically induced moments in membrane bilayers. *Biophys. J.*, 14:923, 1974.

[58] L.D. Landau and E.M. Lifschitz. *Theory of Elasticity.* Pergamon Press, 1986.

[59] D.P. Siegel and M.M. Kozlov. The Gaussian curvature elastic modulus of N-monomethylated dioleoylphosphatidylethanolamine: Relevance to membrane fusion and lipid phase behaviour. *Biophys. J.*, 87:366, 2004.

[60] F. Brochard and J.F. Lennon. Frequency spectrum of the flicker phenomenon in erythrocytes. *J. Physique*, 36:1035, 1975.

[61] H.-G. Döbereiner and U. Seifert. Giant vesicles at the prolate-oblate transition: A macroscopic bistable system. *Europhys. Lett.*, 36:325, 1996.

[62] R. Lipowsky and R. Dimova. Domains in membranes and vesicles. *J. Phys.: Condens. Matter*, 15:S31, 2003.

[63] K. Simons and E. Ikonnen. Functional rafts in cell membranes. *Nature*, 389:569, 1997.

[64] W. Binder, V. Barragan, and F. Menger. Domains and rafts in lipid membranes. *Angew. Chem. Int. Ed.*, 42:5802, 2003.

[65] D.M. Engelman. Membranes are more mosaic than fluid. *Nature*, 438:578, 2005.

[66] N. Chazal and D. Gerlier. Virus entry, assembly, budding, and membrane rafts. *Microbiol. Mol. Biol. Rev.*, 67:226, 2003.

[67] T. Baumgart, S.T. Hess, and W.W. Webb. Imaging coexisting fluid domains in biomembrane models coupling curvature and line tension. *Nature*, 425:821, 2003.

[68] S. Veatch and S. Keller. Miscibility phase diagrams of giant vesicles containing sphingomyelin. *Phys. Rev. Lett.*, 94:148101, 2005.

[69] J.F. Nagle and S. Tristram-Nagle. Structure of lipid bilayers. *Biochim. Biophys. Acta*, 1469:159, 2000.

[70] J.H. Ipsen, G. Karlstrom, O.G. Mouritsen, H. Wennerstrom, and M.J. Zuckermann. Phase equilibria in the phosphatidylcholine-cholesterol system. *Biochim. Biophys. Acta*, 905:162, 1987.

[71] P. Beales. *Phase separation in binary phospholipid vesicles studied using fluorescence microscopy.* PhD thesis, University of Edinburgh, 2005.

[72] P. Beales, V. Gordon, Z. Zhao, S. Egelhaaf, and W. Poon. Solid-like domains in fluid membranes. *J. Phys.: Condens. Matter*, 17:S3341, 2005.

[73] M. Yanagisawa, M. Imai, T. Masui, S. Komura, and T. Ohta. Growth dynamics of domains in ternary fluid vesicles. *Biophys. J.*, 92:115, 2007.

[74] J. Korlach, P. Schwille, W.W. Webb, and G. Feigenson. Characterization of lipid bilayer phases by confocal microscopy and fluorescence correlation spectroscopy. *Proc. Natl. Acad. Sci. (USA)*, 96:8461, 1999.

[75] G. Feigenson and J. Buboltz. Ternary phase diagram of dipalmitoyl-PC/dilauroyl-PC/cholesterol: nanoscopic domain formation driven by cholesterol. *Biophys. J.*, 80:2775, 2001.

[76] D. Scherfeld, N. Kahya, and P. Schwille. Lipid dynamics and domain formation in model membranes composed of ternary mixtures of unsaturated and saturated phosphatidylcholines and cholesterol. *Biophys. J.*, 85:3758, 2003.

[77] S.D. Shoemaker and T.K. Vanderlick. Material studies of lipid vesicles in the L_α and L_α-gel coexistence regimes. *Biophys. J.*, 84:998, 2003.

[78] V.D. Gordon, P.A. Beales, Z. Zhao, C. Blake, F.C. MacKintosh, P.D. Olmsted, M.E. Cates, S.U. Egelhaaf, and W.C.K. Poon. Lipid organization and the morphology of solid-like domains in phase-separating binary lipid membranes. *J. Phys.: Condens. Matter*, 18:L415, 2006.

[79] G. Gompper and D.M. Kroll. Network models of fluid, hexatic and polymerized membranes. *J. Phys.: Condens. Matter*, 9:8795, 1977.

[80] D.R. Nelson, T. Piran, and S. Weinberg, editors. *Statistical Mechanics of Membranes and Surfaces, 2nd ed.* World Scientific, 2004.

[81] N.D. Mermin and H. Wagner. Absence of ferromagnetism or antiferromagnetism in one- or two-dimensional isotropic heisenberg models. *Phys. Rev. Lett.*, 17:1133, 1966.

[82] K.J. Strandburg. Two-dimensional melting. *Rev. Mod. Phys.*, 60:161, 1988.

[83] F. David, P. Ginsparg, and J. Zinn-Justin, editors. *Fluctuating Geometries in Statistical Mechanics and Field Theory.* Elsevier, 1996.

[84] R. Lipowsky. Shape fluctuations and critical phenomena. In H. van Beijeren, editor, *Fundamental Problems in Statistical Mechanics VII.* Elsevier, 1990.

[85] J. Polchinski. *String Theory*, volume I, II. Cambridge University Press, 1998.

[86] E. Frey. *Statistische Physik fluktuierender Mannigfaltigkeiten.* Habilitation thesis, Technische Universität München, 1996.

[87] S.A. Safran. *Statistical Thermodynamics of Surfaces, Interfaces, and Membranes.* Addison-Wesley, 1994.

[88] K.J. Wiese. Polymerized membranes, a review. In C. Domb and J. Lebowitz, editors, *Phase Transitions and Critical Phenomena*, volume 19. Academic Press, 2000.

[89] S.A. Safran. Statistical thermodynamics of soft surfaces. *Surface Science*, 500:127, 2002.

[90] E. Guitter. Méthodes de théorie des champs pour les polymères et les membranes polymérisées. Ecole de Physique de la Matière Condensée. Session Théorie statistique des champs, 25 août - 6 septembre 1997, Beg-Rohu, France.

[91] M.J. Bowick and A. Travesset. The statistical mechanics of membranes. *Phys. Rep.*, 344:255, 2001.

[92] G. Brannigan, L.C.-L. Lin, and F.L.H. Brown. Implicit solvent simulation models for biomembranes. *European Biophysics Journal*, 35:104, 2006.

[93] M. Müller, K. Katsov, and M. Schick. Biological and synthetic membranes: What can be learned from a coarse-grained description? *Phys. Rep.*, 434:113, 2006.

[94] F. David and S. Leibler. Vanishing tension of fluctuating membranes. *J. Phys. II France*, 1:959, 1991.

[95] J.-B. Fournier, A. Ajdari, and L. Peliti. Effective-area elasticity and tension of micromanipulated membranes. *Phys. Rev. Lett.*, 86:004970, 2001.

[96] W. Cai, T.C. Lubensky, P. Nelson, and T. Powers. Measure factors, tension, and correlations of fluid membranes. *J. Phys. II France*, 4:931, 1994.

[97] L. Peliti and S. Leibler. Effects of thermal fluctuations on systems with small surface tension. *Phys. Rev. Lett.*, 54:1690, 1985.

[98] J.A. Santiago and A. Zamora. The one-loop elastic coefficients for the helfrich membrane in higher dimensions. *J. Phys. A: Math. Gen.*, 38:1225, 2005.

[99] O. Berger, O. Edholm, and F. Jähnig. Molecular dynamics simulations of a fluid bilayer of dipalmitoylphosphatidylcholine at full hydration, constant pressure, and constant temperature. *Biophys. J.*, 72:2002, 1997.

[100] V.A. Kazakov, I.K. Kostov, and A.A. Migdal. Critical properties of randomly triangulated planar random surfaces. *Physics Letters*, 157B:295, 1985.

[101] A. Billoire and F. David. Scaling properties of randomly triangulated planar random surfaces. *Nucl. Phys. B*, 275:617, 1986.

[102] J.F. Wheater. Random surfaces: from polymer membranes to strings. *J. Phys. A: Math. Gen.*, 27:3323, 1994.

[103] C. Itzykson. Random geometry, lattices and fields. In M. Asorey J. Abad and A. Cruz, editors, *Proc. GIFT Seminar*, page 130. World Scientific, 1986.

[104] G. Gompper and D.M. Kroll. Random surface discretizations and the renormalization of the bending rigidity. *J. Phys. I France*, 6:1305, 1996.

[105] F. Jülicher. *Die Morphologie von Vesikeln.* PhD thesis, Universität zu Köln, 1994.

[106] J.-L. Maltret and M. Daniel. Discrete curvatures and applications: a survey. preprint Marseille cedex 9, 2003.

[107] D.V. Boulatov, V.A. Kazakov, I.K. Kostov, and A.A. Migdal. Analytical and numerical study of a model of dynamically triangulated random surfaces. *Nucl. Phys. B*, 275:641, 1986.

[108] D.R. Nelson and L. Peliti. Fluctuations in membranes with crystalline and hexatic order. *J. Physique*, 48:1085, 1987.

[109] D. Mermin. The topological theory of defects in ordered media. *Rev. Mod. Phys.*, 51:591, 1979.

[110] C.-F. Chou, A.J. Jin, S.W. Hui, C.C. Huang, and J.T. Ho. Multiple-step melting in two-dimensional hexatic liquid-crystal films. *Science*, 280:1424, 1998.

[111] D. Kaminski, P. Poodt, E. Aret, N. Radenovic, and E. Vlieg. Observation of a liquid phase with an orthorhombic orientational order. *Phys. Rev. Lett.*, 96:056102, 2006.

[112] S.T. Milner and S.A. Safran. Dynamical fluctuations of droplet microemulsions and vesicles. *Phys. Rev. A*, 36:4371, 1987.

[113] D.C. Morse and S.T. Milner. Statistical mechanics of closed fluid membranes. *Phys. Rev. E*, 52:5918, 1995.

[114] A. Baumgärtner and J.-S. Ho. Crumpling of fluid vesicles. *Phys. Rev. A*, 41:5747, 1990.

[115] G. Gompper and D.M. Kroll. Phase diagram of fluid vesicles. *Phys. Rev. Lett.*, 73:2139, 1994.

[116] H. Noguchi and G. Gompper. Dynamics of fluid vesicles in shear flow: Effect of membrane viscosity and thermal fluctuations. *Phys. Rev. E*, 72:011901, 2005.

[117] S. Svetina and B. Zeks. Bilayer couple hypothesis of red-cell shape transformations and osmotic hemolysis. *Biomed. Biochim. Acta*, 42:S86, 1983.

[118] S. Svetina and B. Zeks. Membrane bending energy and shape determination of phospholipid vesicles and red blood cells. *Eur. Biophys. J.*, 17:101, 1989.

[119] L. Miao, U. Seifert, M. Wortis, and H.-G. Döbereiner. Budding transitions of fluid-bilayer vesicles: The effect of area-difference elasticity. *Phys. Rev. E*, 49:5389, 1994.

[120] O.-Y. Zhong-can and W. Helfrich. Bending energy of vesicle membranes: General expressions for the first, second, and third variation of the shape energy and applications to spheres and cylinders. *Phys. Rev. A*, 39:5280, 1989.

[121] J.T. Jenkins. The equation of mechanical equilibrium of a model membrane. *SIAM Journal on Applied Mathematics*, 32:755, 1977.

[122] R. Capovilla and J. Guven. Stresses in lipid membranes. *J. Phys. A: Math. Gen.*, 35:6233, 2002.

[123] M.A. Lomholt and L. Miao. Two different descriptive approaches to the mechanics of membranes and the connection between them. *arXiv: cond-mat/0509664*, 2005.

[124] Y.Yin, Y. Chen, D. Ni, H. Shi, and Q. Fan. Shape equations and curvature bifurcations induced by inhomogeneous rigidities in cell membranes. *Journal of Biomechanics*, 38:1433, 2005.

[125] U. Seifert, K. Berndl, and R. Lipowsky. Shape transformations of vesicles: Phase diagrams for spontaneous-curvature and bilayer-coupling models. *Phys. Rev. A*, 44:1182, 1991.

[126] U. Seifert. The concept of effective tension for fluctuating vesicles. *Zeitschrift für Physik B Condensed Matter*, 97:299, 1995.

[127] H.-G. Döbereiner, G. Gompper, C.K. Haluska, D.M. Kroll, P.G. Petrov, and K.A. Riske. Advanced flicker spectroscopy of fluid membranes. *Phys. Rev. Lett.*, 91:048301, 2003.

[128] J. Rudnick and G. Gaspari. The asphericity of random walks. *J. Phys. A: Math. Gen.*, 19:L191, 1986.

[129] G.T. Linke, R. Lipowsky, and T. Gruhn. Free fluid vesicles are not exactly spherical. *Phys. Rev. E*, 71:051602, 2005.

[130] K. Šolc. Shape of a random-flight chain. *J. Chem. Phys.*, 55:335, 1971.

[131] J.A. Aronovitz and D.R. Nelson. Universal features of polymer shapes. *J. Physique*, 47:1445, 1986.

[132] J.A. Aronovitz and M.J. Stephen. Universal features of the shapes of percolation clusters and lattice animals. *J. Phys. A: Math. Gen.*, 20:2539, 1987.

[133] I. Lyuksyutov, A.G. Naumovets, and V. Pokrovsky. *Two-dimensional Crystals*. Academic Press, 1992.

[134] R. Lipowsky. Budding of membranes induced by intramembrane domains. *J. Phys. II France*, 2:1825, 1992.

[135] T. Kawakatsu, D. Andelman, K. Kawasaki, and K. Taniguchi. Phase transitions and shapes of two component membranes and vesicles I: strong segregation limit. *J. Phys. II France*, 3:971, 1993.

[136] S. Schneider and G. Gompper. Shapes of crystalline domains on spherical fluid vesicles. *Europhys. Lett.*, 70:136, 2005.

[137] Y. Chushak and A. Travesset. Solid domains in lipid vesicles and scars. *Europhys. Lett.*, 72:767, 2005.

[138] V. Vitelli, J.B. Lucks, and D.R. Nelson. Crystallography on curved surfaces. *Proc. Natl. Acad. Sci. (USA)*, 103:12323, 2006.

[139] V. Vitelli and D.R. Nelson. Nematic textures in spherical shells. *Phys. Rev. E*, 74:021711, 2006.

[140] M. Spivak. *A comprehensive Introduction to Differential Geometry I-IV*. Publish or Perish, 1979.

[141] D.R. Nelson. *Defects and Geometry in Condensed Matter Physics*. Cambridge University Press, 2002.

[142] M. Bowick, A. Cacciuto, D.R. Nelson, and A. Travesset. Crystalline order on a sphere and the generalized Thomson problem. *Phys. Rev. Lett.*, 89:185502, 2002.

[143] F.C. MacKintosh and T.C. Lubensky. Orientational order, topology, and vesicle shapes. *Phys. Rev. Lett.*, 67:1169, 1991.

[144] T.C. Lubensky and J. Prost. Orientational order and vesicle shape. *J. Phys. II France*, 2:371, 1992.

[145] R.M.L. Evans. Phase diagrams for deformable toroidal and spherical surfaces with intrinsic orientational order. *J. Phys. II France*, 5:507, 1995.

[146] R.M.L. Evans. Theoretical study of fluid membranes of spherical topology with internal degrees of freedom. *Phys. Rev. E*, 53:935, 1996.

[147] J.-M. Park, T.C. Lubensky, and F.C. MacKintosh. n-atic order and continuous shape changes of deformable surfaces of genus zero. *Europhys. Lett.*, 20:279, 1992.

[148] C.-M. Ghim and J.-M. Park. Morphology of fluctuating spherical vesicles with internal bond-orientational order. *J. Phys.: Condens. Matter*, 15:3891, 2003.

[149] J. Lidmar, L. Mirny, and D.R. Nelson. Virus shapes and buckling transitions in spherical shells. *Phys. Rev. E*, 68:051910, 2003.

[150] A.E. Blaurock and R.C. Gamble. Small phosphatidylcholine vesicles appear to be faceted below the thermal phase transition. *J. Membr. Biol.*, 50:187, 1979.

[151] T.T. Nguyen, R. Bruinsma, and W.M. Gelbart. Elasticity theory and shape transitions of viral shells. *Phys. Rev. E*, 72:051923, 2005.

[152] M. Bowick, D.R. Nelson, and A. Travesset. Interacting topological defects on frozen topographies. *Phys. Rev. B*, 62:8738, 2000.

[153] A.R. Bausch, M.J. Bowick, A. Cacciuto, A.D. Dinsmore, M.F. Hsu, D.R. Nelson, M.G. Nikolaides, A. Travesset, and D.A. Weitz. Grain boundary scars and spherical crystallography. *Science*, 299:1716, 2003.

[154] M. Bowick, D.R. Nelson, and A. Travesset. Curvature-induced defect unbinding in toroidal geometries. *Phys. Rev. E*, 69:041102, 2004.

[155] S.J. Marrink, J. Risselada, and A.E. Mark. Simulation of gel phase formation and melting in lipid bilayers using a coarse grained model. *Chem. Phys. Lip.*, 135:223, 2005.

[156] L. van Hemmen and M. Peterson. Crumpling of curved sheets: Generalizing Föppl-von Kármán. *arXiv: cond-mat/0503158*, 2005.

[157] S. Akimov, P. Kuzmin, S. Akimov, J. Zimmerberg, F. Cohen, and Y. Chizmadzhev. An elastic theory for line tension at a boundary separating two lipid monolayer regions of different thickness. *Journal of Electroanalytical Chemistry*, 564:13, 2004.

[158] P. Kuzmin, S. Akimov, Y. Chizmadzhev, J. Zimmerberg, and F. Cohen. Line tension and interaction energies of membrane rafts calculated from lipid splay and tilt. *Biophys. J.*, 88:1120, 2005.

[159] T. Kohyama, D.M. Kroll, and G. Gompper. Budding of crystalline domains in fluid membranes. *Phys. Rev. E*, 68:061905, 2003.

[160] T. Mora and A. Boudaoud. Thin elastic plates: On the core of developable cones. *Europhys. Lett.*, 59:41, 2002.

[161] K. Brakke. The surface evolver. *Exp. Math.*, 1:141, 1992.

[162] C.-M. Chen. Theory for the bending anisotropy of lipid membranes and tubule formation. *Phys. Rev. E*, 59:6192, 1999.

[163] J. Rudnick and R. Bruinsma. Shape of domains in two-dimensional systems: Virtual singularities and a generalized Wulff construction. *Phys. Rev. Lett.*, 74:2491, 1995.

[164] P.B. Sunil Kumar and M. Rao. Shape instabilities in the dynamics of a two-component fluid membrane. *Phys. Rev. Lett.*, 80:2489, 1998.

[165] P.B. Sunil Kumar, G. Gompper, and R. Lipowsky. Budding dynamics of multicomponent membranes. *Phys. Rev. Lett.*, 86:3911, 2001.

[166] P.G. Dommersnes, J.-B. Fournier, and P. Galatola. Long-range elastic forces between membrane inclusions in spherical vesicles. *Europhys. Lett.*, 42:233, 1998.

[167] P. Biscari, F. Bisi, and R. Rosso. Curvature effects on membrane-mediated interactions of inclusions. *J. Math. Biol.*, 45:37, 2002.

[168] M. Goulian, R. Bruinsma, and P. Pincus. Long-range forces in heterogeneous fluid membranes. *Europhys. Lett.*, 22:145, 1993.

[169] J.-M. Park and T.C. Lubensky. Interactions between membrane inclusions on fluctuating membranes. *J. Phys. I France*, 6:1217, 1996.

[170] J.G. Kirkwood. Statistical mechanics of fluid mixtures. *J. Chem. Phys.*, 3:300, 1935.

[171] T. Baumgart, S. Das, W.W. Webb, and J.T. Jenkins. Membrane elasticity in giant vesicles with fluid phase coexistence. *Biophys. J.*, 89:1067, 2005.

[172] F. Jülicher and R. Lipowsky. Domain-induced budding of vesicles. *Phys. Rev. Lett.*, 70:2964, 1993.

[173] F. Jülicher and R. Lipowsky. Shape transformations of vesicles with intramembrane domains. *Phys. Rev. E*, 53:2670, 1996.

[174] M. Laradji and P.B. Sunil Kumar. Dynamics of domain growth in self-assembled fluid vesicles. *Phys. Rev. Lett.*, 93:198105, 2004.

[175] J.L. Harden, F.C. MacKintosh, and P.D. Olmsted. Budding and domain shape transformations in mixed lipid films and bilayer membranes. *Phys. Rev. E*, 72:011903, 2005.

[176] G. Ayton, J.L. McWhirter, P. McMurtry, and G.A. Voth. Coupling field theory with continuum mechanics: A simulation of domain formation in giant unilamellar vesicles. *Biophys. J.*, 88:3855, 2005.

[177] W.T. Góźdź and G. Gompper. Composition-driven shape transformations of membranes of complex topology. *Phys. Rev. Lett.*, 80:4213, 1998.

[178] S. Leibler. Curvature instability in membranes. *J. Phys. I France*, 47:507, 1986.

[179] U. Seifert. Curvature-induced lateral phase segregation in two-component vesicles. *Phys. Rev. Lett.*, 70:1335, 1993.

[180] D. Benvegnu and H. McConnell. Line tension between liquid domains in lipid monolayers. *J. Phys. Chem.*, 96:6820, 1992.

[181] H.-G. Döbereiner, J. Käs, D. Noppl, I. Sprenger, and E. Sackmann. Budding and fission of vesicles. *Biophys. J.*, 65:1396, 1993.

[182] Yanhong Li. private communication.

[183] J.-M. Allain and M.B. Amar. Biphasic vesicle: instability induced by adsorption of proteins. *Physica A*, 337:531, 2004.

[184] R.C. Sarasij and M. Rao. Tilt texture domains on a membrane and chirality induced budding. *Phys. Rev. Lett.*, 88:088101, 2002.

[185] R.H. Templer, B.J. Khoo, and J.M. Seddon. Gaussian curvature modulus of an amphiphilic monolayer. *Langmuir*, 14:7427, 1998.

[186] S. Semrau, T. Idema, L. Holtzer, T. Schmidt, and C. Storm. Accurate determination of elastic parameters for multi-component membranes. *arXiv: cond-mat/0612554*, 2006.

[187] M.P. do Carno. *Differential Geometry of Curves and Surfaces.* Englewood Cliffs: Prentice-Hall, 1976.

[188] S. Kobayashi and K. Nomizu. *Foundations of Differential Geometry Vol I,II.* John Wiley & Sons, 1996.

[189] Z.C. Tu and Z.C. Ou-Yang. A geometric theory on the elasticity of biomembranes. *J. Phys. A: Math. Gen.*, 37:11407, 2004.

[190] M. Nakahara. *Geometry, Topology and Physics.* Institute of physics publishing, Bristol and Philadelphia, 1990.

[191] J. Cheeger, W. Müller, and R. Schrader. On the curvature of piecewise flat spaces. *Commun. Math. Phys.*, 92:405, 1984.

[192] H. Hadwiger. *Vorlesungen über Inhalt, Oberfläche und Isoperimetrie*. Springer, 1957.

[193] V. Borrelli, F. Cazals, and J.-M. Morvan. On the angular defect of triangulations and the pointwise approximation of curvature. *Computer Aided Geometric Design*, 20:319, 2003.

[194] Z. Xu and G. Xu. Discrete schemes for Gaussian curvature and their convergence. preprint, 2006.

[195] A.M. Polyakov. Fine structure of strings. *Nucl. Phys. B*, 268:406, 1986.

[196] F. David, E. Guitter, and L. Peliti. Critical properties of fluid membranes with hexatic order. *J. Physique*, 48:2059, 1987.

[197] M. Bowick and A. Travesset. The geometrical structure of 2d bond-orientational order. *J. Phys. A: Math. Gen.*, 34:1535, 2001.

[198] M.O. Katanaev and I.V. Volovich. Theory of defects in solids and three-dimensional gravity. *Annals of Physics*, 216:1, 1991.

[199] M.P. Allen and D.J. Tildesley. *Computer Simulations of Liquids*. Clarendon Press, 1989.

[200] D.P. Landau and K. Binder. *Monte Carlo Simulations in Statistical Physics*. Cambridge University Press, 2000.

[201] N. Metropolis and S. Ulam. The Monte Carlo method. *Journal of the American Statistical Association*, 44:335, 1949.

[202] H. Flyvbjerg and H. G. Petersen. Error estimates on averages of correlated data. *J. Chem. Phys.*, 91:461, 1989.

[203] N. Metropolis, A. Rosenbluth, M. Rosenbluth, A. Teller, and E. Teller. Equation of state calculations by fast computing machines. *J. Chem. Phys.*, 21:1087, 1953.

[204] K. Svozil. *Randomness & Undecidability in Physics*. World Scientific, 1993.